Abstract

LIU, QIANG. Fundamental Study and Method Development for Surface-based Laser Desorption Ionization Imaging Mass Spectrometry. (Under the direction of Lin He).

By providing both the chemical identity and the spatial organization of each component in biological samples, Imaging Mass Spectrometry (IMS) becomes an emerging tool in clinic and pharmacological study. Most work in IMS has been focused on protein and peptide mapping in biological samples to take advantage of effective analyte ionization in MALDI-MS, and also partially due to the limitation of MALDI-MS in small molecule detection. The focus of my research is to develop novel tools to image spatial distribution of small molecules in biological samples. A surface-based mass spectrometric imaging method, i.e. Desorption/Ionization on Silicon (DIOS), was used for biological surface analysis in the concept-proof investigation. More over, possible proton transferring pathways and impact of local chemical environment have been systematically investigated in the fundamental understanding of ionization mechanism of SALDI-MS. Based on the finding on the SALDI mechanism, a hybrid ionization approach, ME-SALDI has been developed by combing the strength of the conventional MALDI matrix and SALDI, where the improved detection sensitivity with reduced matrix-analyte interference and the improved imaging capability through analysis of mouse brain and heart sections has been demonstrated. In addition, the impact of vacuum stability of matrix in ME-SALDI-IMS applications has been examined. A solvent free, homogenous and reproducible sublimation method has been developed for ionic matrix in ME-SALDI, by which improved vacuum stability and MS detection have been achieved.

Furthermore, a new generation of meso-porous oxide substrate was developed as a novel ME-SALDI substrate with a superior storage stability, extended detectable mass range and robust substrate preparation.

Fundamental Study and Method Development for Surface-based Laser Desorption Ionization Imaging Mass Spectrometry

by
Qiang Liu

A dissertation submitted to the Graduate Faculty of
North Carolina State University
in partial fulfillment of the
requirements for the Degree of
Doctor of Philosophy

Chemistry

Raleigh, North Carolina

February 25, 2009

APPROVED BY:

Lin He Assistant Professor, Chemistry Chair of Advisory Committee	Morteza G. Khaledi Professor, Chemistry
Edmond F. Bowden Professor, Chemistry	David C. Muddiman Professor, Chemistry

Dedication

To my wife Wei Yue, my lovely daughters Joanna and Judy, my parents Huanxin Liu and Weijun Fan, my parents-in-law Jun Yue and Ruling Liu, and my brothers and sisters Yong Liu, Dan Gao, Qing Yue, and Yan Kou, I appreciate all of your love, encouragement, patience, and support.

Biography

Born: October 14, 1973, Jinan, Shandong, China

Parents: Weijun Fan and Huanxin Liu

Siblings: Yong Liu and Dan Gao

Married: September 25, 1998

Spouse: Wei Yue

Daughters: Joanna Y Liu and Judy Y Liu

Parents-in-law: Ruling Liu and Jun Yue

Siblings-in-law: Qing Yue and Yan Kou

High School: Beizhen High School, graduated 1991

Undergraduate: Beijing Institute of Technology
B.S. Fine Chemistry, graduated 1995

Acknowledgments

My advisor, Professor Lin He, provided guidance, patience, and financial support during my graduate studies. North Carolina State University Department of Chemistry and Canon, Inc also provided financial support.

Dr. Zhong Guo, Yongshen Xiao, Yu Chiu, Coral Pagan-Miranda and John F. Cahill also contributed on the imaging mass spectrometry (IMS) project. Weiming Zheng helped with IMS software installation and upgrade. Dr. Hirokatsu Miyata and Mr. Kimihiro Yoshimura contributed to the development of titania substrate.

I would like to thank Dr. Michael Dykstra for training me the preparation of frozen tissue section. I appreciate Dr. Gary M. Pollack, Dr. Jeannie Padowski, Dr. Wei Yue and Ms. Welker for providing mice tissue samples. I am also thankful to Dr. Markus Stoeckli for the help with MS imaging software. I would like to acknowledge Mr. Fred Stevie and Mr. Matthew M. Lyndon for the help with MS data collection. I thank Drs. Ade's and Feldheim's groups for the usage of optical microscopes.

I also thank the other former and current members of the He group, Nancy Finkel, Amel Ganawi, Abhilasha Shah, Fredrick Jaeger, Peng He, Geoffrey Okelo, Mark Eckert, Hong Qian and Yafeng Wu.

The members of my committee made suggestions and comments during my graduate studies. These faculty members are Professors Edmond F. Bowden, Morteza G. Khaledi and David C. Muddiman. The graduate school representative is Professor Peter Bloomfield from the Department of Statistics.

I would also like to acknowledge all the teachers and professors during my educational journey that helped me get to this point today. I am grateful to my fellow graduate students and postdocs within the department, especially the Gorman group.

Members of the support staff provided prompt assistance with regard to equipment repairs and administrative matters. These persons include Mr. Eddie Barefoot, Mr. Alan Harvell, Ms. Brenda Burgess and Ms. Maria D. Moreno.

Finally, I'd like to sincerely thank all my family and friends. I am indebted to my parents and parents-in-law, who have been taking care of my daughters since they were born with their love and patience. Without the support and love from them, I would not have been able to successfully finish the Ph.D. program. I am very grateful to all brothers and sisters in Chapel Hill Chinese Christian Church. My wife and I will always remember your love and support when Joanna and Judy were born.

Best wishes to all.

Table of Contents

List of Tables

List of Figures

List of Schemes

Chapter 1 Introduction

1.1 Matrix Assisted Laser Desorption Ionization (MALDI)

The use of organic acids as matrix in laser desorption ionization, so-called MALDI, dramatically softens and facilitates the desorption/ionization process of analyte. Therefore, the detectable mass range has been extended to hundreds of thousand (even millions in certain cases) Dalton and the low limit of detection (LOD) routinely reached the low femtomole to attomole range. MALDI, along with electrospray, has revolutionized the use of mass spectrometry in biological science and material sciences. Their applications have expanded to forensics, genomics, proteomics, most recently metabolomics and beyond.[1-5] For instance, MALDI-based peptide mass fingerprint analysis has become one of the primary high-throughput protein identification methods.[6] The application of MALDI MS in targeted detection of neuropeptide families within single cells has led to the discovery of over 400 invertebrate neuropeptides.[7]

Scheme 1.1. Schematic drawing of MALDI ionization source

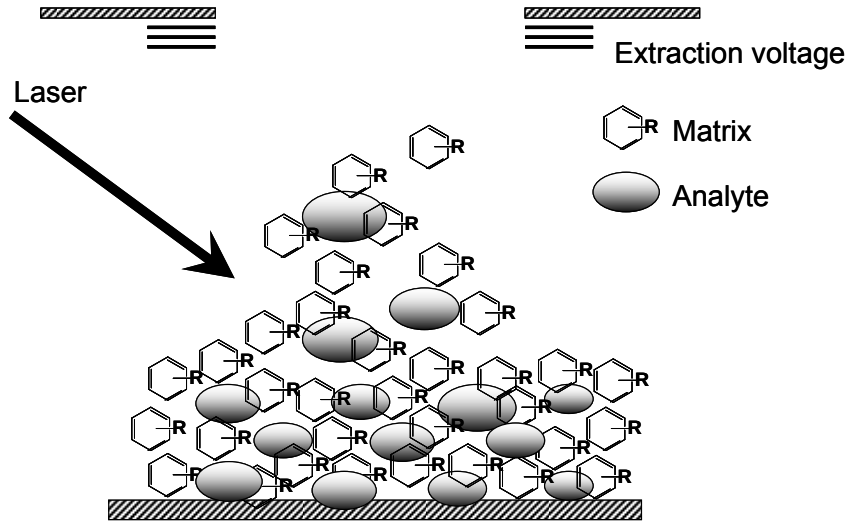

Scheme 1.1 describes a simplified outline of a MALDI ionization source: the analyte is co-crystallized with an organic matrix before depositing on a solid support. Upon irradiated by a pulsed laser beam, the analyte molecule desorb to the gas phase, along with matrix molecules, and ionize. The charged analyte molecules are extracted into the mass analyzer by a high voltage and their chemical nature are analyzed based on their mass-to-charge ratios. The MALDI ion sources are catogorized into UV-MALDI or IR-MALDI based on the equipped laser and the matrice to be used varied accordingly. The research and discussion will be focused on the use of N_2 lasers (337 nm) in this thesis.

Scheme 1.2. Schematic drawing of time-of-flight mass analyzer

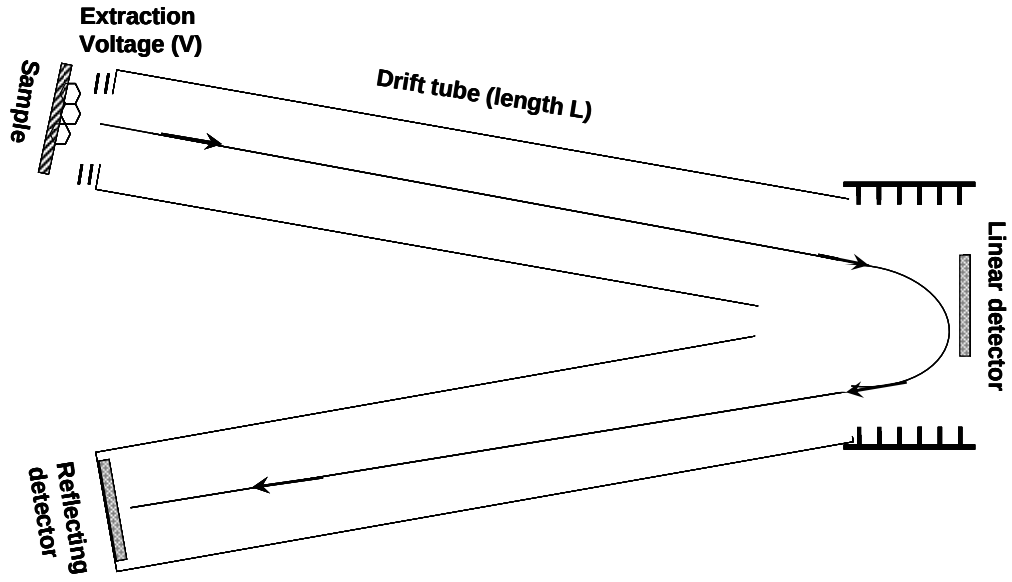

Various mass analyzers have been successfully interfaced with MALDI-MS. Time-of-flight (TOF) mass analyzer is the most widely used one and is used in this thesis. TOF provides the benefits of wide detecting mass range, high duty cycle and good

sensitive.[8] As shown in Scheme 1.2, species of different mass-to-charge ratios exhibit different velocities when they travel inside of the vacuum tube. This difference in the initial velocity allows ions to arrive the detector at different time and to be differentiated. Techniques such as delayed extraction, reflectron detector and orthogonal extraction/acceleration have been developed to significantly improve the resolving power of the TOF analyzer.[9,10] Additional mass analyzers, such as FT-ICR allow analyte detection of sub part-per-million (ppm) mass accuracy and triple quadrupole enable quantitative analysis of pharmaceutical compounds in a sensitive, high-throughput, and inexpensive fashion.[11-14]

The selection of proper matrix and sample preparation method is crucial for a successful MALDI experiment. An aromatic carboxylic acid moiety with a strong absorption coefficient at 337 nm is the common structure shared among most UV-MALDI matrices. It is worth pointing out that the selection of suitable matrix is still a very much empirical task due to the insufficient understanding of their structural roles in MALDI. Compounds with similar chemical structures, such as 2,5-DHB and 3,5-DHB, have been found to behave with stark differences in MALDI experiments.[15]

Although the detail mechanism of MALDI is still under debate, matrix is believed serving both as a photon trap and a proton donor in the MALDI process. Systematic variation of relevant parameters and large scale molecular dynamic simulation are two major approaches to providing insights on the mechanism of MALDI desorption process.[16] The desorption process of MALDI was found to be highly dependent on the experimental parameters, such as laser conditions, structure of matrix/analyte crystal, and

matrix selection. Several theoretical models have been suggested to explain the MALDI process, including thermal desorption of molecules, surface layer by layer sublimation and volume ablation.[17-19] A more complex and mixed process was also reported and was believed to be one step closer to the truth.[20] Briefly, analyte molecules are believed to be surrounded by matrix molecules and isolated from each other in the matrix/analyte co-crystal structure. When a laser is fired on co-crystals, matrix molecules absorb the photon energy and convert it to thermal/mechanic energy. The local temperature of co-crystals could raise up to 600 ℃ within nanoseconds. When the input rate of photon energy is significant larger the energy consuming rate (thermal energy diffusion, matrix melting, matrix evaporation/sublimation, stress relaxing and so on), volume ablation would then occur through phase explosion. During the subsequent sublimation (thermal) /spallation (mechanical) the matrix molecules carry the analyte molecules into the gas phase and protect them from destructive heating.

The ionization process in MALDI could be roughly divided into two stages: primary ion formation and secondary ion formation.[16] The primary ions are directly generated from neutral molecules in condense phase, which are generally matrix ions. Formation of free ions directly from neutral molecules is energetic challenging. Several theoretical models have been proposed for the primary ions formation in MALDI process. For examples, Hillenkamps et al suggested the formation of matrix radical ions through photo-ionization led to subsequent production of matrix ions.[21] However, for most matrix species, the ionization potential (IP) is higher than the energy provided by single photon of commonly used MALDI lasers For example, the IP of DHB is 8.05 eV,

where direct deposition of three N_2 photons (3.68 eV each) is required to overcome the ionization energy barrier. An energy pooling model has also been proposed that suggests multiple excited matrix molecules pool all energy together to generate one matrix radical ion, by which the energetic barrier would be much lower for primary ion formation.[22] Preformed ion during sample preparation is another possible source for primary ions since the formation of ions in solution is easier.[22] However, the charge separation of pre-existing ions from their counter ions also needs high energy input, as high as 4.8 eV for separating Na^+Cl^-. Last but not the least, primary ions can be formed during thermal desorption when the local temperature of matrix crystal raises rapidly during laser irradiation.[23] Complex and mixed pathways leading to primary ion formation likely happened in parallel during actual MALDI experiments.

Secondary ions are generated through charge (proton) transfer between matrix-matrix and matrix-analyte in the MALDI plume (gas phase). It is widely accepted that a high density plume is generated, where proton transfer through collision is possible.[16] In a typical MALDI experiment, a thermal equilibrium could be reached for ion-ion and ion-molecule interaction. For instance, a linear correlation between ion intensities of amino acids with their gas phase basicities has been reported, supporting the suspected equilibrium for proton transfer in gas phase.[24] Gas-phase based secondary ionization also explains the dominant observation of singly charged ions, protonated or deprotonated, in MALDI because large excess of electrons/protons in MALDI plume could easily neutralize most of multiply charged ions and only singly charged species could survive, the so-called “lucky survivor” theory.[25] The fact that the ionized species have been found

to present only a very small fraction of total desorbed molecules further corroborates its importance.[26] An interesting and useful phenomenon, called matrix suppression effect, has been well explained by the secondary ion reaction in plume where the matrix signal could be dramatically suppressed by the analyte signal at certain matrix to analyte ratio.[22,27] Analytes with high gas phase basicity would deplete protons from matrix ions and result in significant decrease of matrix signal. Similar suppression was also commonly observed between analytes with different gas phase basicity in the detection complex sample using MALDI MS.

Regardless exact roles played by matrix molecules during MALDI-MS remains elusive, their importance in enhancing desorption/ionization efficiency of analytes is without a doubt. However, the employment of matrix molecules raises several issues that may adversely impact MALDI applications**.** Dried-droplet method is a routinely used sample preparation method, where matrix and analyte are pre-mixed in an acidic aqueous or organic solution. The concentration of matrix is typically thousands of times higher than the concentration of analyte. The analyte/matrix solution is then loaded onto a MALDI target and co-crystallized together. Improved detection has been reported by using fast evaporation technique, where concentrated matrix solution in volatile organic solvent is loaded onto MALDI target first.[29-32] The analyte solution is then loaded and co-crystallized only with the top thin matrix layer, by which the analyte could be more concentrated in the top layer and much finer crystal could be generated. However, in MALDI experiment, the co-crystallization process is less controllable and often produces a non-uniform matrix film. Consequently, the signal intensity often varied significantly

from different spots of same sample, so called sweet spot phenomenon, by which the reproducibility and quantification capability of MALDI-MS could be significant impaired.[28] This results in a poor spot-to-spot reproducibility, an extended analysis time and a poor performance in quantitative analysis. A new class of matrix has been developed by mixing conventional MALDI matrix with one equivalent organic base, so called ionic matrix, which provides uniform crystal film and have been demonstrated as an attractive approach in quantitative analysis using MALDI MS.[6,33-36]

Another drawback of using matrix is the strong noise background caused by the matrix signal interferes with analyte at low mass range. Great efforts have been made to improve the MALDI detection of small molecules, where matrix additives (such as amino compounds and ammonium salts) are most commonly used approach for suppressing matrix signals.[37,38] Binary matrix by mixing two matrices of different basicity has been successfully applied in the detection of small bio-molecules.[39] Matrix has also been incorporated into silica so-gel to reduce the overlapping of matrix signal with low mass analyte. Matrix with higher molecular weight has been synthesized in order to shift the background noise in to higher mass range. Nevertheless the success is still very limited in the analysis of complex small molecules mixture such as metabolite.

1.2 Surface Assisted Laser Desorption Ionization (SALDI)

With today's mounting scientific interests in metabolite profiling to gain insight into functional biology and facilitate drug discovery and development, there are ever-increasing demands for new tools to effectively identify and quantify a broad range of

low-mass bioactive compounds. Surface-assisted laser desorption ionization mass spectrometry (SALDI-MS) is a matrix-free Laser Desorption/Ionization (LDI) technique, which was developed in parallel to well-known MALDI-MS. SALDI-MS was first demonstrated using a suspension of 30-nm cobalt particles in glycerol as the matrix, resulting in detection of proteins with masses greater than 20,000 Dalton.[40] Since then different materials have been tested as potential SALDI substrates, including graphite, carbon nanotubes, Au, Sn, Si, TiO_2 nanoparticles, etc.[41-45] In addition, the use nanoparticles with or without affinity capping agents could combine the sample purification, analyte enrichment and detection into one single step, which significantly simplifies the sample preparation and improves the detection.[42,46-48] The most successful SALDI medium was reported by Siuzdak et al. in which porous Si was used. The approach is also known as Desorption Ionization on Silicon Mass Spectrometry (DIOS-MS), which has been successfully employed in DIOS-MS to profile metabolites, identify active drug components, monitor organic synthetic products, and image small molecules in biological sample.[49-55] Figure 1.1 displays the scanning electron microscopy (SEM) image of porous silicon substrates, where typical pore size is about 50-200 nm. Inspired by the success of DIOS, liquid initiator compounds was developed and absorbed into porous silicon, by which significantly improvement in the MS performance was achieved in a means of detectable mass range and detection sensitivity. [56,57]

In SALDI, the analyte was directly loaded onto (or mixed with) the SALDI surface/particle without addition of organic matrix. Elimination of matrix molecules in SALDI-MS reduces background noises in low mass range and enables direct detection of

biologically significant small molecules (MW<500). The fact that most SALDI experiment could be easily performed on any conventional MALDI instrument makes it an attractive alternative to SIMS, another low-mass molecule detection method.

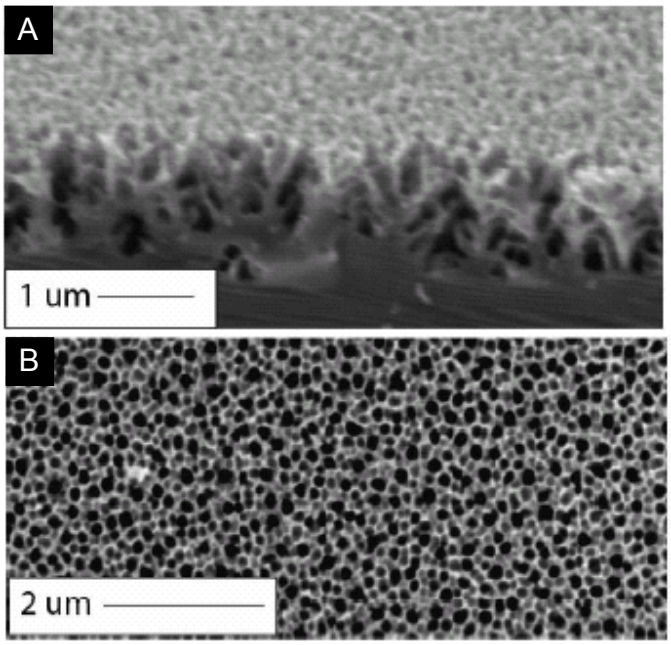

Figure 1.1. (A) Cross section and (B) top view of SEM image of porous silicon.

In general, the low limit of detection (LOD) of SALDI is in the low picomole to femtomole range, which is not as sensitive as MALDI. Lack of fundamental understanding in desorption and ionization processes of SALDI-MS is the primary cause behind this unsatisfied MS performance. Several groups have initiated the efforts and have proposed the contribution from substrate surface morphology, porosity or roughness to analyte ionization.[58-62] The surface chemical properties of porous substrates have also been investigated, which are found to affect ionization threshold but not on molecular fragmentation. Surface derivitization has been applied to change the wet-ability of a

surface to selectively concentrate target molecules, to extend substrate stability by surface passivation, and in some cases, to provide protons. Cleaner MS spectra have also been collected from modified surfaces with little background signals, thus better signal-to-background ratios obtained. However, continuous study, especially on quantitative characterization of the contribution from each physical and chemical parameters involved in DIOS/SALDI is imperial to make the matrix-free MS method competitive in small molecule detection.

1.3 Two-Dimensional Imaging Mass Spectrometry (IMS)

By providing both the chemical identities and the spatial organization of each component on a surface, chemical Imaging Mass Spectrometry (IMS) has created new research opportunities in many fields, such as microelectronics, materials science, and geochemistry.[63] For instance, the imaging secondary ion mass spectrometry (SIMS) has become a standard method in the elementary analysis of various surfaces since the commercialization of instrument in 1960's. New developments in mass spectrometry have dramatically extended the detectable mass range and have enabled the applications of IMS to clinic and pharmacological studies. Comparing to the optical imaging techniques commonly used in medical fields, IMS can track multiple species simultaneously and unveil unknown species involved in cellular communication without the requirement of tagging optically distinctive labels to the molecules of interest. Molecular specific information can be obtained and parent compound can be simultaneously monitored with its metabolites in comparison to the traditional radio-

autographic images. IMS is normally conducted in a point-to-point scanning fashion where a laser beam rasters across a sample surface with a MS spectrum collected at each point. Later reconstruction of the 2-D ion maps of the molecules of interest reveals their spatial distributions and the local concentrations.

MALDI-IMS has shown unique advantages in biomarker discovery and become the major player among IMS techniques since Capriole *et al.* pioneered the use of MALDI-IMS in 1996.[64-66] Most work in MS imaging has been focused on protein and peptide mapping in biological tissue samples to take advantages of effective analyte ionization using MALDI-MS, and also partially due to the limitation of MALDI-MS in small molecules detection as discussed in previous section. Great efforts have been made to improve analysis of small molecules with MALDI IMS. For example, with careful selection of appropriate matrix systems, pharmaceutically compounds with known structures have been profiled and imaged to study metabolite activity and drug efficacy.[67,68] Application of high resolving power MALDI FT-ICR instrument and tandem mass spectrometry MS/MS have also been demonstrated in small bio-molecules imaging.[69-71] However, success is still limited in imaging complex unknown small molecule mixtures, such as metabolites in biological sample.

From the practical aspect, sample preparation for IMS experiment, including the sectioning of biological sample and the deposition of matrix are the most challenge steps in MALDI-IMS. In general, a fresh tissue sample would be preferably quick frozen without any chemical treatment to avoid the potential redistribution, decomposition and denature of bio-component. Because the signal intensity of an analyte may vary with

different matrix crystal sizes or different matrix to analyte ratios, homogeneous matrix deposition is another critical factor to minimize distortion in analyte spatial distribution. Automated dropping and electro-spray are two commonly used matrix deposition approach, where potential redistribution of analyte is the major concern for all solution based methods.[72,73] Therefore, a solvent free approach, homogeneous matrix deposition through sublimation, has shown great potential in the IMS analysis of small molecule attracted great research interest by completely eliminates the possibility of redistribution.[74]

In recent years, serious research efforts from both industry and academia have been devoted to improving the imaging interface of MALDI-MS instruments. For instance, the equipped laser foot-print has been reduced to 20 μm with the precision of translation stage movement has reached <5 μm in routine operation. Sherrod *et. al.* have demonstrated the use of digital micromirror device (DMD) in imaging MALDI-MS that exhibits great potentials in improving imaging spatial resolution, laser homogeneity and throughput.[75] Imaging specific software for hardware control and data analysis have been developed for all major MALDI instruments since a huge number of spectra (tens of thousand) would be collected during imaging experiment.

Since its first demonstration in 1999, DIOS has opened the opportunities of MS-based small molecule profiling.[49] It has reportedly exhibited advantages in reducing background noise in the low mass region (m/z <500), which makes DIOS-based MS imaging a potentially attractive approach to detecting unknown small molecules that are not always addressable with the conventional MALDI-MS techniques. In comparison to

SIMS, direct adoption of the MALDI-MS interface in DIOS imaging reduces the instrument cost associated with SIMS imaging, especially when the use of cluster beams is required. Therefore, this dissertation is devoted to a systematic study and method development for DIOS-based IMS techniques.

1.4 Research Overview

This dissertation entails my effort in understanding the mechanism behind SALDI-MS technique and employing it as a complementary approach to MALDI-MS for 2-D small biomolecules mass spectrometry imaging. Chapter 1 describes the concept-proof investigation on using SALDI-MS to image mouse liver tissues and HEK 293 cancer cells. Basic imaging parameters, such as the laser footprint and the stage movement, on the quality of DIOS imaging, have also been studied.

To further improve the detection sensitivity, the fundamental understanding of ionization mechanism of SALDI is conducted. In Chapter 2, I have shown a systematic investigation of proton transferring pathways by using deuterated chemical reagents as a MS-distinctive tag and have semi-quantitatively assesses contributions from the local chemical environment surrounding analytes.

Based on the finding on the SALDI mechanism, a hybrid ionization approach has been developed by combing the strength of the conventional MALDI matrix and SALDI, termed as matrix enhanced surface assisted laser desorption ionization (ME-SALDI). Chapter 3 describes the demonstrated improved detection sensitivity with reduced matrix-

analyte interference and the improved imaging capability through analysis of mouse brain and heart sections.

To further improve the performance of ME-SALDI in imaging-based applications, the impact of vacuum stability of matrix was investigated in Chapter 4. Experimental conditions for sublimation deposition of several matrix molecules were systematically studied and the results rationalized. Improved vacuum stability has been reported for sublimation-coated ionic matrix. Employment of ionic matrix in ME-SALDI IMS has been successfully demonstrated and an improved MS detection of small molecules was observed in comparison to conventional MALDI using.

Last but not the least, Chapter 5, a new generation of meso-porous oxide substrate was developed as a novel ME-SALDI substrate through collaborations with Canon. Preliminary results show it exhibiting benefits of providing a superior storage stability, extended detectable mass range and robust substrate preparation.

1.5 References

(1) Dunn, J. D.; Allison, J. *J. Forensic Sci.* 2007, 52, 1205-1211.

(2) Ragoussis, J.; Elvidge, G. P.; Kaur, K.; Colella, S. *PLoS Genet* 2006, 2, e100.

(3) Nakazawa, T.; Yamaguchi, M.; Okamura, T.-A.; Ando, E.; Nishimura, O.; Tsunasawa, S. *Proteomics.* 2008, 8, 673-685.

(4) Rainer, M.; Najam-ul-Haq, M.; Huck, C. W.; Vallant, R. M.; Heigl, N.; Hahn, H.; Bakry, R.; Bonn, G. K. Recent Pat. *Nanotechnol*. 2007, 1, 113-119.

(5) Szpunar, J. *Analyst.* 2005, 130, 442-465.

(6) Zabet-Moghaddam, M.; Heinzle, E.; Lasaosa, M.; Tholey, A. *Anal. Bioanal. Chem.* 2006, 384, 215-224.

(7) Hummon, A. B.; Sweedler, J. V.; Corbin, R. W. TrAC *Trends Analyt. Chem.* 2003, 22, 515-521.

(8) Doig, M. V.; Higton, D. M. *Princ. Pract. Bioanal. (2nd Ed.)* 2008, 193-222.

(9) Uphoff, A.; Grotemeyer, *J. Eur. J. Mass Spectrom.* 2003, 9, 151-164.

(10) Vestal, M. L. *NATO ASI Ser., Ser. C* 1997, 504, 239-262.

(11) Peters, E. C.; Brock, A.; Phung, Q.; Fitchett, J.; Horn, D. M.; Ericson, C.; Ficarro, S. B.; Salomon, A. R. *Am. Pharm. Rev.* 2002, 5, 72, 74, 76, 78, 80-81.

(12) Jing, L.; Li, C.; Wong, R. L.; Kaplan, D. A.; Amster, I. J. *J. Am. Soc. Mass Spectrom.* 2008, 19, 76-81.

(13) van Kampen, J. J. A.; Burgers, P. C.; Gruters, R. A.; Osterhaus, A. D. M. E.; de Groot, R.; Luider, T. M.; Volmer, D. A. *Anal. Chem.* 2008, 80, 4969-4975.

(14) Gobey, J.; Cole, M.; Janiszewski, J.; Covey, T.; Chau, T.; Kovarik, P.; Corr, J. *Anal. Chem.* 2005, 77, 5643-5654.

(15) Yassin, F. H.; Marynick, D. S. *J. Phys. Chem. A* 2006, 110, 3820-3825.

(16) Knochenmuss, R. *Analyst* 2006, 131, 966-986.

(17) Johnson, R. E. *Inter. J.Mass Spectrom. Ion Proc.* 1994, 139, 25-38.

(18) Akos Bencsura, V. N. M. S. A. V. *Rapid Commun. Mass Spectrom.* 1997, 11, 679-682.

(19) Knochenmuss, R.; Zhigilei, L. V. *J.Phys. Chem. B* 2005, 109, 22947-22957.

(20) Dreisewerd, K. *Chem. Rev.* 2003, 103, 395-426.

(21) Ehring, H.; Karas, M.; Hillenkamp, F. *Org. Mass Spectrom.* 1992, 27, 472-480.

(22) Knochenmuss, R.; Dubois, F.; Dale, M. J.; Zenobi, R. *Rapid Commun. Mass Spectrom.* 1996, 10, 871-877.

(23) Fujii, T. *Eur. Mass Spectrom.* 1996, 2, 91-114.

(24) Kinsel, G. R.; Yao, D.; Yassin, F. H.; Marynick, D. S. *Eur. J. Mass Spectrom.* 2006, 12, 359-367.

(25) Michael Karas, M. G. J. S. *J. Mass Spectrom.* 2000, 35, 1-12.

(26) Curtis D. Mowry, M. V. J. *Rapid Commun. Mass Spectrom.* 1993, 7, 569-575.

(27) McCombie, G.; Knochenmuss, R. *Anal. Chem.* 2004, 76, 4990-4997.

(28) Tholey, A.; Heinzle, E. *Anal. Bioanal. Chem.* 2006, 386, 24-37.

(29) Koomen, J. M.; Russell, W. K.; Hettick, J. M.; Russell, D. H. *Anal. Chem.* 2000, 72, 3860-3866.

(30) Dai, Y.; Whittal, R. M.; Li, L. *Anal. Chem.* 1999, 71, 1087-1091.

(31) Nicola, A. J.; Gusev, A. I.; Proctor, A.; Jackson, E. K.; Hercules, D. M. *Rapid Commun. Mass Spectrom.* 1995, 9, 1164-1171.

(32) Vorm, O.; Roepstorff, P.; Mann, M. *Anal. Chem.* 1994, 66, 3281-3287.

(33) Samuel Carda-Broch, A. B. D. W. A. *Rapid Commun. Mass Spectrom.* 2003, 17, 553-560.

(34) Fukuyama, Y.; Nakaya, S.; Yamazaki, Y.; Tanaka, K. *Anal. Chem.* 2008, 80, 2171-2179.

(35) Laremore, T. N.; Zhang, F.; Linhardt, R. J. *Anal. Chem.* 2007, 79, 1604-1610.

(36) Armstrong, D. W.; Zhang, L.-K.; He, L.; Gross, M. L. *Anal. Chem.* 2001, 73, 3679-3686.

(37) Asara, J. M.; Allison, J. *Anal. Chem.* 1999, 71, 2866-2870.

(38) Kjellstrom, S.; Jensen, O. N. *Anal. Chem.* 2004, 76, 5109-5117.

(39) Guo, Z.; He, L. *Anal. Bioanal. Chem.* 2007, 387, 1939-1944.

(40) Koichi Tanaka, H. W., Yutaka Ido, Satoshi Akita, Yoshikazu Yoshida, Tamio Yoshida, T. Matsuo, *Rapid Commun. Mass Spectrom.* 1988, 2, 151-153.

(41) Su, C.-L.; Tseng, W.-L. *Anal. Chem.* 2007, 79, 1626-1633.

(42) Chen, C.-T.; Chen, Y.-C. *Anal. Chem.* 2005, 77, 5912-5919.

(43) Hoang, T. T.; Chen, Y.; May, S. W.; Browner, R. F. *Anal. Chem.* 2004, 76, 2062-2070.

(44) Kim, J.; Paek, K.; Kang, W. *Bullet. Kore. Chem. Soc.* 2002, 23, 315-319.

(45) Sunner, J.; Dratz, E.; Chen, Y.-C. *Anal. Chem.* 1995, 67, 4335-4342.

(46) Kailasa, S. K.; Kiran, K.; Wu, H.-F. *Anal. Chem.* 2008, 80, 9681-9688.

(47) Shrivas, K.; Wu, H.-F. *Rapid Commun. Mass Spectrom.* 2008, 22, 2863-2872.

(48) Chiu, T.-C.; Huang, L.-S.; Lin, P.-C.; Chen, Y.-C.; Chen, Y.-J.; Lin, C.-C.; Chang, H.-T. *Recent Pat. Nanotechnol.* 2007, 1, 99-111.

(49) Wei, J.; Buriak, J. M.; Siuzdak, G. *Nature* 1999, 399, 243-246.

(50) Go, E. P.; Uritboonthai, W.; Apon, J. V.; Trauger, S. A.; Nordstrom, A.; O'Maille, G.; Brittain, S. M.; Peters, E. C.; Siuzdak, G. *J. Proteo. Res.* 2007

(51) Okuno, S.; Wada, Y. *J. mass spectrum.* 2005, 40, 1000-1004.

(52) Xu, S.; Pan, C.; Hu, L.; Zhang, Y.; Guo, Z.; Li, X.; Zou, H. *Electrophoresis* 2004, 25, 3669-3676.

(53) Budimir, N.; Blais, J.-C.; Fournier, F.; Tabet, J.-C. *Rapid Commun. Mass Spectrom.* 2005, 20, 680-684.

(54) Deng, G.; Sanyal, G. *J. Pharm. Biomed. Anal.* 2006, 40, 528-538.

(55) Kraj, A.; Jarzebinska, J.; Gorecka-Drzazga, A.; Dziuban, J.; Silberring, J. *Rapid Commun. Mass Spectrom.* 2006, 20, 1969-1972.

(56) Northen, T. R.; Lee, J.-C.; Hoang, L.; Raymond, J.; Hwang, D.-R.; Yannone, S. M.; Wong, C.-H.; Siuzdak, G. *Proc. Nat. Acad. Sci.* 2008, 105, 3678-3683.

(57) Northen, T. R.; Yanes, O.; Northen, M. T.; Marrinucci, D.; Uritboonthai, W.; Apon, J.; Golledge, S. L.; Nordstrm, A.; Siuzdak, G. *Nature* 2007, 449, 1033-1036.

(58) Alimpiev, S.; Nikiforov, S.; Karavanskii, V.; Minton, T.; Sunner, J. *J. Chem. Phys.* 2001, 115, 1891-1901.

(59) Luo, G.; Chen, Y.; Siuzdak, G.; Vertes, A. *J. Chem. Phys. B* 2005, 109, 24450-24456.

(60) Chen, Y.; Vertes, A. *Anal. Chem.* 2006, 78, 5835-5844.

(61) Xiao, Y.; Retterer, S. T.; Thomas, D. K.; Tao, J.-Y.; He, L. *J. Phys. Chem.*

(62) Alimpiev, S. S.; Nikiforov, S. M.; Karavanski, V. A.; Grechnikov, A. A.; Sunner, *J. Proc.SPIE* 2004, 5506, 95-106.

(63) Chaurand, P.; Schwartz, S. A.; Caprioli, R. M. *Curr. Opin. Chem. Biol.* 2002, 6, 676-681.

(64) Chaurand, P.; Schwartz, S. A.; Billheimer, D.; Xu, B. J.; Crecelius, A.; Caprioli, R. M. *Anal. Chem.* 2004, 76, 1145-1155.

(65) Caldwell, R. L.; Caprioli, R. M. *Mol Cell Proteomics* 2005, 4, 394-401.

(66) Zhang, H.; Caprioli, R. M. *J Mass Spectrom* 1996, 31, 690-692.

(67) Rubakhin, S. S.; Greenough, W. T.; Sweedler, J. V. *Anal. Chem.* 2003, 75, 5374-5380.

(68) Chandra, S.; Tjarks, W.; Lorey, D. R., II; Barth, R. F. *J. Microsc.* 2007, 229, 92-103.

(69) Koestler, M.; Kirsch, D.; Hester, A.; Leisner, A.; Guenther, S.; Spengler, B. *Rapid Commun. Mass Spectrom.* 2008, 22, 3275-3285.

(70) Taban, I. M.; Altelaar, A. F. M.; van der Burgt, Y. E. M.; McDonnell, L. A.; Heeren, R. M. A.; Fuchser, J.; Baykut, G. *J. Am. Soc. Mass Spectrom.* 2007, 18, 145-151.

(71) Naito, Y.; Miyabayashi, K.; Tsujimoto, K. *Int. J. Mass Spectrom.* 2002, 221, 83-92.

(72) Aerni, H.-R.; Cornett, D. S.; Caprioli, R. M. *Anal. Chem.* 2006, 78, 827-834.

(73) Altelaar, A. F. M.; Van Minnen, J.; Jimenez, C. R.; Heeren, R. M. A.; Piersma, S. R. *Anal. Chem.* 2005, 77, 735-741.

(74) Hankin, J. A.; Barkley, R. M.; Murphy, R. C. *J. Am. Soc. Mass Spectrom.* 2007, 18, 1646-1652.

(75) Sherrod, S. D.; Castellana, E. T.; McLean, J. A.; Russell, D. H. *Int. J. Mass Spectrom.* 2007, 262, 256-262.

Chapter 2 Mass Spectrometry Imaging of Small Molecules Using DIOS-MS

2.1 Introduction

More and more small biomolecules (MW<500) have been found to play important roles in regulating cellular functions.[1-4] Development of novel tools to map the distribution of these molecules in cells is imperative to probe spatial organization of intercellular processes and investigate signal transduction pathways. In spite of great strides being made in optical imaging techniques to directly visualize selected biomolecules, the requirement in tagging optically distinctive labels to molecules of interest has limited their applications in unveiling unknown species involved in cellular communication and in tracking multiple species (>10) simultaneously. In this regard, mass spectrometry (MS) is an ideal tool that offers highly specific structural information to discover unknown molecules involved in bioprocesses and provides a multiplexing capability to monitor concurrent molecular fluctuations in complex biological systems. Indeed, growing academic and commercial interest has been evident in the development of two dimensional MS imaging.[5-11]

Caprioli *et al.* have pioneered the use of matrix-assisted laser desorption/ionization (MALDI) MS imaging in biomarker discovery.[12-14] It is normally conducted in a point-to-point scanning fashion where a laser beam rasters across a sample surface with a MS spectrum collected at each point. Later reconstruction of the 2-D ion maps of the molecules of interest reveals their spatial distributions and the local concentrations. Most work in MS imaging has been focused on protein and peptide

mapping in biological tissue samples to take advantages of effective analyte ionization in MALDI-MS. With the careful selection of appropriate matrix systems, pharmaceutically important small molecules of known structures have also been profiled in a similar fashion to study metabolite activity and drug efficacy at the molecular level by the same group.[7, 15] Various groups have since joined the efforts to further exploit the applications of MALDI-MS imaging in low-mass molecule studies. For example, Takach *et al.* have successfully identified the dosed drug and metabolites in rat tissue sections that accompanied with an increase of phospholipids after the treatment.[16] Atkinson *et al.* have studied lipid variations between tumor cells and liver tissues and have validated the results with conventional histology (H&E) staining.[17] In parallel to MALDI-MS, another MS technique, secondary ion MS (SIMS), has been well-demonstrated in mapping of small molecules and atomic ions as well. By electromagnetically focusing a high energy ion beam to a smaller foot-point, SIMS exhibits a better imaging resolution than MALDI-MS and has allowed detailed investigations of local chemical conditions at a subcellular level.[10, 18-21] The recent uses of cluster ion beams have further improved its performance in larger molecule detection (MW>1000), as well as in 3-D depth profiling of active drug components.[22-26] The third MS imaging method, matrix-enhanced SIMS, combines the better ionization efficiency in the presence of a matrix and a smaller foot-print of an ion beam; it has enabled larger molecule detection (up to 2500 Da) without the use of expensive cluster ion beams and has provided better imaging resolution than MALDI-MS.[27, 28] Other emerging 2-D MS imaging techniques include Desorption ElectroSpray Ionization (DESI) and Surface Sampling Probe Electrospray ionization MS (SP/ES-MS)

that have also started to attract attention.[11, 29, 30]

In this section, I report the employment of a laser beam-based MS imaging concept using Desorption/Ionization on Silicon (DIOS) as the MS ionization source. Since its first demonstration in 1999, DIOS has opened the opportunities of MS-based small molecule profiling.[31-33] It has reportedly exhibited advantages in reducing background noise in the low mass region (MW <500), which makes DIOS-based MS imaging a potentially attractive approach to detecting unknown small molecules that are not always addressable with the conventional MALDI-MS techniques.[31, 34-38] The elimination of the matrix addition step in DIOS further circumvents the potential problem of analyte dissolvation, which has been the most challenging step during sample preparation in MALDI-MS and ME-SIMS imaging. In comparison to SIMS, direct adoption of the MALDI-MS interface in DIOS imaging reduces the instrument cost associated with SIMS imaging, especially when the use of cluster beams is required. This report details our study of the imaging parameters, such as the laser footprint and the stage movement, on the quality of DIOS imaging. The concept-proof imaging of mouse liver tissues and HEK 293 cancer cells on a DIOS substrate is conducted as well.

2.2 Experimental Section

Materials Antimony-doped (100) single-crystalline silicon wafers at 0.005-0.02 Ω/cm were purchased from Silicon Sense, Inc. (Nashua, NH), and stored under vacuum upon use. 1,2-Dipalmitoyl-sn-glycero-3-phosphocholine (DPPC) was purchased from Avanti Polar Lipids, Inc. (Alabaster, AL). des-Arg-bradykinin, reserpine,

dodecyltrimethylammonium chloride (DTMA), and propidium iodide (PI) were purchased from Sigma Aldrich (St. Louis, MO). Human embryonic kidney (HEK) 293 cells were received as a gift. The DER 736 Epoxy Resin mixture was purchased from Electron Microscopy Sciences (Hatfield, PA). The TEM reference copper grids were purchased from Ted Pella, Inc. (Redding, CA). Hydrofluoric acid (HF, 49%), H_2SO_4 and H_2O_2 (30%) were purchased from Fisher Scientific (Pittsburgh, PA). Ethanol (EtOH, CH_3CH_2OH) was purchased from Aaper Alcohol (Shelbyville, KY). DI H_2O of 18 MΩ (Millipore, PO) was used throughout the experiments.

DIOS Substrate Preparation. DIOS were prepared as previously described.[38] Briefly, the Si wafer was cut into squared chips at the size of approximately 1x1 cm^2 and dipped into 5% HF/EtOH solution for 1 min to remove the oxidized layer prior to etching. The surface was electrochemically etched in a 25% HF/EtOH solution for 1 min at a current density of 5 mA/cm^2, followed by long-term storage in EtOH. Prior to the MS applications, the DIOS substrates were dipped into 15% H_2O_2 for 1 min, followed by a 1-min dip in a 5% HF/EtOH solution to refresh the surface.

MS Instrument Parameters. An Applied Biosystems Voyager DE-STR MALDI-TOF mass spectrometer (Framingham, MA) was operated at an accelerating voltage of 20 kV in a linear mode. A 20-Hz N_2 laser was used, and the delay time was varied from 100-250 ns to achieve optimal MS performance. An adjustable pinhole was placed close to the laser entrance window to adjust the diameter of the laser beam. The laser radiant energy was adjusted by a neutral density filter wheel. The actual laser footprint, i.e. the beam size, was obtained by measuring the burn marks on the DIOS surface. The signal-

to-background ratio (S/B) of different ion peaks were calculated by the instrument manufacture.

In the tissue thickness studies, two standard solutions (a solution of 100 pmol/μL DTMA and 100 pmol/μL Angiotensin I and a mixture of 100 pmol/μL of reserpine and 200 pmol/μL of Bradykinin) were drop-coated onto the substrates coated with or without 50-nm thick mouse liver tissue samples. The typical laser fluxes of 44 μJ/mm^2 and 14 μJ/mm^2 were used for tissue-coated DIOS and direct pSi imaging in detection of DTMA, respectively; and fluxes of 119 μJ/mm^2 and 60 μJ/mm^2 were used in detection of reserpine/bradykinin on tissue-coated DIOS and direct PSi, respectively, to achieve the best S/B ratios of the targeting analytes. The irradiation energy indicated here was measured *outside* of the sample chamber using a FieldMax-P laser energy meter (Coherent Inc.). Six spectra were collected from each substrate, and five substrate replicates were studied. Relative standard deviation (RSD%) were calculated based on the absolute mass peak intensity of DTMA.

Mass Spectrometry Imaging To prepare the copper grid sample for MS imaging, a DIOS substrate was first dipped into a 300 pmol/μL DPPC/EtOH solution for 30 min. A copper grid (pitch width 450 μm; bar width 50 μm) was then placed atop the dried substrate, and stabilized by a double-sided tape on the edge. The Cu grid was imaged with a laser beam size of 25 μm in diameter.

Fixed mouse liver tissue was first embedded with DER 736 Epoxy Resin. Specifically, 6.3 g of DER 736 were mixed with 100 g ERL 4221, 26 g NSA and 0.4 g DMAE.[39] After filtration, the mouse tissue sample was placed in the polymer solution

and baked at an approximately 70°C for 8 hrs to allow the resin to solidify. A thin slice of the tissue cross sections (50 nm) was prepared by cutting the resin-coated tissues using a Leica UCT ultramicrotome and transferred onto a DIOS substrate. Another piece of 50-nm liver tissue was transferred to a flat Si wafer as the control sample. The mouse tissue samples were also imaged with a laser beam size of 25 μm in diameter. Electron and optical microscope imaging was also conducted on the slices from the same tissue sample.

HEK 293 cells were cultured in Dulbecco's modified Eagle's medium (DMEM, Sigma) supplemented with 10% fetal bovine serum (FBS, Sigma) and antibiotic. Exponentially growing HEK 293 cells were digested with trypsin and seeded onto the DIOS substrates that were placed at the bottoms of a 6-well plate. After 24 h of culturing, the cells were washed with phosphate buffered saline (PBS) and fixed with 70% EtOH for MS analysis. The staining of the cell nucleus with PI was conducted by incubating cells with 300 nM PI solution for 30 min, followed by rinsing with EtOH to remove any nonspecifically adsorbed dye molecules. The HEK 293 cells were imaged using a 15-μm laser beam size.

All MS spectra in this study were collected in an automatic MS control mode and five laser shots were averaged to yield one accumulated spectrum at each location. Due to hardware limitation, most MS spectra were collected with a narrow mass window of Δmass = 50 amu. Mass spectra data were extracted using in-house developed software and imported in an excel spreadsheet. The reconstruction of the 2-D MS ion maps were conducted by manually plotting the MS intensity of the ions of certain *m/z* values as a

function of their corresponding x-y coordination using Origin 6.0 (Microcal Software, Inc.).

The bright-field images of the mouse liver tissue and the HEK 293 cells on the DIOS substrates were collected using a Leica DMRX light microscope in a reflection mode combined with a Donpisha XC-003P CCD camera. Fluorescence images were collected with a Carl Zeiss AxioVert 35 microscope combined with a Nikon Dxm1200 digital camera. A fluorescent filter set with bandpasses at 470±40nm for excitation and 525±50nm for emission was used in the measurements.

2.3 Result and Discussion

Scheme 2.1. Schematic Drawing of 2-D DIOS Imaging.

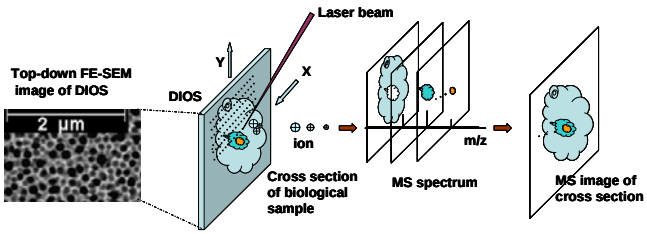

In DIOS imaging, the laser beam rasters across the DIOS surface with a MS profile generated at every sampling point. An ion map of each analyte is reconstructed afterwards to illustrate its spatial distribution (Scheme 2.1). By eliminating the matrix-induced analyte diffusion and the physical size of MALDI matrix crystals, the resolving power of the 2-D DIOS imaging should be a simple convolution of the laser beam size and the movement consistency of the x-y translational sample stage. An understanding on how the change in the laser beam size and the stage movement affects the quality of

MS spectra collected therefore is critical in attaining accurate reconstruction of ion distribution on a surface.

Laser Footprint in DIOS Imaging

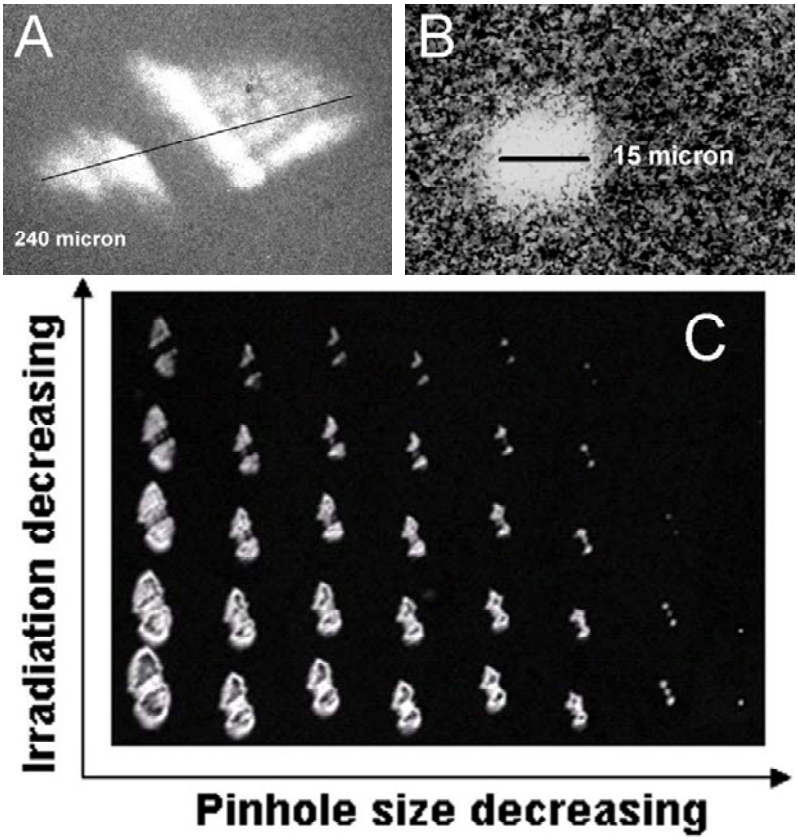

Figure 2.1. Optical microscopic images of laser footprint measurements: (A) a laser spot size of 250 μm in diameter; (B) a laser spot size reduced to 15 μm in diameter; and (C) a plot of laser spot sizes as a function of laser radiation energy and the pinhole open sizes. Panel B was the zoom-in of the smallest spot in C.

A commercial MALDI instrument equipped with an inexpensive N_2 pulse laser often has a beam diameter of several hundreds of microns. It is a common practice to reduce the laser beam size using an iris in order to tune the diameter of the laser beam and distinguish the chemical information present in the specimen in greater details. The actual size of the laser beam on the DIOS surface was measured as the diameter of the

burn marks left behind when the porous Si surface slightly melted upon heating (Figure 2.1). When the pinhole was opened to its fullest extent, an ellipsoidal shaped burning spot was observed on the surface. The breakage of the laser spot in the middle was due to the presence of the ion-extraction grid close to the DIOS surface that partially blocked the laser beam. Reducing the pinhole size by physically blocking the incoming laser beam using an iris, the size of the laser footprint reaching the substrate became smaller and smaller, until a perfectly circular shaped laser spot was realized, mirroring the shape of the pinhole aperture. As shown in Figure 2.1B, the laser beam size was reducible to 15 μm, the same length scale of a typical mammalian cell. Further reduction in the laser beam size could be achieved by improving the initial laser beam quality with additional collimating lenses.[9]

It is important to note that the size of the burn mark varied with increasing laser irradiation energy (Figure 2.1C). In particular, an increasing laser irradiation slightly enlarged the mark diameter, despite the pinhole remained unchanged. This is attributed to the fact that a minimal temperature threshold needs to be reached on the DIOS surface in order to leave the burn mark. Considering the lower energy fluence of the peripheral area of the laser beam, it is not surprising that the visible laser footprint was slightly smaller than the actual one when the laser energy borderlined on the threshold. An increase in the irradiation power could easily elevate surface temperature, making the peripheral area visible. Therefore, consistent laser irradiation energy was applied during each imaging experiment in our subsequent imaging studies to eliminate any possible flocculation in the laser beam size. It is noted, however, a constant beam diameter size

was observed beyond certain laser energy, suggesting that at this point the pinhole aperture became the dominant size-controlling factor.

Sample Plate Movement in DIOS Imaging

In most MALDI or DIOS imaging experiments, the laser beam is pre-fixed at certain angle, whereas the sample plate is moved to different locations during scanning in a step-wise fashion. Therefore, the second important factor to the achievable spatial resolution in DIOS imaging is related to the plate movement, such as the smallest movable step and moving precision. Taking advantage of our capability of imprinting the laser footprint on the surface by melting porous Si locally, optical images showing the burn marks generated at each moving step were obtained to assess this experimental parameter. Figure 2.2 shows the movement of the sample stage at 30 and 20 μm/step with burn marks being generated by a 25 μm diameter laser beam. At 30 μm/step, DIOS imaging was intentionally carried out in an undersampling fashion to illustrate the subtle but nevertheless non-negligible variations in column-to-column and row-to-row spacing. This unsteady stage movement was mainly due to mechanic inconsistency of the translation stage. An approximately 8% error was calculated from Figure 2.2A. Considering reconstruction of 2-D MS images was built on the assumption of the well-preserved x-y scanning coordinates, this error inevitably comprised final MS imaging resolution. It is interesting to note that, although the inter-row or inter-column spacing was less consistent, the alignment inside the same row or column was relatively steady. Therefore it is possible to overcome this 8% moving error, if necessary, by generating an internal calibration line where the burn marks in the first scanning row and the first spot

of each row (i.e. the first column) were use to back-calculate the actual imaging coordinates.

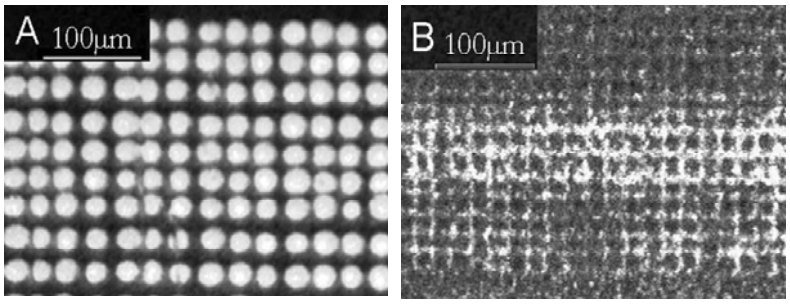

Figure 2.2. Optical images of patterned laser burn marks on the DIOS substrates with a stage moving step of (A) 30 μm and (B) 20 μm. The laser footprint was kept at 25 μm in diameter.

While most tissue MALDI-MS imaging was done in an undersampling fashion to achieve high throughput, an oversampling approach could be useful to improve spatial resolution beyond the resolving limit set by the minimal laser beam size and to better reflect the chemical distribution of analytes.[40] Figure 2.2B demonstrated a 20-μm scanning resolution with a laser beam size of 25 μm. The overlapping of the laser footsteps yielded a ~20 μm resolving map of the sample.[40] But in comparison to the previous 30 μm scanning steps, extra time was needed to map a sample of similar sizes. A judicious decision on the step size of stage movement should be made based on the needs of detection sensitivity, imaging throughput, and the movement precision.

Sample Thickness in DIOS Imaging

Both MALDI-MS and SIMS are "top-layer" imaging methods in which the laser or ion beams interact with the matrix applied on the top of the sample or with the sample top layer directly. In DIOS, however, the porous Si surface is where analyte desorption and ionization occurs; therefore it would be best suited to have analytes in direct contact

with the Si surface. This unique feature imposes a challenge in DIOS imaging where the biological sample of a certain thickness is placed atop the substrate; thus the surface to be imaged is not in direct contact with the DIOS surface.

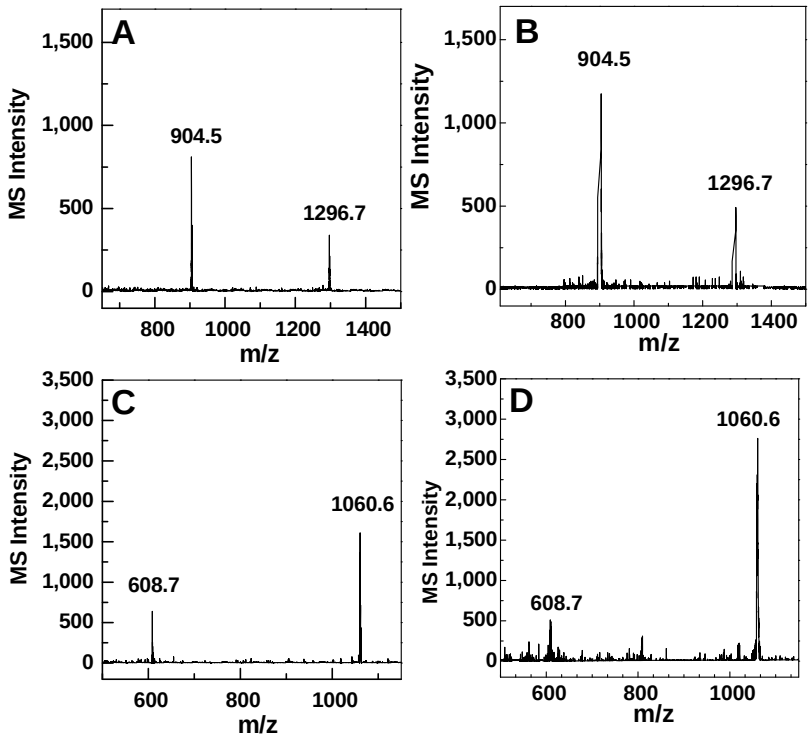

Figure 2.3. DIOS mass spectra of (A) 100 pmol/μL des-Arg-Bradykinin and Angiotensin I detected atop of 50-nm thick mouse liver tissue, (B) 100 pmol/μL des-Arg-Bradykinin and Angiotensin directly atop of the DIOS substrate, (C) 100 pmol/μL of reserpine and 200 pmol/μL of Bradykinin atop of 50-nm thick mouse liver tissue, and (D) 100 pmol/μL of reserpine and 200 pmol/μL of Bradykinin directly atop of the same DIOS substrate. The typical laser fluxes of 119 μJ/mm^2 and 60 μJ/mm^2 were used for tissue-coated DIOS and direct pSi imaging, respectively, to achieve the best S/N ratios of the targeting analytes. Other experimental conditions see the text.

Conceptually it is feasible to image biological samples through tissue blotting, a standard technique used in histological staining experiments. However, the difficulties in keeping the exact spatial relationship between molecules of interest during blotting and in ensuring transferring analytes of different kinds consistently make this approach

undesirable. A direct imaging of the top-layer of the sample is preferred, but the impacts of the natural thickness of any biological samples placed atop the DIOS surface on MS detection sensitivity needs to be investigated first.

DER 736 Epoxy Resin was used to support mouse liver tissues in our preliminary DIOS imaging following the well-established protocol.[39] In particular, the resin-embedded mouse liver tissues were sliced into 50 nm thin layers and were placed atop the DIOS substrates. Drops of the solutions containing different MS standards, including small peptides (such as bradykinin) and organic compounds (such as DTMA and reserpine), were loaded on the top surface of the tissue samples. No bradykinin, reserpine, or DTMA were detected from the tissue sample before analyte loading; thus they were chosen as the MS standards to avoid any ambiguity in later MS spectra interpretation. Figure 2.3 shows clear detection of all three analytes placed atop 50 nm tissue samples versus directly deposited on the DIOS surfaces. Higher absolute ion currents for the analytes were observed from the uncoated DIOS surface, but comparable S/B ratios (S/B = 8064 vs S/B = 7194 from Figure 2.3, parts A and B, respectively) were calculated from both substrates, regardless of the presence of the tissue samples in

Table 1. Calculated Relative Standard Deviation (RSD%) of the Molecular Ion Peak of DTMA (100 pmol/μL, *m/z* = 228.3) Detected Atop DIOS or 50 nm Mouse Liver Tissue

intrasubstrate RSD%	substrate 1# %	substrate 2# %	substrate 3# %	substrate 4# %	substrate 5# %	av intrasubstrate RSD%	intersubstrate RSD%
DIOS	27	20	35	67	58	41	20
tissue	37	65	42	58	56	52	11

between or not, which confirmed the feasibility of direct DIOS imaging of the tissue top layer when the sample was reasonably thin. The intrasubstrate RSD% of the DTMA

peak intensity (m/z = 228.3) was calculated based on six spectra collected from the same DIOS substrate with or without 50 nm thick mouse liver tissue, and the intersubstrate RSD% values were calculated from five different substrates (Table 2.1). The RSD% values calculated from the tissue surface were similar to those from the DIOS surface, suggesting the negligible impact of thin biological layers on the reproducibility of MS measurements. Note that the DTMA solution was loaded on both surfaces in a drop-coating fashion; thus, the uneven solvent drying could partially contribute to the large intra-substrate RSD%. It is also interesting to note that a slightly better peak resolution was observed for those detected atop the tissue layer, although the cause is unknown. Further investigation is underway to quantitatively examine the impacts of tissue thickness in greater details. The possibilities of analyte detection with direct laser desorption/ionization (LDI) was eliminated by the control experiment in which no MS signals were observed when the same sample was placed atop a smooth Si wafer chip and investigated under the same laser fluence.

2-Dimensional DIOS Imaging

The concept-proof of DIOS imaging was first demonstrated in a reversed spectrometric image of a reference copper grid placed on top of a dipalmitoylphos-phatidylcholine (DPPC)-coated DIOS substrate. Phosphatidylcholine (PC) is one of the most abundant lipid molecules present in animal membranes and its inherent positive charge makes it an ideal MS target. Figure 2.4A shows a typical DIOS spectrum of DPPC with the Na^+ adduct of molecular ion peak at m/z=756.1 (**a**). The phosphoester bond broke easily during ionization, generating headgroup fragments at m/z=184.1

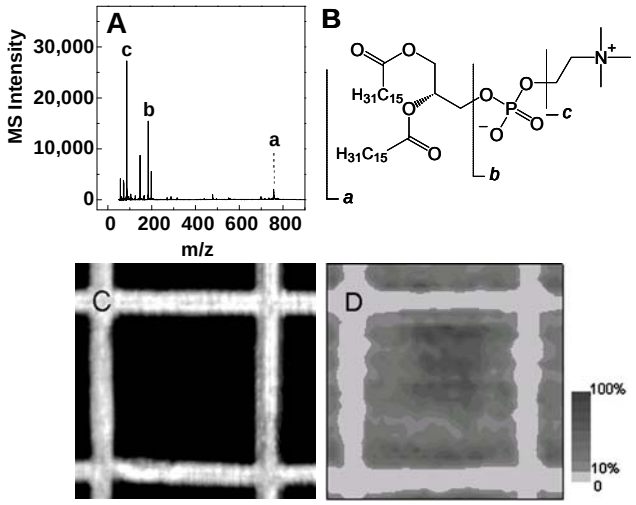

Figure 2.4. (A) A DIOS spectrum of DPPC, with the signature peaks labeled; (B) the chemical structure of DPPC and the corresponding major fragments; (C) an optical image of a reference copper grid on top of a DIOS substrate; and (D) the corresponding reconstructed ion imaging of the DPPC headgroup fragment **b**. The dark gray scale on the right indicates the corresponding ion intensities with the light gray of zero MS intensity. The DIOS spectra were collected at 25 μm stepwise in both X and Y directions with a 25-μm diameter laser beam. Other experimental conditions see the text.

($[C_5H_{15}NPO_4]^+$, **b**) and *m/z*=86.1 ($[C_5H_{12}N]^+$, **c**) as the dominant species (Figure 2.4B). In traditional MALDI-MS detection, the molecular ion peak of DPPC was often used, despite the presence of stronger MS signals from its headgroup fragments. This was mainly due to the presence of the MALDI matrix peaks in the *m/z* =50-300 region that often overshadowed these two fragment ions. In DIOS, however, the elimination of the matrix reduces the background signals; thus these fragment ion peaks were the logical choice to be closely monitored in PC detection for their better detection sensitivity. It also eliminates the needs to differentiate the PC molecules of different alkyl chains. Figure 2.4C shows an optical image of the reference copper grid placed on the DIOS substrate. One complete grid window was shown with 475-μm pitch and 50-μm bars. The MS imaging was conducted using a 25 μm-dia laser beam at a 25-μm scanning step. The reconstructed ion map of one of the DPPC head group ($[C_5H_{15}NPO_4]^+$, *m/z*=184.1)

was shown in Figure 2.4D. A good correlation to the optical image was evident with a clear-cut TEM grid frame. The rough edge of the reconstructed ion map was probably due to the inconsistency in the stage movement. The lower ion currents observed near the grid edges were from the shadowing effect of the grids since the laser irradiated the surface at a 45-degree angle.

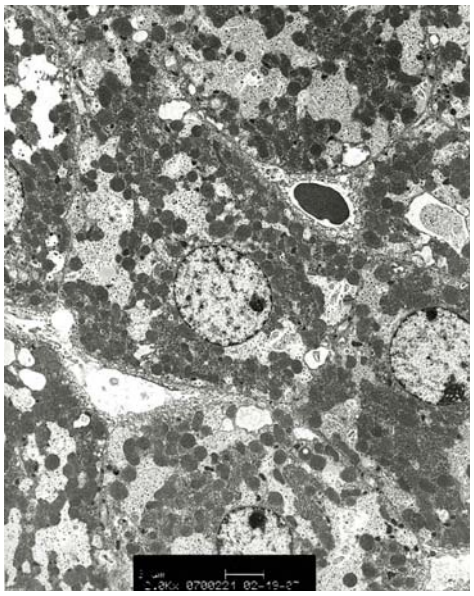

Figure 2.5. A typical TEM image of a stained mouse liver tissue section.

To examine the actual biological tissues in DIOS imaging, a piece of 50 nm thick DER 736 epoxy resin-fixed mouse liver tissue was placed atop a DIOS substrate. No apparent sample texture was visible due to the thin layer of the tissue sample. The tissue texture became visible when a thicker tissue sample was examined optically. The cellular components within the 50 nm tissue sample could also be visualized in electron microscope imaging (Figure 2.5). A typical mass spectrum of the mouse liver tissue showed numerous intense ions clearly observed. The mouse liver tissue of the same thickness on a smooth Si surface in the control experiment did not yield any detectable

signals. The chemical standard, DTMA (m/z = 228.3), was purposely deposited on the tissue top layer uniformly to examine the spot-to-spot reproducibility of MS measurements. Its steady detection across the sample suggested relatively consistent MS

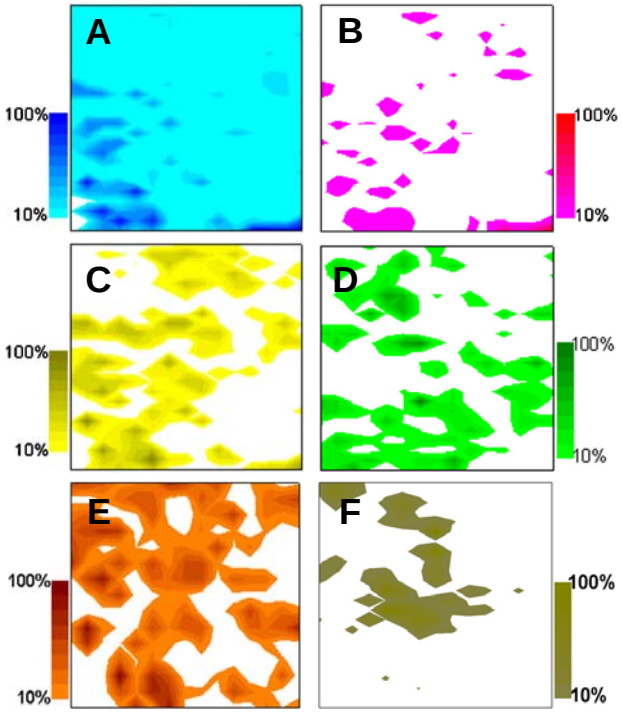

Figure 2.6. The reconstructed ion maps of (A) *m/z* = 228.3, (B) *m/z* = 184.1, (C) *m/z* = 218.6, (D) *m/z* = 189.2, (E) *m/z* = 203.1, and (F) *m/z* = 214.2.

ionization efficiency (Figure 2.6A). Several representative ions detected from the tissue sample were mapped (Figure 2.6B-F): the *m/z*=184.1 peak was likely from the headgroup of PC, one of the major animal membrane component (confirmed by the detection of the molecular ion peak at *m/z* = 758)[41]. The *m/z*=218.6 peak may be related to N-acetylserotonin but was not confirmed.[42] Additional ions at *m/z* = 189.2, 203.1, and 214.2 were reconstructed as well, but a tandem MS or a high-resolution mass spectrometer would be needed for structural identification. The non-overlapping distribution of these ions suggested the presence of chemical heterogeneity in the tissue

that was undetectable by the optical means. While further structural analysis is needed to identify these ions, the reconstructed ion maps directly confirmed the feasibility of 2-D DIOS imaging to profile the biological samples. Under current MS conditions, little background was observed from DER 736 epoxy resin (data not shown). Note that due to the hardware limitation on handling a large stream of data generated during high-resolution imaging, we have focused on collecting MS images with a narrow MS window of $\Delta m/z$ = 50 (e.g., m/z = 180-230). However, for each sample, several full MS spectra (m/z = 50-1000) were collected at random locations to verify PC detection by the presence of the molecular ion peaks and to monitor the presence of other highly abundant ions that may be of interest.

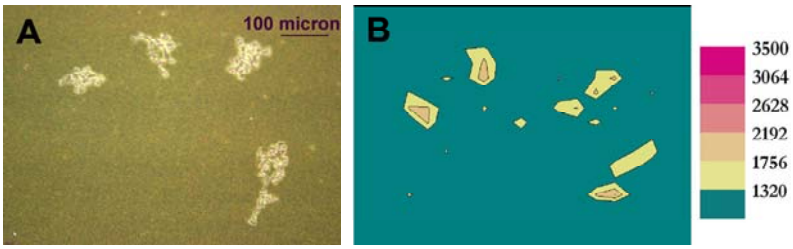

Figure 2.7. (A) An optical image of HEK 293 cells grown on the DIOS substrate; and (B) the corresponding MS ion maps of the PC headgroup (m/z =184.1). The DIOS spectra were collected at 15 μm stepwise in both X and Y directions with a 15-μm diameter laser beam. Other experimental conditions see the text.

DIOS-MS imaging was further demonstrated in direct detection of mammalian cells. Figure 2.7A shows the optical images of several HEK293 cells that were cultured directly on the DIOS substrate and simply fixed with 70% ethanol afterwards. The reconstruction of the ion maps of PC, one of the cell membrane major components, was shown in Figure 2.7B. A good correlation to the optical image was observed. The lack of detection from the cells of similar density but on a flat Si wafer surface confirmed that

the detection of the PC headgroup was indeed due to the presence of the active DIOS

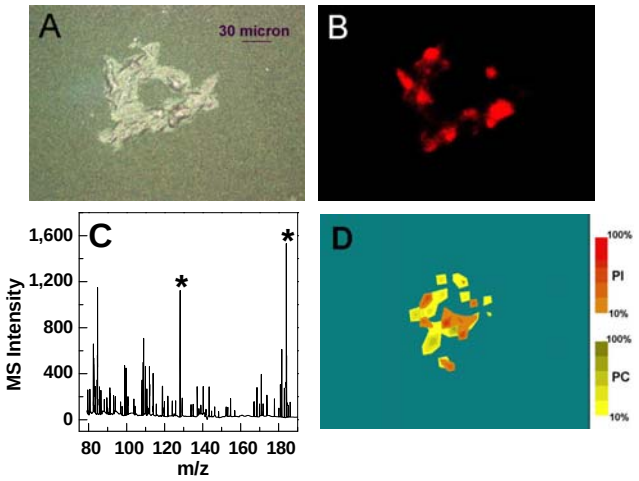

Figure 2.8. (A) An optical image of HEK 293 cells grown on the DIOS substrate; (B) the corresponding fluorescence image of the same cell cluster with nucleuses stained by PI; (C) a typical DIOS MS spectrum collected from HEK 293 cell detection; both PC and PI peaks were labeled with asterisks. (D) Corresponding ion maps of PC (yellow) and PI fragments (orange) overlaid. The DIOS spectra were collected at 15 µm stepwise in both X and Y directions with 15 µm diameter. Other experimental conditions see the text.

surface underneath. In a parallel experiment, the fixed HEK293 cells (Figure 2.8A) were incubated in a solution containing PI, a nucleic acid specific dye commonly used as a nucleus marker. As showing in Figure 2.8B, a fluorescence image of a cluster of HEK293 cells illustrated the exact staining of cell nucleuses. Figure 2.8C shows a typical DIOS mass spectrum, showing the detection of the cell membrane (PC, *m/z*=184.1) and the nucleuses (PI, *m/z*=128.1). The reconstructed ion maps were overlaid in Figure 2.8D. A reasonable correlation of the reconstructed ion map to the optical images was evident, with the ring-shaped cell cluster clear distinguishable.

2.4 Conclusion

In this report, we have concept-demonstrated the use of DIOS in 2-D MS bioimaging. The preliminary study has shown the ability to directly monitor spatial

distribution of small molecules at cellular levels using a simple/inexpensive MALDI-MS interface. By eliminating the matrix application step, the current imaging resolution is limited by the stage movement precision and, ultimately, the amount of the analyte molecules available for detection and the ionization efficiency of each analyte. Further research in sample preparation to improve imaging performance and clinical validation is needed before DIOS imaging could be employed in spatial profiling of biologically relevant small molecules.

2.5 References

(1) Rochfort, S. J. Nat. Prod. 2005, 68, 1813-1820.

(2) Rivkin, A.; Chou, T.-C.; Danishefsky, S. J. Angew. Chem. Int. Ed. 2005, 44, 2838-2850.

(3) Want, E. J.; O'Maille, G.; Smith, C. A.; Brandon, T. R.; Uritboonthai, W.; Qin, C.; Trauger, S. A.; Siuzdak, G. Anal. Chem. 2006, 78, 743-752.

(4) Smith, C. A.; O'Maille, G.; Want, E. J.; Qin, C.; Trauger, S. A.; Brandon, T. R.; Custodio, D. E.; Abagyan, R.; Siuzdak, G. Ther. Drug. Monit. 2005, 27, 747-751.

(5) Caldwell, R. L.; Caprioli, R. M. Mol. Cell. Proteomics 2005, 4, 394-401.

(6) Luxembourg, S. L.; Mize, T. H.; McDonnell, L. A.; Heeren, R. M. A. Anal. Chem. 2004, 76, 5339-5344.

(7) Rubakhin, S. S.; Greenough, W. T.; Sweedler, J. V. Anal. Chem. 2003, 75, 5374-5380.

(8) Chaurand, P.; Schwartz, S. A.; Caprioli, R. M. Curr. Opin. Chem. Biol. 2002, 6, 676-681.

(9) Spengler, B.; Hubert, M. J. Am. Soc. Mass. Spectrom. 2002, 13, 735-748.

(10) Ostrowski, S. G.; Van Bell, C. T.; Winograd, N.; Ewing, A. G. Science 2004, 305, 71-73.

(11) Van Berkel, G. J.; Ford, M. J.; Deibel, M. A. Anal. Chem. 2005, 77, 1207-1215.

(12) Chaurand, P.; Schwartz, S. A.; Billheimer, D.; Xu, B. J.; Crecelius, A.; Caprioli, R. M. Anal. Chem. 2004, 76, 1145-1155.

(13) Stoeckli, M.; Chaurand, P.; Hallahan, D. E.; Caprioli, R. M. Nat. Med. 2001, 7, 493-496.

(14) Caprioli, R. M.; Farmer, T. B.; Gile, J. Anal. Chem. 1997, 69, 4751-4760.

(15) Caldwell, R. L.; Caprioli, R. M. Mol. Cellular Proteom. 2005, 4, 394-401.

(16) Takach, E. J.; Zhu, Q.; Hsieh, F. Proc. 54th ASMS Conf. on Mass Spectrom. 2006, ThP18.

(17) Atkinson, S. J.; Majeed, A.; Bird, N.; Mangnall, D.; Burrell, M. M.; Clench, M. R. Proc. 54th ASMS Conf. on Mass Spectrom. 2006, ThP18.

(18) Lockyer, N. P.; Vickerman, J. C. Appl. Surf. Sci. 2004, 231-232, 377-384.

(19) Hindie, E.; Coulomb, B.; Beaupain, R.; Galle, P. Biol. Cell 1992, 74, 81-88.

(20) Sostarecz, A. G.; McQuaw, C. M.; Ewing, A. G.; Winograd, N. J. Am. Chem. Soc. 2004, 126, 13882-13883.

(21) Winograd, N. Anal. Chem. 2005, 77, 143A-149A.

(22) Wong, S. C. C.; Hill, R.; Blenkinsopp, P.; Lockyer, N. P.; Weibel, D. E.; Vickerman, J. C. Appl. Surf. Sci. 2003, 203-204, 219-222.

(23) Weibel, D. E.; Lockyer, N.; Vickerman, J. C. Appl. Surf. Sci. 2004, 231-232, 146-152.

(24) Crossman, L.; McHugh, N. A.; Hsieh, Y.; Korfmacher, W. A.; Chen, J. Rapid Commun. Mass Spectrom. 2006, 20, 284-290.

(25) Mahoney, C. M.; Roberson, S. V.; Gillen, G. Anal. Chem. 2004, 76, 3199-3207.

(26) Cheng, J.; Wucher, A.; Winograd, N. J. Phys. Chem. B 2006, 110, 8329-8336.

(27) McDonnell, L. A.; Piersma, S. R.; Altelaar, A. F. M.; Mize, T. H.; Luxembourg, S. L.; Verhaert, P. D. E. M.; Van Minnen, J.; Heeren, R. M. A. J. Mass Spectrom. 2005, 40, 160-168.

(28) Altelaar, A. F. M.; Van Minnen, J.; Jimenez, C. R.; Heeren, R. M. A.; Piersma, S. R. Anal. Chem. 2005, 77, 735-741.

(29) Takats, Z.; Wiseman, J. M.; Gologan, B.; Cooks, R. G. Science 2004, 306, 471-473.

(30) Leuthold, L. A.; Mandscheff, J.-F.; Fathi, M.; Giroud, C.; Augsburger, M.; Varesio, E.; Hopfgartner, G. Rapid Commun. Mass Spectrom. 2005, 20, 103-110.

(31) Wei, J.; Buriak, J. M.; Siuzdak, G. Nature 1999, 399, 243-246.

(32) Go, E. P.; Prenni, J. E.; Wei, J.; Jones, A.; Hall, S. C.; Witkowska, H. E.; Shen, Z.; Siuzdak, G. Anal. Chem. 2003, 75, 2504-2506.

(33) Shen, Z.; Thomas, J. J.; Averbuj, C.; Broo, K. M.; Engelhard, M.; Crowell, J. E.; Finn, M. G.; Siuzdak, G. Anal. Chem. 2001, 73, 612-619

(34) Tanaka, K.; Waki, H.; Ido, Y.; Akita, S.; Yoshida, Y.; Yohida, T. Rapid Commun. Mass Spectrom. 1988, 2, 151-153.

(35) McLean, J. A.; Stumpo, K. A.; Russell, D. H. J. Am. Chem. Soc. 2005, 127, 5304-5305.

(36) Cuiffi, J. D.; Hayes, D. J.; Fonash, S. J.; Brown, K. N.; Jones, A. D. Anal. Chem. 2001, 73, 1292-1295.

(37) Kruse, R. A.; Rubakhin, S. S.; Romanova, E. V.; Bohn, P. W.; Sweedler, J. V. J. Mass Spectrom. 2001, 36, 1317-1322.

(38) Finkel, N. H.; Prevo, B. G.; Velev, O. D.; He, L. Anal. Chem. 2005, 77, 1088-1095.

(39) http://www.cvm.ncsu.edu/research/laelom/Assets/resin_preparation.pdf.

(40) Jurchen, J. C.; Rubakhin, S. S.; Sweedler, J. V. J. Am. Soc. Mass. Spectrom. 2005, 16, 1654-1659.

(41) Brügger, B.; Erben, G.; Sandhoff, R.; Wieland, F. T.; Lehmann, W. D. Proc. Natl. Acad. Sci. USA, 1997, 94, 2339-2344.)

(42) Slominski, A.; Pisarchik, A.; Semak, I.; Sweatman, T.; Wortsman, J. Eur. J. Biochem. 2003, 270, 3335-3344.

Chapter 3 Quantitative Study of Solvent and Surface Effects on Analyte Ionization in Desorption Ionization on Silicon (DIOS) Mass Spectrometry

3.1 Introduction

Extensive research in metabolite profiling in recent years has revived interest in Desorption Ionization on Porous Silicon mass spectrometry (DIOS-MS). Elimination of matrix molecules in DIOS-MS reduces background noise in the low-mass range and enables direct detection of biologically significant small molecules.[1-4] It also overcomes matrix-induced analyte redistribution on a sample surface, which allows 2-dimensional imaging of tissue samples with good spatial accuracy.[5] Recent studies have shown that the local chemical properties of a DIOS substrate, including the residual solvent on the surface and the surface functional groups, are critical in analyte ionization.[6-9] Quantitative investigation of these factors, however, is still lacking. In this report, we semi-quantitatively assess attributions of various proton sources in DIOS-MS and the feasibility of improved MS detection of lipids and peptides by purposely optimizing experimental conditions.

3.2 Experimental Section

Materials Phosphorus-doped (100) single-crystalline silicon wafers at 0.005-0.02 Ω/cm were purchased from Silicon Sense, Inc. (Nashua, NH). 1,2-Dipalmitoyl-s*n*-glycero-3-phosphocholine (DPPC) was purchased from Avanti Polar Lipids, Inc. (Alabaster, AL). Triethylamine (TEA), pentanedione, and deuterium oxide (D_2O) were purchased from

Sigma Aldrich (St. Louis, MO). 3-Aminopropyltrimethoxysilane (APTMS) was purchased from Fluka (Milwaukee, WI). Acetone-d_6, toluene-d_8 and methanol-d_4 were purchased from Cambridge Isotope Laboratories (Andover, MA). Deuterium peroxide (D_2O_2, 30% in D_2O) was purchased from Icon Isotopes (Summit, NJ). Hydrofluoric acid (HF, 49%) and H_2O_2 (30%) were purchased from Fisher Scientific (Pittsburgh, PA). CH_3CH_2OH (EtOH) was purchased from Aaper Alcohol (Shelbyville, KY). DI H_2O of 18 MΩ (Millipore, PO) was used throughout the experiments.

DIOS Substrate Preparation DIOS substrates were prepared as previously described by dipping the wafer into a solution of 5% HF/EtOH for 1 min to remove the oxidized layer, followed by a 1.5-min anodic etching in 25% HF/EtOH at 5 mA/cm^2.[10, 11] Prior to MS experiments, the DIOS substrates were dipped in 5 %HF/EtOH to regenerate the H-terminated surface. For OH-terminated surfaces, the DIOS substrates were dipped in a solution of 15% H_2O_2/MeOH (or 15% D_2O_2/MeOH-d_4) for 30 min. For RNH_2-terminated surfaces, the same OH-terminated surfaces were refluxed in a solution of 10% APTMS/toluene under N_2 for 4 h. To remove residual solvent molecules, the DIOS or chemically modified DIOS substrates were dried under high vacuum overnight, unless specified otherwise.

DIOS-MS Measurements. An Applied Biosystems Voyager DE-STR MALDI-TOF mass spectrometer (Framingham, MA) was operated at an accelerating voltage of 20 kV in a linear mode. The delay time was varied from 100-250 ns to achieve optimal MS performance. For each data point 30 spectra were collected from different locations on

the same substrate and were accumulated to yield the final spectrum. Three replicate substrates were used in each experiment to calculate measurement variations.

TEA was dissolved in deuterated solvents at 20 pmol/μL. In most studies, after an overnight storage under high vacuum the DIOS or chemically modified DIOS substrates were immersed in the TEA solutions. The exception was made in the study of surface acidity where 20 pmol/μL of TEA/D_2O was drop-coated on the H-, OH-, and RNH_2-terminated DIOS substrates to minimize surface hydrolysis. DPPC was dissolved in 2,4-pentanedione/methanol (1:1) or methanol at 100 pmol/μL. DPPC in the 2,4-pentanedione/methanol solution was then drop-coated on a OH-terminated DIOS substrate and the one in the methanol solution was drop-coated on a freshly prepared H-terminated DIOS substrate, respectively.

Surface Characterization. Surfaces of H-terminated and OH-terminated DIOS substrates were quantitatively analyzed using a Physical Electronics TRIFT I TOF-SIMS instrument with a 25 keV Gallium primary beam (Eden Prairie, MN). For each experiment the spectra were collected from two different locations as replicates. All spectra were normalized by the dominant $[Si]^+$ peak.

3.3 Result and Discussion

Tracking hydrogen migration with a deuterium reagent has been well established in physicochemical studies.[12] Given in DIOS-MS most analytes are detected as protonated species, the same methodology was used in this report by deliberately replacing protons with deuterium in the local environment to isolate and quantify the

source(s) of analyte protonation. Triethylamine (TEA, $C_6H_{15}N$) was used as the MS model molecule for its high basicity and good thermal stability.

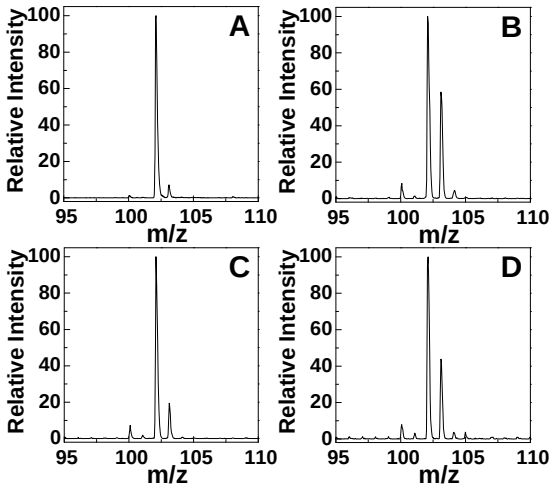

Figure 3.1. Mass spectra of TEA collected from (**A**) a DIOS substrate immersed in a TEA/H_2O solution, (**B**) a DIOS substrate immersed in a TEA/D_2O solution, (**C**) the same DIOS substrate re-loaded with 10 μL of ethanol, and (**D**) the same DIOS substrate reloaded with 10 μL of D_2O again. $[M+1]^+$ was the base peak at 100% RI. Detailed experimental conditions see

Figure 3.1A shows the natural isotopic distribution of TEA with the molecular ion, $[M+H]^+$, at m/z=102.13 and an isotopic peak, mainly from the presence of isotope ^{13}C, ^{15}N (0.37%) and ^{2}D (0.24%), at m/z=103.13 (relative intensity (RI) = 7.3±0.6%). In our studies, the RI of the isotopic mass peak at m/z=103.13 beyond 7.3% was used to estimate the incorporation of deuterium during protonation (i.e. $[M+D]^+$). The monoisotopic mass peak of protonated TEA was labeled as $[M+H]^+$ and was used as the base peak in intensity normalization. A small peak at m/z=100.11 was also noticed throughout the MS spectra collected and was assigned as $[M-H]^+$. Note that the absence of $[M-H]^-$ ions during negative-ion detection (data not shown) reduced the likelihood of proton exchange among analyte molecules themselves. The previous findings of the

aqueous phase basicity of an analyte being more important than the gas-phase basicity of the same analyte on analyte protonation suggested proton transferring in the condensed phase.[6] Consequently, this investigation focused on protonation between analytes and their surrounding molecules in the condensed phase, i.e. proton exchange with (a) the solvent where the analytes were dissolved in, (b) the solid surface where they were deposited on, and (c) other chemical species co-adsorbed on the surface. In addition, several assumptions have been made in the following discussions: a) the ionization cross-sections of the deuterated and non-deuterated species were considered relatively similar; b) in the concentration range studied here, the ion intensities were linearly dependent on the amount of the species in the system, i.e. the $[M+H]^+$ or $[M+D]^+$ peak intensities were proportional to the amount of $[M+H]^+$ or $[M+D]^+$ ions formed; and c) the absolute amount of protons donated from the same solvent was constant, regardless surface chemistry, and vice versa.

Analyte Protonation by Solvent

A freshly prepared DIOS substrate was dried under high vacuum overnight to remove solvent molecules adsorbed during substrate preparation and storage. After taking the substrate out of the vacuum chamber, it was immediately immersed in a 20 pmol/μL solution of TEA/D_2O for 3 h, followed by MS measurements. A MS peak of $[M+2]^+$ was clearly observed with a calculated RI of 54±7% (Figure 3.2B). It was significantly more intense than that from the natural isotopes, which confirmed direct analyte protonation from the solvent. Additional evidence of solvent contribution was obtained when 10 μL of ethanol was added to the same substrate to displace residual D_2O

molecules adsorbed on the surface. A visible decrease of the $[M+2]^+$ signal to a RI of 22±7% was observed (Figure 3.3C). Note that this $[M+2]^+$ peak was more intense than that from the natural isotope abundance (7.3%) due to incomplete displacement of D_2O molecules. The $[M+2]^+$ peak intensity was recovered by reloading the substrate with 10 μL of D_2O (Figure 3.4D).

In the condensed phase, residual solvent molecules left on the surface are known to directly participate in analyte protonation:[6, 12]

$$[\text{solvent}] + [\text{TEA}] \rightarrow [\text{solvent-H}]^- + [\text{TEA+H}]^+$$

Thus, the proton affinity (pKa) and the amount of the selected solvent in the condense phase are expected to play important roles in analyte protonation. The notion was supported by two experiments: in the first experiment TEA was dissolved in solvents of similar vapor pressures but different proton affinities. The measured $[M+2]^+$ peaks had the RIs of 54±7 % or 11±1 % for TEA in D_2O or d_8-toluene, respectively, consistent with water being more acidic than toluene (i.e. pK_a = 15.7 vs. 41) (Table 3.1).

Table 3.1. Calculated proton donating effectiveness of the solvent.

Solvent	pKa	Vapor Pressure[19] (25 ℃, mmHg)	MS RI of $[M+2]^+$	ΔRI = measured RI ─ 7.3%	Calculated Protonation Effectiveness
d_8-Toluene	41[16]	26	11±1%	4±1%	4±1%
D_2O	15.74[17]	23.74	54±7%	47±7%	32±5%
d_4-Methanol	15.54[17]	127.05	29.6±0.5%	22.3±0.8%	18.2±0.6%
d_6-Acetone	19.3[18]	229.52	14.8±0.3%	7.5±0.7%	7.0±0.6%

In the second set of experiments three pre-dried DIOS substrates were dipped in the TEA solutions where D_2O, d_4-methanol, and d_6-acetone were used as the solvent to study the

contribution of solvents of similar proton affinities but drastically different vapor pressures (i.e. different amounts of solvent residuals left on the surface). D_2O has the lowest vapor pressure due to strong hydrogen bonding; therefore the highest amount of solvent molecules was retained on the surface, and subsequently the most intense $[M+2]^+$ peak was observed (Table 3.1). The use of acetone with the highest vapor pressure among the three resulted in the smallest RI of the $[M+2]^+$ peak due to fast evaporation. Continuous removal of solvent molecules through constant pumping at $<2\times10^{-7}$ Torr led to reduction of RIs in all three solvents, in spite that the MS spectra were collected from different spots on the same substrate to avoid analyte depletion (Figure 3.2).

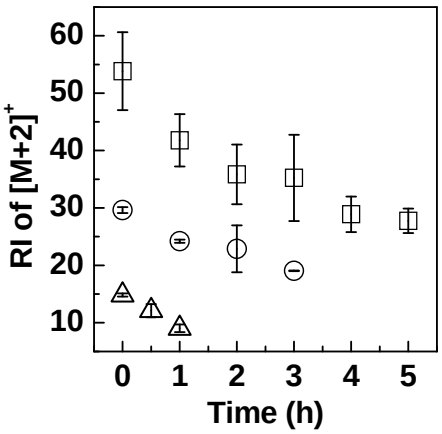

Figure 3.2. The calculated RIs of $[M+2]^+$ peaks plotted as a function of storage time of the substrates s under 2×10^{-7} Torr. The substrates were pretreated with 20 pmol/μL TEA in D_2O (□), methanol-d_4 (○) or acetone-d_6 (Δ). All mass spectra were collected with same instrument

The decreasing rate of $[M+D]^+$ intensities slowed down over time with fewer solvent molecules to be removed from the surface. The RIs of the $[M+D]^+$ peaks later became relatively stable and the plots leveled off when only a few layers of solvent molecules were left on the surface.

A semi-quantitative calculation of the proton donating effectiveness from the solvent was carried out by comparing the RI values of the $[M+2]^+$ peaks collected with and without the use of deuterated solvents. For example, the $[M+2]^+/[M+1]^+$ in Figure 3.1A and 3.1B can be written as the following:

$$\frac{\left[^{13}CC_5H_{15}N+H\right]^+}{\left[C_6H_{15}N+H\right]^+}\times 100\% = 7.3\pm 0.6\%$$

$$\frac{\left[C_6H_{15}N+D\right]^+ + \left[^{13}CC_5H_{15}N+H\right]^+}{\left[C_6H_{15}N+H\right]^+}\times 100\% = \frac{\left[C_6H_{15}N+D\right]^+}{\left[C_6H_{15}N+H\right]^+}\times 100\% + (7.3\pm 0.6)\% = 54\pm 7\%$$

$$\text{or: } \frac{\left[M+D_{solvent}\right]^+}{\left[M+H_{others}\right]^+}\times 100\% + (7.3\pm 0.6)\% = 54\pm 7\%$$

where $[M+D_{solvent}]^+$ refers to D_2O contribution and $[M+H_{others}]^+$ refers to contributions from other factors. Several assumptions were made in the following calculations: a) the ionization cross-sections of the deuterated and non-deuterated species were considered relatively similar; b) in the concentration range studied here, the ion intensities were linearly dependent on the amount of the species in the system, i.e. the $[M+H]^+$ or $[M+D]^+$ peak intensities were proportional to the amount of $[M+H]^+$ or $[M+D]^+$ ions formed; and c) the absolute amount of protons donated from the same solvent was constant, regardless surface chemistry, and vice versa. Step-by-step calculation of fraction of protonation from solvent (proton donating effectiveness) was then demonstrated as following.

Ions from triethyl amine (TEA, $C_6H_{16}N$) are theoretically possible if only one ^{13}C isotope and one H-D exchange event (-H+D) are considered:

m/z=100.11 ($[M-1]^+$): $[C_6H_{16}N\text{-}H]^+$

m/z=101.12([M]$^+$): $[C_6H_{16}N]^+$, $[C_6H_{15}DN\text{-}H]^+$, $[^{13}CC_5H_{16}N\text{-}H]^+$
m/z=102.13 ([M+1]$^+$): $[C_6H_{16}N+H]^+$, $[C_6H_{15}DN]^+$, $[^{13}CC_5H_{15}DN\text{-}H]^+$,
m/z=103.13 ([M+2]): $[C_6H_{16}N+D]^+$, $[^{13}CC_5H_{16}N+H]^+$, $[^{13}CC_5H_{15}DN]^+$
m/z=104.13 ([M+3]): $[^{13}CC_5H_{16}N+D]^+$

Contributions from ^{15}N (0.37%) and natural occurring ^2D (0.24%) are within MS measurement error; thus are neglected. Among these ion species, given that few $[C_6H_{16}N]^+$ ions are observed at m/z=101.12 due to high basicity of TEA, $[C_6H_{15}DN]^+$ and $[^{13}CC_5H_{15}DN]^+$are highly unlikely. $[C_6H_{15}DN\text{-}H]^+$ and $[^{13}CC_5H_{16}N\text{-}H]^+$ are negligible as well due to the lack of a MS peak at m/z=101.12. The small $[C_6H_{16}N\text{-}H]^+$ makes the presence of $[C_6H_{15}DN\text{-}H]^+$ and $[^{13}CC_5H_{15}DN\text{-}H]^+$ less likely, too. Together, only these ion species are considered during our calculations:

m/z=100.11 ([M-1]$^+$): $[C_6H_{16}N\text{-}H]^+$
m/z=102.13 ([M+1]$^+$): $[C_6H_{16}N+H]^+$,
m/z=103.13 ([M+2]$^+$): $[C_6H_{16}N+D]^+$ and $[^{13}CC_5H_{16}N+H]^+$
m/z=104.13 ([M+3]$^+$): $[^{13}CC_5H_{16}N+D]^+$

Define the contribution from deuterated solvent as:

$$\left[M+D_{solvent}\right]^+ = \left[C_6H_{15}N+D\right]^+ + \left[^{13}CC_5H_{15}N+D\right]^+ \quad (1)$$

and the contribution from all other factors as:

$$\left[M+H_{others}\right]^+ = \left[C_6H_{15}N+H\right]^+ + \left[^{13}CC_5H_{15}N+H\right]^+ \quad (2)$$

Mathematically

$$\frac{\left[C_6H_{15}N+D\right]^+}{\left[C_6H_{15}N+H\right]^+} = \frac{\left[^{13}CC_5H_{15}N+D\right]^+}{\left[^{13}CC_5H_{15}N+H\right]^+} = \frac{\left[C_6H_{15}N+D\right]^+ + \left[^{13}CC_5H_{15}N+D\right]^+}{\left[C_6H_{15}N+H\right]^+ + \left[^{13}CC_5H_{15}N+H\right]^+}$$

$$\text{thus } \frac{\left[M+D_{solvent}\right]^+}{\left[M+H_{others}\right]^+} = \frac{\left[C_6H_{15}N+D\right]^+}{\left[C_6H_{15}N+H\right]^+} \quad (3)$$

The natural isotopic distribution of TEA was measured as:

$$\frac{\left[^{13}CC_5H_{15}N+H\right]^+}{\left[C_6H_{15}N+H\right]^+} \times 100\% = \frac{\left[^{13}CC_5H_{15}N+D\right]^+}{\left[C_6H_{15}N+D\right]^+} \times 100\% = 7.3 \pm 0.6\% \quad (4)$$

The measured relative intensity (RI) of $[M+2]^+/[M+1]^+$ equals to:

$$\frac{[C_6H_{15}N+D]^+ + [^{13}CC_5H_{15}N+H]^+}{[C_6H_{15}N+H]^+} \times 100\% = \frac{[C_6H_{15}N+D]^+}{[C_6H_{15}N+H]^+} \times 100\% + (7.3 \pm 0.6)\% \quad (5)$$

Bring (3) to (5):

$$\frac{[M+D_{solvent}]^+}{[M+H_{others}]^+} \times 100\% + (7.3 \pm 0.6)\% = RI$$

$$\frac{[M+D_{solvent}]^+}{[M+H_{others}]^+} \times 100\% = RI - (7.3 \pm 0.6)\% = \Delta RI$$

Therefore the fraction of protonation from the solvent is calculated as (Table 3.1):

$$f_{solvent} = \frac{[M+D_{solvent}]^+}{[M+H_{others}]^+ + [M+D_{solvent}]^+} \times 100\% = \frac{\Delta RI}{1+\Delta RI}$$

Mathematic rearrangement of these equations shows that the fraction of the protons donated by water (i.e. proton donating effectiveness of the solvent) in overall analyte protonation was estimated to be 32±5 %. Applying the same calculation to TEA dissolved in methanol or acetone showed that the fraction of protons from the solvent were at ~18.2% and ~7.0%, respectively (Table 3.1). Note that these calculated numbers were slightly smaller than the actual values, mainly due to fast adsorption of H_2O molecules from the air during the short period of air-exposure when the substrate was taken out of the vacuum but before its immediate immersion in the TEA/D_2O solution. It is interesting to point out that the calculated proton donating effectiveness from different solvents of similar acidity was in linear reciprocal to their vapor pressures.

Additional consideration was given to potential indirect proton transferring to the analytes from solvent-induced surface modification because silicon is known to react with H_2O.[13-15] MS spectra were collected from the same DIOS surface at different time

points to monitor surface oxidation. If there was any oxidation, a slow but steady increase in the $[M+2]^+$ peak intensity would be expected from more and more surface groups being oxidized to Si-OD groups over time. No increase in $[M+2]^+/[M+1]^+$ was observed in our experiment, suggesting that this indirect proton transfer pathway played a minor role, if any, in analyte protonation.

Analyte Protonation by Porous Si Surface

Table 3.2. Calculated proton donating effectiveness of the surface.

	Surface	MS RI of $[M+2]^+$	ΔRI = measured RI - 7.3%)	Calculated Protonation Effectiveness of Surface
Dip coating	Si-OH DIOS	34±6%	27±6%	21±5%
	Si-OD DIOS	80±9%	73±9%	
Drop coating	Si-OH DIOS	17±6%	10±6%	N/A
	Si-H DIOS	33±9%	26±9%	N/A
	$Si-NH_2$ DIOS	70±11%	63±11%	N/A

Surface functional groups of DIOS substrates are decided by substrate preparation and storage.[11,20,21] For example, surface oxidation occurs immediately after a brief exposure of the substrate in air and has been found to be the culprit for performance degradation of DIOS-MS.[22] In our studies, two DIOS substrates were carefully oxidized in H_2O_2/MeOH or D_2O_2/MeOH-d_4. The use of deuterated peroxide introduced deuterium to the surface as in Si-OD, and possibly other deuterated functional groups through isotopic exchange. After drying both substrates under vacuum, they were dipped in a

TEA/D_2O solution before MS measurements. As expected, the calculated RI of the $[M+2]^+$ peak increased from 34±6% from the H_2O_2-treated surface to 80±9% from the D_2O_2-treated one, due to the deuterated silanol groups on the latter substrate.

Similarly, the fraction of protonation from the surface can be estimated by comparing the RI values of the $[M+2]^+$ peaks collected from the H_2O_2 or D_2O_2-oxidized substrates (Table 3.2). For example, $[M+2]^+/[M+1]^+$ in the previous experiment can be written as:

$$\frac{\left[M+D_{solvent}\right]^+}{\left[M+H_{others}\right]^+ + \left[M+H_{Si-OH}\right]^+} \times 100\% + (7.3 \pm 0.6)\% = 34 \pm 6\%$$

$$\text{and } \frac{\left[M+D_{solvent}\right]^+ + \left[M+D_{Si-OD}\right]^+}{\left[M+H_{others}\right]^+} \times 100\% + (7.3 \pm 0.6)\% = 80 \pm 9\%$$

where $[M+D_{solvent}]^+$ refers to D_2O contribution, $[M+H_{Si\text{-}OH}]^+$ or $[M+D_{Si\text{-}OD}]^+$ refers to the contribution of the oxidized –OH/OD groups, and $[M+H_{others}]^+$ refers to contribution from other factors, including residual H_2O, un-oxidized Si-H groups, and other co-adsorbents. Step-by-step calculation of proton donating effectiveness from surface was then demonstrated as following.

In D_2O_2 modified Si-OD DIOS, the contribution from D_2O and Si-OD as:

$$\left[M+D_{D_2O}\right]^+ + \left[M+D_{Si-OD}\right]^+ = \left[C_6H_{15}N+D\right]^+ + \left[^{13}CC_5H_{15}N+D\right]^+ \quad (6)$$

and the contribution from all other factors as:

$$\left[M+H_{others}\right]^+ = \left[C_6H_{15}N+H\right]^+ + \left[^{13}CC_5H_{15}N+H\right]^+ \quad (7)$$

In H_2O_2 modified Si-OH DIOS, the contribution from D_2O as:

$$\left[M+D_{D_2O}\right]^+ = \left[C_6H_{15}N+D\right]^+ + \left[^{13}CC_5H_{15}N+D\right]^+ \quad (8)$$

and the contribution from all other factors and Si-OH as:

$$\left[M+H_{others}\right]^{+}+\left[M+H_{Si-OH}\right]^{+}=\left[C_6H_{15}N+H\right]^{+}+\left[^{13}CC_5H_{15}N+H\right]^{+} \quad (9)$$

Assume a similar chemical derivatization efficiency was obtained using H_2O_2 or D_2O_2, i.e.

$$\left[M+H_{Si-OH}\right]^{+}=\left[M+D_{Si-OD}\right]^{+} \quad (10)$$

and the same donating efficiency from the solvent D_2O on both surfaces,

Similar to equation (5), the measured relative intensity (RI) of $[M+2]^+/[M+1]^+$ equals to:

$$\frac{\left[C_6H_{15}N+D\right]^{+}+\left[^{13}CC_5H_{15}N+H\right]^{+}}{\left[C_6H_{15}N+H\right]^{+}}\times 100\%=\frac{\left[C_6H_{15}N+D\right]^{+}}{\left[C_6H_{15}N+H\right]^{+}}\times 100\%+(7.3\pm 0.6)\%$$

Therefore, for D_2O_2 modified Si-OD DIOS:

$$\begin{aligned}&\frac{\left[C_6H_{15}N+D\right]^{+}+\left[^{13}CC_5H_{15}N+H\right]^{+}}{\left[C_6H_{15}N+H\right]^{+}}\times 100\%\\&=\frac{\left[M+D_{D_2O}\right]^{+}+\left[M+D_{Si-OD}\right]^{+}}{\left[M+H_{others}\right]^{+}}\times 100\%+(7.3\pm 0.6)\%=RI_D\end{aligned} \quad (11)$$

$$\text{thus: } \frac{\left[M+D_{D_2O}\right]^{+}+\left[M+D_{Si-OD}\right]^{+}}{\left[M+H_{others}\right]^{+}}\times 100\%=RI_D-(7.3\pm 0.6)\%=\Delta RI_D \quad (12)$$

Similarly, for H_2O_2 modified Si-OH DIOS:

$$\begin{aligned}&\frac{\left[C_6H_{15}N+D\right]^{+}+\left[^{13}CC_5H_{15}N+H\right]^{+}}{\left[C_6H_{15}N+H\right]^{+}}\times 100\%\\&=\frac{\left[M+D_{D_2O}\right]^{+}}{\left[M+H_{others}\right]^{+}+\left[M+H_{Si-OH}\right]^{+}}\times 100\%+(7.3\pm 0.6)\%=RI_H\end{aligned} \quad (13)$$

$$\text{thus: } \frac{\left[M+D_{D_2O}\right]^{+}}{\left[M+H_{others}\right]^{+}+\left[M+H_{Si-OH}\right]^{+}}\times 100\%=RI_H-(7.3\pm 0.6)\%=\Delta RI_H \quad (14)$$

Mathematic rearrangement shows:

$$\left[M+D_{D_2O}\right]^{+}=\Delta RI_H\times\left[M+H_{others}\right]^{+}+\Delta RI_H\times\left[M+H_{Si-OH}\right]^{+} \quad (15)$$

$$\left[M+D_{D_2O}\right]^{+}+\left[M+D_{Si-OD}\right]^{+}=\Delta RI_D\times\left[M+H_{others}\right]^{+} \quad (16)$$

(16) – (15) renders:

$$\left[M+D_{Si-OD}\right]^{+}=(\Delta RI_D-\Delta RI_H)\times\left[M+H_{others}\right]^{+}-\Delta RI_H\times\left[M+H_{Si-OH}\right]^{+} \quad (17)$$

Bring (10) to (17):

$$\left[M + D_{Si-OD}\right]^+ = \frac{\Delta RI_D - \Delta RI_H}{1 + \Delta RI_H} \times \left[M + H_{others}\right]^+ \quad (18)$$

$$\left[M + D_{D_2O}\right]^+ = \frac{\Delta RI_H + \Delta RI_H \times \Delta RI_D}{1 + \Delta RI_H} \times \left[M + H_{others}\right]^+ \quad (19)$$

Therefore the fraction of protonation from D_2O and Si-OD/H can be calculated as (Table 3.2):

$$f_{D_2O} = \frac{\left[M + D_{D_2O}\right]^+}{\left[M + H_{others}\right]^+ + \left[M + D_{D_2O}\right]^+ + \left[M + D_{Si-OD}\right]^+} \times 100\% = \frac{\Delta RI_H + \Delta RI_H \times \Delta RI_D}{1 + \Delta RI_H + \Delta RI_D + \Delta RI_D \times \Delta RI_H}$$

Mathematic rearrangement of the equations shows that the calculated fraction of protonation from SiOD/H was 21±5 % and the solvent contribution was reduced to 21±4 %.

The pKa value of a surface functional group is also found to affect its ability of donating protons in the condensed phase. A set of porous silicon substrates were modified to introduce three different functional groups: Si-RNH_2, Si-H, and Si-OH with increasing acidity. While a 100% surface conversion to any particular surface functional group was unlikely, a more acidic surface was expected from the one with a higher density of Si-OH, and a more basic one for the substrate of Si-RNH_2 groups that competed with the analyte for protons. D_2O was used as an internal calibrator to evaluate the relative contribution of various surface functional groups because the proton-donating capability of a solvent was found to be largely decided by the chemical nature of the solvent itself. As shown in Table 3, the relative intensities of the $[M+2]^+$ peaks increase as the acidity of the corresponding surface function group decreases, correlated well with the reduced protonation contribution of the surface (i.e. formation of $[M+H]^+$). However, quantitative assessment of surface contribution was not feasible due to the lack of

deuterated surface modification reagents. Note that in this set of experiments, the modified porous silicon substrates were drop-coated with a 20 pmol/uL solution of TEA/D_2O to minimize surface hydrolysis by reducing incubation time. As the result, the amount of the residual solvent, i.e. D_2O, was much less than what was observed in the previous experiments. Consequently, a significant decrease in the $[M+2]^+$ ion intensity was observed from the hydroxyl-modified surface, comparing to Table 3.2.

Analyte Protonation by Other Environmental Factors

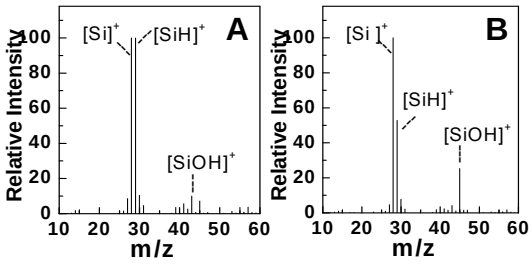

Figure 3.3. SIMS mass spectra of (A) a HF-rinsed DIOS substrate and (B) a H_2O_2-modified DIOS substrate. The relative intensity of $[Si\text{-}OH]^+$ was increased from 9±2% to 23±2% after oxidation. The relative intensity of Si-H only reduced to 51±2 % from 97±2 %, suggesting that more than 50% surface functional groups were not accessible.

Despite of the efforts to replace hydrogen in the solvent and on the surface with deuterium, a strong $[M+H]^+$ peak was observed throughout the MS spectra collected. The residual Si-H groups on the porous Si surface were believed to be the main culprit to the remaining $[M+H]^+$ peak. The speculation was supported by surface characterization using secondary ion mass spectrometry (SIMS), in which the relative intensity of $[Si\text{-}OH]^+$ was found to increase from 9±2 % to 23±2 % after oxidation. Meanwhile, the relative intensity of Si-H only reduced to 51±2 % from the previous 97±2 % (Figure 3.3). Although a quantitative estimation of the absolute conversion percentage of the surface functional groups was difficult due to the varying ionization probabilities of

$[SiOH]^+/[SiOD]^+$, $[SiH]^+$ and $[Si]^+$, this experimental observation suggests that a significant amount of surface functional groups was not accessible during surface oxidation. Additional proton source(s) in the analyte local chemical environment in the forms of adsorbed hydrocarbons and H_2O vapor in the sample chamber were also attributed to the remaining presence of $[M+H]^+$, grouped together in this report as the "other" factors.

Improvement in DIOS-MS performance

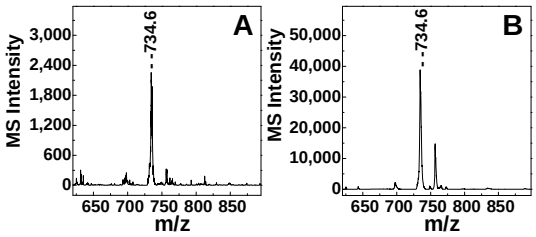

Figure 3.4. Mass spectra of (**A**) a DPPC/Methanol solution drop-coated on an unmodified DIOS substrate, and (**B**) a DPPC/2,4-pentadione/methanol mixture at the same concentration drop-coated on an oxidized DIOS substrate. The detected analyte were labeled by their molecular ion peaks.

The findings that analyte protonation is directly related to the properties of DIOS surface and the solvent suggest that DIOS-MS detection can be enhanced by purposely modifying the substrate surface with low-pKa functional groups and selecting solvents of low-pKa values and low vapor pressures. Figure 3.4 shows detection of dipalmitoylphosphatidyl- choline (DPPC) that was dissolved in 2,4-pentanedione/methanol and the mixture was drop-coated on an oxidized DIOS substrate. 2,4-Pentanedione was selected as the appropriate solvent for its low acidity, low vapor pressure and good bio-compatibility (pKa = 9.8, vapor pressure = 6 mmHg). In comparison, DPPC was dissolved in methanol at the same concentration and was loaded

on a control DIOS piece where the surface was freshly regenerated (i.e. Si-H-rich). A remarkable enhancement of 17 folds in the molecular ion intensity was obtained with the Si-OH/pentanedione treatment to that of the control experiment. Similar result was also observed in detection of des-Arg^1-bradykinin and angiotensin I (data not shown).

3.4 Conclusions

The local chemical environment of the analyte, including residual solvent and surface function groups, were identified as the major proton sources in DIOS-MS and their contributions were semi-quantified. The experimental conclusions allowed further optimization of DIOS-MS conditions with improve performance in lipid and peptide detection. It is important to note, however, that chemical modification of the Si surface changes not only the functional groups but also the physical properties of the porous surface. For example, moderate oxidation leads to the formation of acidic Si-OH groups that benefit analyte ionization. However, the formation of an over-oxidized silicon oxide layer slowed down thermal dissipation and reduces overall ionization efficiency. As a result, the degree of surface modification needs to be carefully monitored to achieve optimal MS results.

3.5 References

(1) Wei, J.; Buriak, J. M.; Siuzdak, G. Nature 1999, 399, 243-246.

(2) Deng, G.; Sanyal, G. J. Pharm. Biomed. Anal. 2006, 40, 528-538.

(3) Lee, J.-C.; Wu, C.-Y.; Apon, J. V.; Siuzdak, G.; Wong, C.-H. Angew. Chem. Int. Ed. 2006, 45, 2753-2757.

(4) Go, E. P.; Uritboonthai, W.; Apon, J. V.; Trauger, S. A.; Nordstrom, A.; O'Maille, G.; Brittain, S. M.; Peters, E. C.; Siuzdak, G., J. Proteome Res. 2007, 6; 1492-1499.

(5) Liu, Q.; Guo, Z.; He, L. Anal. Chem. 2007, 79, 3535-3541.

(6) Alimpiev, S.; Nikiforov, S.; Karavanskii, V.; Minton, T.; Sunner, J. J. Chem. Phys. 2001, 115, 1891-1901.

(7) Kruse, R. A.; Li, X.; Bohn, P. W.; Sweedler, J. V. Anal. Chem. 2001, 73, 3639-3645.

(8) Luo, G.; Chen, Y.; Siuzdak, G.; Vertes, A. J. Phys. Chem. B 2005, 109, 24450-24456.

(9) Tuomikoski, S.; Huikko, K.; Grigoras, K.; Oestman, P.; Kostiainen, R.; Baumann, M.; Abian, J.; Kotiaho, T.; Franssila, S. Lab Chip 2002, 2, 247-253.

(10) Finkel, N. H.; Prevo, B. G.; Velev, O. D.; He, L. Anal. Chem. 2005, 77, 1088-1095.

(11) Shen, Z.; Thomas, J. J.; Averbuj, C.; Broo, K. M.; Engelhard, M.; Crowell, J. E.; Finn, M. G.; Siuzdak, G. Anal. Chem. 2001, 73, 612-619.

(12) Wen, X.; Dagan, S.; Wysocki, V. H., Anal. Chem. 2007, 79, 434-444.

(13) Irene, E. A. J. Electrochem. Soc. 1978, 125, 1708-1714.

(14) Graef, D.; Grundner, M.; Schulz, R. J. Vac. Sci. Technol., A 1989, 7, 808-813.

(15) Graef, D.; Grunder, M.; Schulz, R.; Muehlhoff, L. J. Appl. Phys. 1990, 68, 5155-5161.

(16) Buncel, E.; Menon, B. C., Canadian J. Chem. 1976, 54, 3949-3954.

(17) Ballinger, P.; Long, F. A., Acid Ionization Constants of Alcohols. Ii. J. Am. Chem. Soc. 1960, 82, 795-798.

(18) Pearson, R. G.; Dillon, R. L., J. Am. Chem. Soc. 1953, 75, 2439-2443.

(19) http://www.sigmaaldrich.com/catalog/search/ProductDetail

(20) Trauger, S. A.; Go, E. P.; Shen, Z.; Apon, J. V.; Compton, B. J.; Bouvier, E. S. P.; Finn, M. G.; Siuzdak, G., Anal. Chem. 2004, 76, (15), 4484-4489.

(21) Gorecka-Drzazga, A.; Bargiel, S.; Walczak, R.; Dziuban, J. A.; Kraj, A.; Dylag, T.; Silberring, J. Sens. Actuators, B 2004, B103, 206-212.

(22) Lewis, W. G.; Shen, Z.; Finn, M. G.; Siuzdak, G. Int. J. Mass spectrom. 2003, 226, 107-116.

Chapter 4 Metabolite Imaging Using Matrix-Enhanced Surface-Assisted Laser Desorption Ionization Mass Spectrometry (ME-SALDI-MS)

4.1 Introduction

By providing both the chemical identities and the spatial distribution of hundreds of components in biological systems simultaneously without pre-tagging distinctive labels, Imaging Mass Spectrometry (IMS) has created new research opportunities in many fields[1-7]. However, regardless rapid developments in the field of IMS, several fundamental issues remain to be addressed. In particular, analyte ionization efficiency is in an urgent need for improvement, giving its importance in enhancing detection sensitivity of less-abundant bioactive species as the imaging footprint decreases[8].

Technology development leaps forward when two complementary methodologies are combined to overcome the inherent difficulties encountered by each one. It is especially true in mass spectrometry (MS) where hybrid approaches constantly change the landscape of the field. Indeed, in addition to numerous hyphened mass analyzers, hybrid mass ionization techniques, such as matrix-enhanced secondary ion mass spectrometry (ME-SIMS)[3, 9], desorption electrospray ionization (DESI)[10], electrospray-assisted laser desorption ionization (ELDI)[11], laser desorption atmospheric-pressure chemical ionization (LD-APCI)[12] and matrix assisted laser desorption electrospray ionization (MALD-ESI)[13], have together augmented the overall applicability of MS in solving increasingly complex biological problems. The concept of mixing solid photon-absorbing materials (metal nanoparticles and graphite particles, etc) with non-absorbing

liquid (such as glycerol derivative) has also been demonstrated for improved detectable upper mass limit where glycerol mainly served to improve mixing of analytes with suspended particles and to dissipate excess heating energy[14-17]. Alternatively, mixing the conventional solid MALDI matrix with a porous Si surface, the surface has served as a solid-phase extraction medium to concentrate selected analytes[18].

Adapting the similar concept but aiming to improve the ionization efficiency of *low-mass* species in a 2-D IMS format, we describe here the use of this hybrid ionization method, i.e. matrix-enhanced SALDI (ME-SALDI), that combines valuable attributes from both conventional MALDI and SALDI methods. In particular: (1) the introduction of the solid conventional MALDI matrix, such as CHCA, to SALDI is purposely designed to take advantage of its strong proton donating capability and to protect analyte from deconstructive overheating for enhancing the detection sensitivity, based on the previous findings that a proton-rich local environment is critical during SALDI[19, 20]; (2) the application of ME-SALDI in MS imaging is demonstrated for the first time that provides a complementary tool to widely-used MALDI IMS by addressing analytes in a different mass range that overlaps with traditional MALDI. Experimental results from ME-SALDI IMS show substantially improved MS performance over conventional MALDI and SALDI methods in small molecule detection, including reduced matrix interference and analyte fragmentation, expanded mass detection window to 10,000+ amu, and much improved analyte ionization efficiency in small-footprint, high-spatial resolution MS imaging.

4.2 Experimental Section

Materials. N-type Sb-doped (100) single-crystalline silicon wafers at 0.005-0.02 Ω/cm were purchased from Silicon Sense, Inc. (Nashua, NH), and stored under vacuum upon use. 1,2-Dimyristoyl-s*n*-glycero-3-phosphocholine (DMPC) was purchased from Avanti Polar Lipids, Inc. (Alabaster, AL). L-Histidine, caffeine, 2,5-dihydroxybenzoic acid (DHB), α-cyano-4-hydroxycinnamic acid (CHCA), and 37% formaldehyde solution were purchased from Sigma Aldrich (St. Louis, MO). Prednisone and methylene blue zinc chloride double salt were purchased from MP Biomedicals (Solon, OH). Hydrofluoric acid (HF, 49%), acetone and H_2O_2 (30%) were purchased from Fisher Scientific (Pittsburgh, PA). CH_3CH_2OH was purchased from Aaper Alcohol (Shelbyville, KY). DI H_2O of 18 MΩ (Millipore, PO) was used throughout the experiments. Insulin (bovine) and thioredoxin (E. coli) were purchased from Applied Biosystems (Framingham, MA). CD-1 female mouse heart tissues were fixed with 37% formaldehyde solution prior to the use. Mouse brain tissues were fresh frozen and stored at -80 °C upon use.

Porous Si Substrate Preparation Porous Si substrates were prepared as previously described[6, 21]. Briefly, 1-cm^2 square-shaped Si wafer chips were dipped into a 5% HF solution in ethanol for 1 min to remove the oxidized layer first. These Si chips were then electrochemically etched in a 25% HF/ethanol solution for 1 min at a current density of 5 mA/cm^2. White light from a 50 W tungsten lamp was used to irradiate silicon during etching. The produced porous Si substrates were then dipped into 15% H_2O_2 for 1 min, followed by a 1-min dip in 5% HF/ethanol solution to refresh the surface prior to analyte deposition.

Sample Preparation for MS measurements Analyte molecules were deposited on the solid surface either by conventional drop-coating method or spin-coating method. In the drop-coating method, a 0.5-μM DMPC solution in acetone:ethanol=2:1 that contained (or not) 10 mg/mL of CHCA was drop-loaded onto porous silicon or a stainless steel MALDI target to compare the performance of MALDI, SALDI and ME-SALDI. To demonstrate the extended mass range of ME-SALDI, a standard mix solution of 2.5-μM insulin and 13.5-μM thioredoxin in 10 mg/mL of CHCA was also loaded onto various substrates for MALDI, SALDI and ME-SALDI comparison. In the spin-coating method, a 1-mM DMPC solution was prepared in acetone:ethanol=2:1 with or without 10 mg/mL of CHCA. Porous Si substrates (for ME-SALDI and SALDI) or flat Si substrates (for MALDI) were placed on a Laurell WS-400E-6NPP-LITE spin coater (North Wales, PA), followed by dropping 50 μL of the DMPC solution with (for MALDI and ME-SALDI) or without (for SALDI) CHCA to the center of the substrates. The spin coater was then operated at 300 rpm for 1 min that yielded a homogenous DMPC/CHCA or a DMPC-only film, respectively. The average size of matrix crystals was smaller than 5 μm (Figure 4.1).

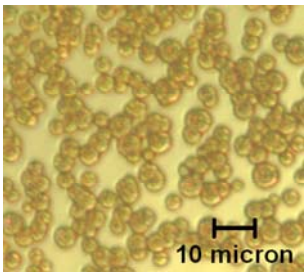

Figure 4.1. An optical image of a CHCA standard solution in ethaol:methanol:acetonitrile:0.1% TFA (water)=2:2:1:1 spin-coated on a flat Si substrate.

Typically a less than complete surface coverage was observed. In some cases as specified in the text, only matrix molecules or matrix spiked with other internal standard molecules were deposited. Optical microscopic images were taken routinely to examine the quality of surface coatings with a Leica DMRX light microscope equipped with a Donpisha XC-003P CCD camera.

MS Instrument Parameters An Applied Biosystems Voyager DE-STR MALDI-TOF mass spectrometer (Framingham, MA) was operated at an accelerating voltage of 20 kV. All experiments were operated in a linear mode except during brain MS imaging where the reflector mode was used. The laser intensity and delay time was varied to achieve optimal performance. An adjustable pinhole was placed close to the laser entrance window to adjust the diameter of the laser beam, though the laser size changed slightly as the laser input energy increased[22]. The largest measurable laser burnmark at each pinhole opening position was used to label the laser beam size (90-μm and 35-μm) in the study. The laser radiation energy at various pinhole opening positions was measured outside of the sample chamber using a FieldMax-P laser energy meter (Coherent Inc.). Note the actual laser radiation energy on the substrate surface would be less; therefore the numbers sited in the following discussions only serve for relative comparison within this manuscript. Twenty laser shots were fired to yield one MS spectrum and ten spectra were averaged to obtain one accumulated MS spectrum before further data analysis. At any given size of the laser beam, five MS replicates were collected at each laser irradiation energy level. Mass spectra data were extracted using in-house developed software and plotted using Origin 6.0 (Microcal Software, Inc.).

Limit of detection The limit of detection values (LOD) for DMPC molecular ions were measured under a 90-μm size laser beam using MALDI, SALDI and ME-SALDI, respectively. LOD was defined as the lowest concentration of DMPC at which the signal-to-background ratio (S/B) and signal intensity (SI) of molecular ion fulfill the following requirements:

$$\text{S/B of DMPC molecular ion} \geq 10 \quad (1)$$

$$\text{Absolute SI of DMPC molecular ion} \geq \text{SI of blank sample} + 3 \times \text{stdev} \quad (2)$$

During the measurements a series of dilution points was prepared as the DMPC standard solutions, where the concentration of CHCA matrix remained at 10 mg/mL for MALDI and ME-SALDI experiments. A 10 mg/mL CHCA solution was used as the blank for MALDI and ME-SALDI, respectively, whereas a blank solvent solution was as the blank for SALDI. Mass spectra were optimized under various laser conditions for each ionization method at each dilution, until one of the requirements could not be reached. The corresponding concentration of the DMPC solution was then reported as the LOD of that ionization method. Note that due to heavy fragmentation of DMPC in SALDI and ME-SALDI, the reported LOD values from molecular ion measurements were conservative estimates with the bias giving to the conventional MALDI technique.

Mass Spectrometry Imaging The mouse heart and brain tissue samples were mounted on a chunk with optical cutting temperature (OCT) compounds and were sliced to 10-40-μm thick sections with a Cryo-cut microtome (American Optical Corp., Buffalo, NY, USA) at -20 °C. The tissue sections were then transferred onto a porous silicon substrate. In the mouse heart experiment, a hydrophobic barrier surrounding the tissue section was drawn with an ImmEdge Pen (Vector Laboratories, Inc.) to confine the solution during

matrix deposition[23]. A mixture of small molecules, including L-histidine, phenylalanine, caffeine and prednisone, were dissolved in a solution of 30 mg/mL of CHCA in ethaol:methanol:acetonitrile:0.1% TFA (water)=2:2:1:1 as the internal standards. 10 μL of the matrix solution was homogenously spin-coated onto the heart tissue sample before MS measurements. In mouse brain imaging experiment, matrix DHB was sublimated onto the 10 μm thick tissue section at 110 °C under vacuum for MS imaging[24]. Meanwhile, a similar section microtomed at the adjacent location was placed on a glass slide and stained with methylene blue. Limited by the view of microscope, the optical images of stained brain sections were mosaics of several individual images in some cases. All tissue sections were imaged under a 35-μm laser beam at 50-μm stepwise. The MS instrument was controlled by MMSIT MALDI Imaging Tool software V2.2.0 (© 2004 by Markus Stoeckli, Novartis Institutes for BioMedical Research, Basel, Switzerland). 20 Laser shots in mouse heart imaging and 50 shots in mouse brain imaging were averaged to yield one accumulated spectrum at each imaging pixel. The final ion maps, as well as the Y-axis profiles, were reconstructed using BioMap 3.7.5.4.

4.3 Result and Discussion

Figure 4.2 illustrates the concept of hybrid ME-SALDI in which the analyte molecules were co-deposited with matrix onto a porous silicon surface prior to MS measurements. Detection of 1,2-dimyristoyl-*sn*-glycero-3-phospho-choline (DMPC) was used in ME-SALDI, MALDI, and SALDI under individually optimized conditions, for its ease of ionization and fragmentation. The molecular ion peak (*m/z*=678.5) and two major

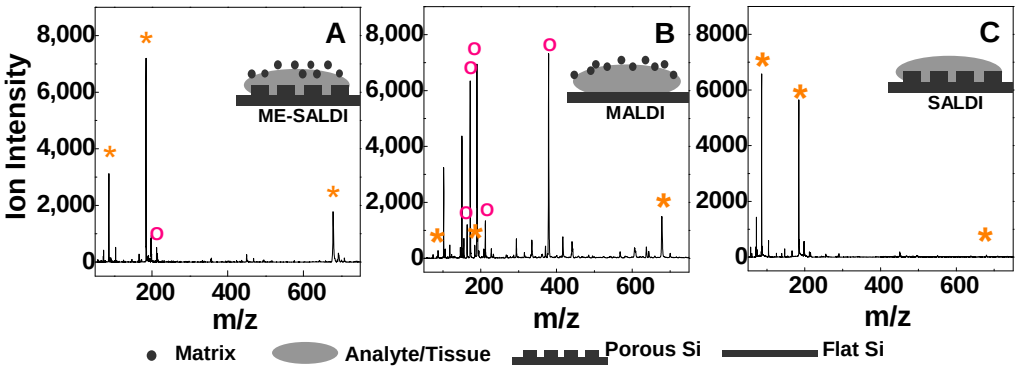

Figure 4.2. MS spectra of DMPC (0.5 μM) using (A) ME-SALDI, (B) MALDI and (C) SALDI. MS peaks associated with the analyte were labeled with asterisks (∗) and the matrix peaks by circles (o). The insets were schematic drawings of each method. All data were collected under a 90-μm laser beam.

fragments ($[C_5H_{15}NPO_4]^+$, *m/z*=184.1, and $[C_5H_{12}N]^+$, *m/z*=86.1) of DMPC were clearly visible in ME-SALDI (Figure 4.2A). Only one matrix peak from α-cyano-4-hydroxycinnamic acid (CHCA), $[CHCA+Na]^+$ was observed, yet with much lower ion intensity. In comparison, the low mass region in MALDI was crowded with the matrix fragments and clusters (Figure 4.2B). Only the molecular ion peak of DMPC was unambiguously observed because it located beyond the region of matrix background. SALDI detection showed similarly clean background in the low mass region as in ME-SALDI, but the fragment ion peaks dominated and the molecular ion peak was indistinctive (Figure 4.2C), suggesting a harsher ionization condition.

Reduced Matrix Interference and Analyte Fragmentation. A clean and low-background MS spectrum in the low-mass region (*m/z* < 500) is essential in complex metabolite profiling. Matrix suppression effect scores (MSE) were calculated using $MSE = \frac{\sum I_{[\text{Analyte Ions}]}}{\sum I_{[\text{Analyte Ions}]} + \sum I_{[\text{Matrix Ions}]}}$ to quantify the impacts of matrix interference[25]. The

MSE of DMPC was then calculated as following. In the positive mode detection of DMPC ($C_{36}H_{72}NPO_8$), most ions are in the form of the molecular ion ($[DMPC+H]^+$ or

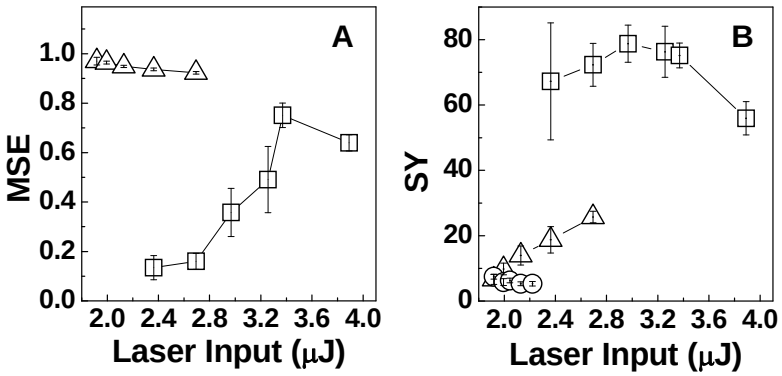

Figure 4.3. (A) MSE scores for DMPC detection using MALDI (□) and ME-SALDI (Δ) at different laser inputs. (B) The survival yields of DMPC molecular ion (m/z=678.5) using MALDI (□), ME-SALDI (Δ) and SALDI (o) at different laser inputs. The error bars were calculated from five replicates.

one of the two fragment ions ($[C_5H_{15}NPO_4]^+$ and $[C_5H_{12}N]^+$). The matrix CHCA ions include $[CHCA+H-H_2O]^+$, $[CHCA+H]^+$, $[CHCA+Na]^+$ and $[2CHCA+H]^+$. Therefore,

for the analyte (DMPC):

$$\sum I_{[\text{Molecular Ion}]} = I_{[DMPC+H]^+}$$

$$\sum I_{[\text{Fragment Ions}]} = I_{[C_5H_{15}NPO_4]^+} + I_{[C_5H_{12}N]^+}$$

$$\sum I_{[\text{Analyte Cations}]} = \sum I_{[\text{Molecular Ion}]} + \sum I_{[\text{Fragment Ions}]}$$

for the matrix (CHCA):

$$\sum I_{[\text{Matrix Cations}]} = I_{[CHCA+H-H_2O]^+} + I_{[CHCA+H]^+} + I_{[CHCA+Na]^+} + I_{[2CHCA+H]^+}$$

As shown in Figure 4.3A, in MALDI the relative matrix signal intensities closely correlated to the laser energy input, varying from less than 15% to a maximum of 75% when the laser energy was varied within the range of 2.4-3.9 μJ. In contrast, in ME-SALDI an average MSE score of (95 ± 2)% quantitatively confirmed the presence of

cleaner mass spectra. The significantly improved MSE score in ME-SALDI is believed to be the result of selective enhancement of analyte ionization. It is also interesting to note that the MSE scores spanning across the broad range of laser irradiation energy studied (1.8-2.6 μJ) were relatively constant in ME-SALDI, a feature important in profiling unknown complex biological samples where little or no prior knowledge was available to allow optimization of laser fluence.

While conventional SALDI also exhibits little background interference in the low mass region, fragmentation often occurs due to destructive overheating during analyte desorption. The survival yields (SY) of DMPC molecular ions in each ionization method were quantified as the relative intensity of the molecular ions: $SY = \frac{\sum I_{[\text{Molecular Ion}]}}{\sum I_{[\text{Molecular Ion}]} + \sum I_{[\text{Fragment Ions}]}} \times 100\%$. In SALDI, relatively low SYs were calculated because most DMPC molecules degraded and were detected in fragments (Figure 4.3B). A slight decrease was noticed with increasing laser inputs. In MALDI, on the other hand, analyte molecules were protected from direct photon excitation and destructive overheating. Subsequently, most molecules were detected intact and the average SY of the molecular ion was at (71 ± 8)%, despite more intense of laser irradiation was employed. Note that the SY values calculated for ME-SALDI was at the same level as that in SALDI under low laser irradiation energy where MALDI matrix molecules were yet to be photo-excited. However, a steady increase in SY (i.e. less fragmentation) was observed under elevated laser energy in ME-SALDI, which was in drastic contrast to what was observed in conventional SALDI. This observation suggests

the presence of a "softer" and a more "MALDI-like" mechanism in analyte ionization with increasing laser irradiation. Benefiting from this "softer" ionization process and improved ionization efficiency, the detectable mass range of ME-SALDI was easily

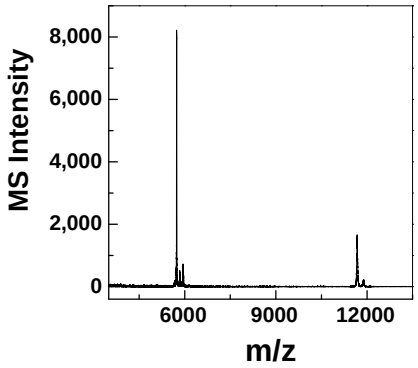

Figure 4.4. A representative MS spectrum of 0.5 pmol/μL insulin (m/z=5734.6) and 2.75 pmol/μL thioredoxin (m/z=11674.5) in 3mg/ml CHCA 50% acetonitrile aqueous solution using ME-SALDI-MS.

extended to >10,000 Da in comparison to SALDI without compromising the qualities of MS signals, even when the irradiation laser fluence was kept below matrix sublimation point (Figure 4.4).

Although the survival yield of DPMC in ME-SALDI was still lower than that in MALDI, the detection sensitivity of DMPC was nevertheless improved due to significantly enhanced overall ionization efficiency in ME-SALDI. The limits of detection (LODs) of DMPC molecular ions using three ionization sources under individually optimized experimental conditions were conservatively quantified as 0.01, 0.05 and 0.5 μM (or 10, 50 and 500 fmol) for ME-SALDI, MALDI, and SALDI, respectively. An improvement of 5 folds over MALDI and 50 folds over SALDI was achieved with ease (data not shown). Note that due to fragmentation of DMPC in SALDI and ME-SALDI, these LOD values calculated from DMPC molecular ion measurements

were conservative estimates with the bias giving to the conventional MALDI technique. For example, at least one more order of magnitude improvement in LOD was achievable in ME-SALDI detection of DMPC if the major fragment ion (m/z=184.1) was used instead in identification.

Suggested ME-SALDI Mechanism. Laser-induced analyte desorption and ionization is a complex process. Various theories have been presented to address the basic mechanisms underlying MALDI or SALDI[20, 26-29]. ME-SALDI, as a hybrid of MALDI and SALDI, is believed to share the energy transfer pathways of both. In particular, the laser threshold in ME-SALDI was found to be similar to that in SALDI but was significantly lower than that of MALDI (Figure 4.3B). This observation suggests the porous silicon surface, rather than the matrix molecules, behaves as the energy mediating center to effectively convert absorbed photons to local thermal energy and to facilitate desorption of analyte molecules; hence the coined name of ME-SALDI instead of surface-enhanced MALDI. During analyte desorption, the matrix molecules primarily serve as a carrying reagent that co-desorb with analyte molecules through phase explosion, increasing the amount of analyte molecules in the gas phase and reducing the amount of energy directly transferred to the analyte molecules. Subsequently more analyte ions (i.e. better sensitivity) and fewer fragments are detected. The control experiments where matrix molecules were deposited on a flat Si surface (as in conventional MALDI) did not show any appreciable signals of matrix nor analyte molecules under the same low laser energy level, further confirmed the critical role played by the porous structure of Si substrates in ME-SALDI.

In addition to serving as the carrying agent, the matrix molecules play a pivotal

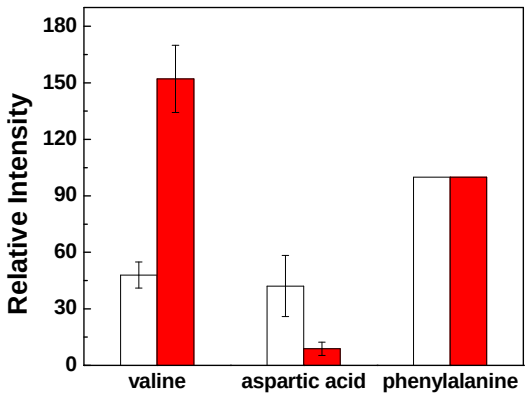

Figure 4.5. A standard solution of three amino acids (valine, aspartic acid and phenylalanine) with CHCA in 1:1:1:3 molar ratios were examined by MALDI (white) and ME-SALDI (red). The signal intensity of amino acids was normalized with signal intensity of phenylalanine.

role in analyte protonation. Three amino acids (valine, aspartic acid and phenylalanine) of different gas-phase proton affinity (PA) were mixed with CHCA at the 1:1:1:3 molar ratio for MALDI and ME-SALDI (Figure 4.5). In MALDI, consistent with their gas-phase proton affinity (PA), the ion signal intensities were similar for valine (PA=217.4kcal/mol) and aspartic acid (PA=217.1kcal/mol), but both were weaker than what from phenylalanine (PA=220.5 kcal/mol). In ME-SALDI, a ~1.5-time stronger ion signal was observed from valine (PI=5.96) while the signal of aspartic acid (PI=2.77) reduced significantly to ~10% of phenylalanine (PI=5.48) signal, consistent with the general trend of their pI values. These results suggest that unlike in MALDI where charge exchange occurs mostly in the gas phase, in ME-SALDI most analytes are probably ionized at the vacuum-substrate interface before and during desorption. Therefore, similar to SALDI, the condense-phase acidity (pKa) of an analyte seems to

play a more important role whereas gas-phase secondary ionization is limited due to the relatively low plume density[19, 20]. The lack of proton donors that often leads to disappointing detection sensitivity in SALDI, however, is no longer an issue in ME-SALDI: acidic matrix molecules become the main source of protons in analyte ionization, as supported by the detection of significant enhanced (~12 folds) matrix anions in the negative-mode detection (Figure 4.6). Previously observed reduction of matrix interference in ME-SALDI can also be rationalized as the result of a large portion of matrix ions were negatively charged species after donating the protons in ME-SALDI.

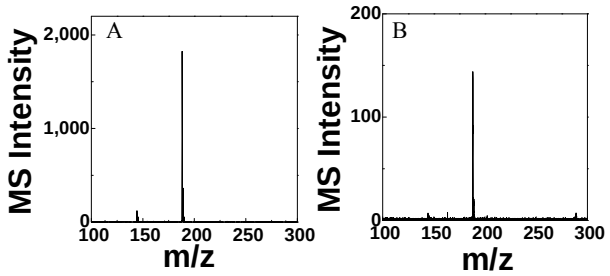

Figure 4.6. MS spectra of CHCA collected under the same MS conditions in (**A**) ME-SALDI and (**B**) MALDI in a negative mode. A 10 mg/mL CHCA matrix solution was loaded onto a porous silicon substrate and a stainless steel MALDI target before measurements. Two negative CHCA anions were observed as $[CHCA\text{-}H]^-$ and $[CHCA\text{-}H\text{-}CO_2]^-$.

Impact of Laser Beam Size. A more pronounced improvement in detection sensitivity using ME-SALDI was realized during high resolution IMS where the use of a size-reduced laser beam was essential. The absolute ion currents from any laser-based MS ionization technique are expected to decrease when the laser beam size is reduced, primarily due to the loss of photon influx from beam blockage and fewer analyte molecules present in the field of analysis. An increase in the level of laser irradiation energy has been traditionally opted as the common remedy of the problem. However, in

MALDI IMS, the increase of ion currents by increasing laser fluence slows down significantly as the laser beam size becomes smaller[27, 30]. When the laser beam was reduced to ~ 35 μm using an iris, little improvement in the ion current was observed, even after the laser irradiation reached the upper-limit of the instrument hardware output

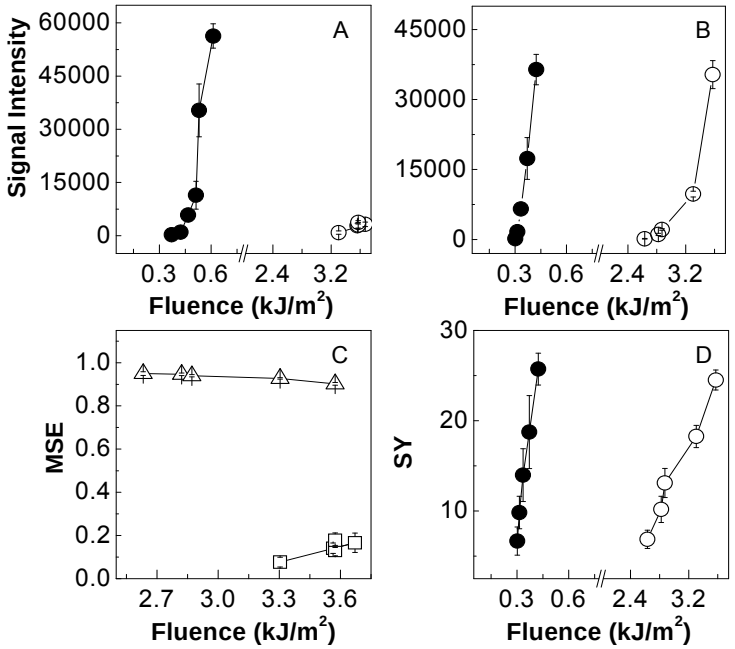

Figure 4.7. Signal intensities of the DMPC molecular ion in (A) MALDI and (B) ME-SALDI MS under the 90-μm (•) or 35-μm (o) laser beam at different laser fluence. (C) The MSE scores of DMPC detection using MALDI (□) and ME-SALDI (Δ) under the 35μm-size laser beam. (D) The survival yield of DMPC molecular ion using ME-SALDI under the 90-μm (•) and 35-μm (o) size laser beam. The error bars were calculated from five replicates.

(Figure 4.7A). The laser size dependence of MALDI MS performance is suggested as the result of the changes in the projectile shape or the gas density within the desorption plume[26]. It is also likely related to faster dissipation of the absorbed energy to the surrounding environment under the smaller laser beam. In SALDI, however, ionization mainly occurs on the porous silicon surface, which is less dependent on the plume geometry and density. Furthermore, the nanoporous structure of the SALDI substrate (~50 nm <<35 μm) effectively "confines" the absorbed energy locally, independent of the

size of the laser beam used[31, 32]. Therefore, comparable MS performance was achievable in SALDI even when the laser beam was reduced, *albeit* high energy input is needed to make up the overall flux (data not shown). Given that ME-SALDI shares the same condense-phase ionization pathway as SALDI, the MS response is expected and was indeed found to be less dependent on the beam size as well (Figure 4.7B).

The previously described benefits of ME-SALDI over MALDI and SALDI were also exemplified at the reduced laser size: a relatively unchanged MSE score was calculated in ME-SALDI at (93 ± 2)%, 7 folds higher than that of MALDI, (14±4)%, under the 35-μm laser beam (Figure 4.7C). Unlike under the 90-μm laser beam, the background interference observed in MALDI can hardly be improved over the range of laser flux. On the other hand, the increased laser energy input at the reduced laser size did not necessarily result in a decreased SY of molecular ion in ME-SALDI. As shown in Figure 4.7D, similar SYs were calculated, which demonstrated relatively independent analyte fragmentation to the laser beam size in ME-SALDI. Together, in comparison to conventional MALDI and SALDI, ME-SALDI exhibits reduced dependency of laser beam sizes. Along with its reduced matrix interference, reduced fragmentation and improved detection sensitivity; ME-SALDI is shown to potentially provide the best overall MS performance for high resolution 2D IMS.

MS Imaging of Mouse Tissue Sections. Although there was no physical contact between analytes atop of the tissue section and the porous silicon underneath the tissue, direct imaging of small bio-molecules with DIOS-MS has been reported[6]. The photon energy absorbed by porous silicon was likely converted to thermal energy and then transferred to

the top-layer of the tissue surface in desorption/ionization process. To confirm the feasibility of using ME-SALDI in 2D imaging, tissue sections with 10, 20, 30 and 40-μm in thicknesses were placed on a porous or a flat silicon surface side by side, followed by coating a standard molecule, lysine, atop to ensure the same amount of analyte molecules was examined.. Comparing to those from a flat surface in the conventional MALDI mode, it is astonishing to see that much stronger MS signals from the tissue placed atop the porous surface, i.e. in the ME-SALDI mode, were observed, regardless the 40-μm thick tissue section lied in-between (Figure 4.8). The exact cause behind this enhancement in the presence of a thick insulating layer is not understood at the moment. Yet, the benefit of using ME-SALDI in tissue imaging is apparent.

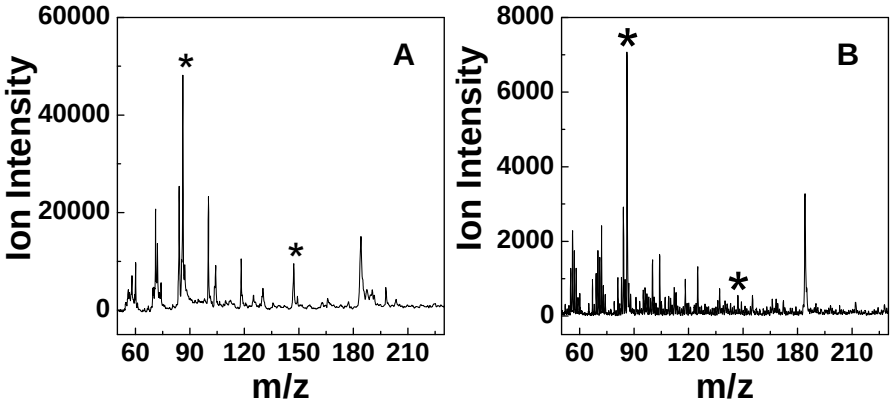

Figure 4.8. Mouse heart tissue sections of 40-μm thickness were placed onto porous/flat silicon surface and immersed to a 1mM L-lysine solution in 2 mg/mL CHCA. The signal intensity of L-lysine detected from the tissue atop of (A) a porous silicon substrate in ME-SALDI was ~20 folds stronger than that from (B) the flat silicon in MALDI. The ion intensity of the m/z =86.1 peak was ~7 folds stronger.

The use of ME-SALDI in MS imaging under a reduced laser beam was examined using mouse brain and heart tissues. Figure 4.9B shows an optical image of the mouse

heart tissue collected before deposition of a thin layer of CHCA matrix atop. The tissue was purposely placed on the boarder of a porous silicon substrate such that half of the tissue was rested on the porous substrate to be imaged in the ME-SALDI mode, whereas the other half was on the flat Si surface to be imaged in the conventional MALDI mode. The blue dotted line outlined the boundary of the tissue sample and the virtual boundary

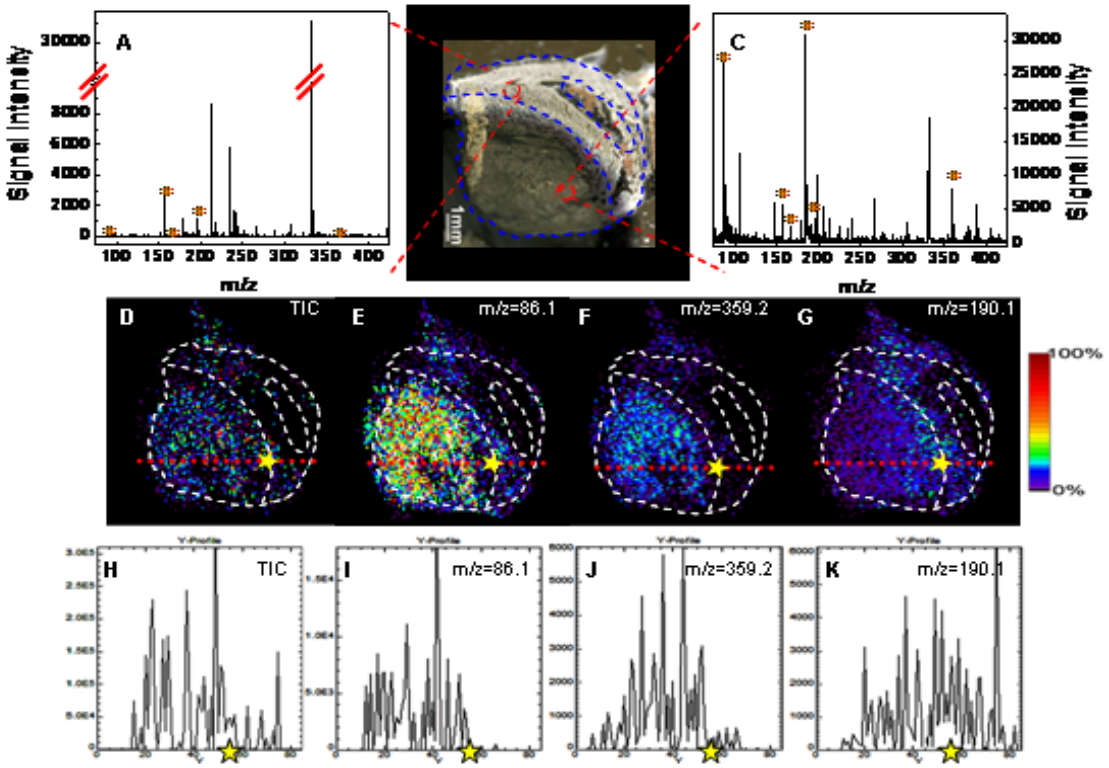

Figure 4.9. Representative MS spectra collected from the tissue atop of (A) the flat silicon in MALDI and (C) the porous silicon in ME-SALDI. MS peaks associated with the phosphocholine headgroups and the internal standards were labeled with asterisks (∗). (B) An optical image of a CB1 mouse heart tissue section placed half-inside-half-outside of a porous silicon substrate. The blue-dotted line shows the virtual boundary of two surfaces and the outline of the tissue. Small tissue damage in the right-middle portion was blocked by a hydrophobic barrier. The reconstructed 2-D images for (D) total ion chromatogram (TIC), and the ions at (E) *m/z*=86.1, (F) *m/z*=359.2 and (G) *m/z*=190.1 are representative ion maps. Panels H, I, G, and K are the scanning profiles in the corresponding MS images at the location indicated by the red-dotted lines. The yellow star indicates the border where the porous and the flat surface underneath the tissue met along the red line.

of the porous surface where the tissue atop the porous Si portion showed a darker shade in the picture. This experimental setup allowed direct side-by-side performance comparison of two MS ionization methods and eliminated any ambiguity introduced by

using different tissue samples. MS spectra were collected with a 35-μm laser beam at 50-μm scanning steps. Despite the experimental conditions were optimized for MALDI IMS whose performance was more sensitive to instrumental parameters and required higher laser irradiation energy, stronger overall signal intensities were observed in the representative spectrum of ME-SALDI (Figure 4.9C vs 4.9A). Figure 4.9D-F show the reconstructed ion maps of total ions or selective species. Stronger ion intensities were universally observed from the left-bottom section of the tissue atop of the porous silicon than from the right-top half of the tissue on the flat surface. A linear-scanning profile of the ion maps was carried out pixels along the red dotted line with a yellow star located on the border of two surfaces (the right side of the yellow star corresponds to the flat portion). A clear difference in average ion intensity was observed for 4.9H-J. The species at *m/z*=86.1 was likely from the headgroup of phosphatidylcholine, and the one at m/z=359.2 was an internal standard prednisone spiked into the matrix solution prior to matrix deposition**.** Much smaller differences were observed between MALDI and ME-SALDI for matrix ions at m/z=190.1, i.e. $[CHCA+H]^+$.

To quantify the degree of improved MS imaging performance, ~1,800 spectra were averaged for both MS ionization methods. Statistic calculation shows that an average of a ~20-fold improvement for detection of seven representative analytes was achieved in ME-SALDI imaging to MALDI. Meanwhile, the matrix background only exhibited an average of 1.5-fold enhancement (for three matrix related ion peaks) to that of MALDI imaging, confirming again the reduced matrix interference. A higher degree

of improvement was obtained when 2D IMS was conducted under the conditions more suitable for ME-SALDI (data not shown).

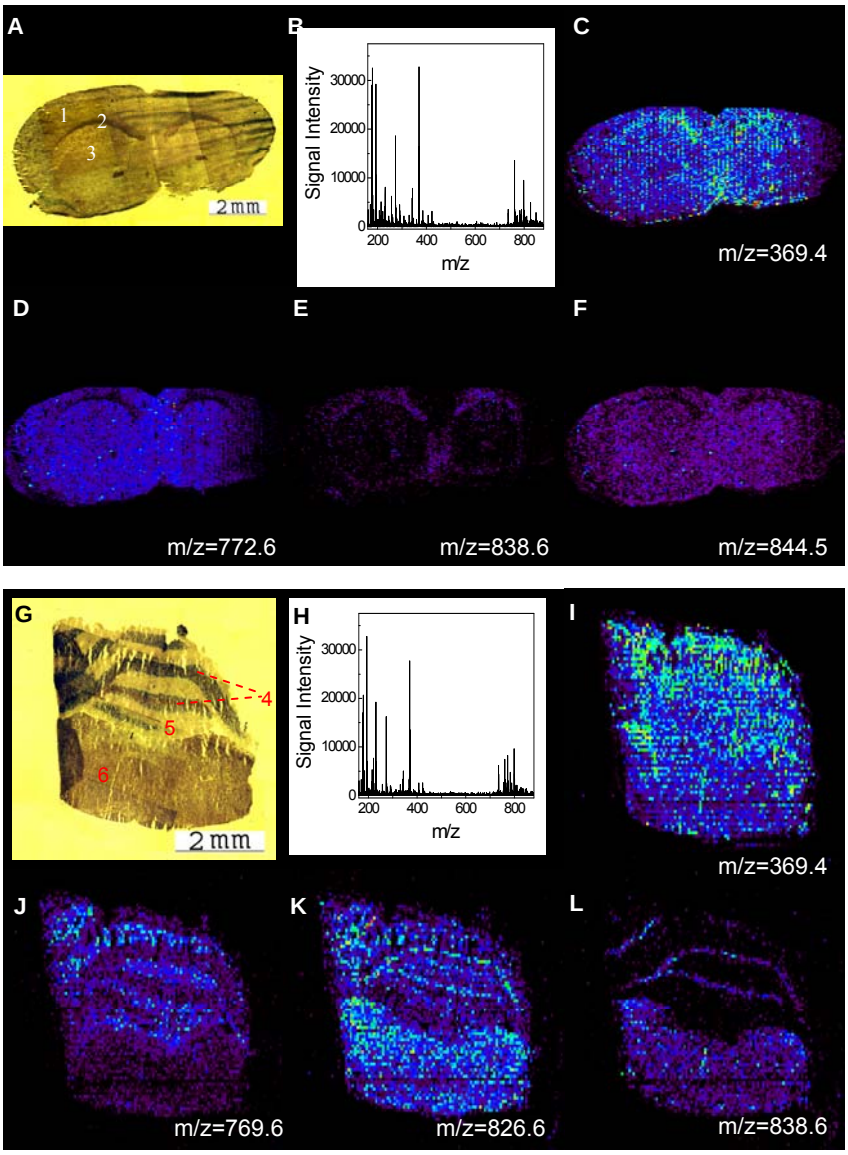

Figure 4.10. Optical images of the coronal sections of (A) mouse cerebrum and (G) mouse cerebellum. Representative MS spectra collected from the adjacent coronal sectioning of (B) mouse cerebrum and (H) mouse cerebellum in Me-SALDI, respectively. Also shown are reconstructed 2-D images for ions at (C) m/z=369.4, (D) m/z=772.6, (E) m/z= 838.6 and (F) m/z= 844.5 from the mouse cerebrum coronal section, and for ions at (I) m/z=369.4, (J) m/z=769.6, (K) m/z= 826.6 and (L) m/z= 838.6 from mouse cerebellum coronal section. Molecular identification sees the text. 1, cerebral cortex; 2, corpus callosum; 3, striatum; 4, cerebellar nuclei; 5, molecular layer in cerebellum; 6, brain stem.

The capability of ME-SALDI-IMS in visualizing distribution of natural biomolecules was further demonstrated in the examination of mouse brain tissues. Figure 4.10A and G shows the optical images of the coronal sections of mouse cerebrum and mouse cerebellum, respectively. Clear detection of cholesterol and phospholipids was visible in the MS spectra (Figure 4.10B and H). The 2-D reconstructed ion maps show that cholesterol and certain phospholipids were differentially expressed at specific regions of mouse brain. As shown in Figure 4.10C and I, the cholesterol ions $[M-H_2O+H]^+$ (m/z=369.4) was found highly concentrated in the white matter at corpus callosum and cerebellum. In contrast, the adducts of phosphocholine (PC) 32:0 (m/z=772.6) and PC 38:6 (m/z=844.5) were complementary distributed in cerebral cortex and striatum, but almost absent in corpus callosum (Figure 4.10D and F). The PC 40:4 molecular ions $[M+H]^+$ (m/z=838.6) were concentrated in corpus callosum, brain stem and the cerebellar nuclei, but absent in the molecular layer of cerebellum (Figure 4.10E and L). As shown in Figure 4.10J, the potassium adducts of sphingomyelin (SM) 18:0 (m/z=769.6) were highly expressed in the molecular layer of cerebellum but barely in brain stem, complementary to the spatial distribution of PC 36:1 and PC 40:4 in the grey matter. While these findings were consistent with the reported histological and traditional MS studies, it is the first time that the complementary spatial distribution of cholesterol and whole lipids was visualized simultaneously using a laser-based MS imaging method.[33, 34]

4.4 Conclusions

In summary, we have demonstrated that by synergically combining the traditional MALDI and SALDI methods, the hybrid ME-SALDI ionization method provides an attractive approach to imaging small molecules under a reduced laser beam. The demonstrated benefits include better detection sensitivity, lower background noise, and a broader detectable mass range. Furthermore, by separating the primary photon-absorption medium (i.e. porous surface-facilitated desorption) from the primary protonation step (i.e. matrix-assisted proton transferring), ME-SALDI enables independent optimization of desorption and ionization processes to achieve the best imaging outcome. The demonstrated simultaneous imaging of cholesterol and lipids in mouse brain tissue opens opportunities in further investigation of their roles in brain development and damage repairs.

4.5 References.

(1) Caprioli, R. M.; Farmer, T. B.; Gile, J., Anal. Chem. 1997, 69, 4751-4760.

(2) Ostrowski, S. G.; Van Bell, C. T.; Winograd, N.; Ewing, A. G., Science 2004, 305, 71-73.

(3) Altelaar, A. F. M.; Van Minnen, J.; Jimenez, C. R.; Heeren, R. M. A.; Piersma, S. R., Anal. Chem. 2005, 77, 735-741.

(4) Drexler, D. M.; Garrett, T. J.; Cantone, J. L.; Diters, R. W.; Mitroka, J. G.; Prieto Conaway, M. C.; Adams, S. P.; Yost, R. A.; Sanders, M., J. Pharmaco. Toxico. Methods 2007, 55, 279-288.

(5) Nemes, P.; Vertes, A., Anal. Chem. 2007, 79, 8098-8106.

(6) Liu, Q.; Guo, Z.; He, L., Anal. Chem. 2007, 79, 3535-3541.

(7) Cha, S.; Yeung Edward, S., Anal. Chem. 2007, 79, 2373-2385.

(8) Cornett, D. S.; Reyzer, M. L.; Chaurand, P.; Caprioli, R. M., Nat. Methods 2007, 4, 828-833.

(9) Wu, K. J.; Odom, R. W., Anal. Chem. 1996, 68, 873-882.

(10) Cooks, R. G.; Ouyang, Z.; Takats, Z.; Wiseman, J. M., Science 2006, 311, 1566-1570.

(11) Shiea, J.; Huang, M.-Z.; Hsu, H.-J.; Lee, C.-Y.; Yuan, C.-H.; Beech, I.; Sunner, J., Rapid Commun. Mass Spectrom. 2005, 19, 3701-3704.

(12) Coon, J. J.; Steele, H. A.; Laipis, P. J.; Harrison, W. W., J. Mass Spectrom. 2002, 37, 1163-1167.

(13) Sampson, J. S.; Hawkridge, A. M.; Muddiman, D. C., J. Am. Soc. Mass Spectrom. 2006, 17, 1712-1716.

(14) Tanaka, K.; Waki, H.; Ido, Y.; Akita, S.; Yoshida, Y.; Yohida, T., Rapid Commun. Mass Spectrom. 1988, 2, 151-153.

(15) Sunner, J.; Dratz, E.; Chen, Y.-C., Anal. Chem. 1995, 67, 4335-4342.

(16) Dale, M. J.; Knochenmuss, R.; Zenobi, R., Anal. Chem. 1996, 68, 3321-3329.

(17) Dale, M.; Knochenmuss, R.; Zenobi, R., Rapid Commun. Mass Spectrom. 1997, 11, 136-142.

(18) Zhou, H.; Xu, S.; Ye, M.; Feng, S.; Pan, C.; Jiang, X.; Li, X.; Han, G.; Fu, Y.; Zou, H., J. Proteome Res. 2006, 5, 2431-2437.

(19) Liu, Q.; He, L., J. Am. Soc. Mass. Spectrom. 2008, 19, 8-13.

(20) Chen, C.; Chen, H.; Aleksandrov, A.; Orlando, T. M., J. Phys. Chem. C 2008, 112, 6953-6960.

(21) Finkel, N. H.; Prevo, B. G.; Velev, O. D.; He, L., Anal. Chem. 2005, 77, 1088-1095.

(22) Chaurand, P.; Schriver, K. E.; Caprioli, R. M., I J. Mass Spectrom. 2007, 42, 476-489.

(23) Agar, N. Y. R.; Yang, H. W.; Carroll, R. S.; Black, P. M.; Agar, J. N., Anal. Chem. 2007, 79, 7416-7423.

(24) Hankin, J.A.; Barkley, R.M.; Murphy, R.C. J Am. Soc. Mass Spectrom. 2007, 18, 1646-1652.

(25) McCombie, G.; Knochenmuss, R., Anal. Chem. 2004, 76, 4990-4997.

(26) Dreisewerd, K., Chem. Rev. 2003, 103, 395-426.

(27) Knochenmuss, R., Analyst 2006, 131, 966-986.

(28) Alimpiev, S.; Grechnikov, A.; Sunner, J.; Karavanskii, V.; Simanovsky, Y.; Zhabin, S.; Nikiforov, S., J. Chem. Phys. 2008, 128, 014711-1-19.

(29) Luo, G.; Chen, Y.; Daniels, H.; Dubrow, R.; Vertes, A., J. Phys. Chem. B 2006, 110, 13381-13386.

(30) Dreisewerd, K.; Schurenberg, M.; Karas, M.; Hillenkamp, F., Int. J. Mass Spectrom. Ion Processes 1995, 141, 127-148.

(31) Schuerenberg, M.; Dreisewerd, K.; Hillenkamp, F., Anal. Chem. 1999, 71, 221-229.

(32) Alimpiev, S.; Nikiforov, S.; Karavanskii, V.; Minton, T.; Sunner, J., J. Chem. Phys. 2001, 115, 1891-1901.

(33) Puolitaival, S. M.; Burnum, K. E.; Cornett, D. S.; Caprioli, R. M. J Am Soc Mass Spectrom 2008, 19, 882–886.

(34) Sjovall, P; Johansson, B.; Lausmaa, J. App. Sur. Sci. 2006, 252, 6966–6974.

Chapter 5 Ionic Matrix for Matrix-Enhanced Surface-Assisted Laser Desorption Ionization Imaging Mass Spectrometry (ME-SALDI-IMS)

5.1 Introduction

Surface-assisted laser desorption ionization mass spectrometry (SALDI-MS) has been used as a complementary tool to matrix-assisted laser desorption ionization mass spectrometry (MALDI-MS) in small molecule profiling.[1-6] Its applications in tissue imaging have been demonstrated by various groups where porous surfaces or inorganic nanoparticles have been successfully utilized as the energy mediating reagents.[7-9] To further improve imaging sensitivity, a hybrid ionization approach, matrix-enhanced SALDI (ME-SALDI), has been recently reported in which conventional matrix molecules were deposited atop a porous SALDI substrate to provide a proton-rich environment for enhanced ionization of low-mass species. Meanwhile, the porous SALDI substrate effectively reduced laser flux needed for analyte desorption and few matrix ions were observed in the background. Both features are in particularly crucial for MS imaging of metabolites under a reduced laser beam size in order to achieve better spatial resolution.[10]

However, a new challenge arises with the adaptation of ME-SALDI in imaging MS (IMS): it is known that most conventional MALDI matrices slowly vaporize under vacuum (10^{-7}~10^{-8} torr) due to their low sublimation points.[11] The loss of materials becomes more severe when the matrix is in an amorphous form. While matrix sublimation under vacuum does not necessarily impose a problem in traditional MALDI profiling applications where most measurements occur in seconds, the loss of matrix can

not be ignored during MS imaging because of extended interrogation time and the preferred solvent-free approach for matrix deposition, i.e. sublimation that results in formation of an amorphous matrix layer.[12] For example, a commercial MALDI-TOF instrument equipped with a 20-Hz N_2 laser, approx. 720 pixels can be imaged in an hour when 100 laser shots were needed per pixel not counting in time needed for translational stage movement, which translates to ~55.6 h of instrument time to examine a 1-cm^2 tissue section with spatial resolution of 50 μm. It is sufficiently long to experience the impacts of matrix loss during MS inquisition, including the inevitable change in ionization efficiency over time and across tissue. Consequently the actual spatial distribution of chemical compounds in the sample imaged could be skewed.

A new class of MALDI matrices by mixing an equal molar of conventional MALDI matrix with an organic base to form so called ionic matrix have been developed in recent years.[13] In comparison to conventional MALDI matrices, ionic matrices afford several advantages, including improved deposition homogeneity, suppressed matrix interference, reduced matrix fragmentation, and more importantly for imaging applications, superior stability under high vacuum over extended imaging duration. Many types of ionic matrices have since been synthesized and evaluated. Their applications in detection and quantification of oligonucleotides, lipids and saccharides have gained great research interest.[14-17] Direct tissue analysis in the MALDI mode using ionic matrices has shown better spectral quality and ionization efficiency over their conventional analogs.[18]

Here we describe the use of an ionic matrix, i.e. CHCA/ANI synthesized with α-cyano-4-hydroxycinnamic acid (CHCA) and aniline (ANI), in the place of conventional MALDI matrix for ME-SALDI imaging. Reproducible and homogenous deposition of CHCA/ANI through sublimation has been developed for the first time to eliminate solvent interference. Spectral qualities in terms of detectable mass range and mass resolution of ionic matrix-based ME-SALDI are comparable to those of ionic matrix-based MALDI. Reduced spectral background and better MS ionization efficiency of ionic matrix-based ME-SALDI over ionic matrix-based MALDI renders it an ideal solution for 2-D metabolite imaging.

5.2 Experimental Section

Materials. N-type Sb-doped (100) single-crystalline silicon wafers at 0.005-0.02 Ω/cm were purchased from Silicon Sense, Inc. (Nashua, NH), and stored under vacuum upon use. 2,5-Dihydroxybenzoic acid (DHB), α-cyano-4-hydroxycinnamic acid (CHCA), quinidine, and aniline (ANI) were purchased from Sigma Aldrich (St. Louis, MO). Methylene blue ($C_{18}H_{22}N_3SCl \cdot 1/2ZnCl_2$) was purchased from MP Biomedicals (Solon, OH). Hydrofluoric acid (HF, 49%), acetone, methanol and H_2O_2 (30%) were purchased from Fisher Scientific (Pittsburgh, PA). CH_3CH_2OH was purchased from Aaper Alcohol (Shelbyville, KY). DI H_2O of 18 MΩ (Millipore, PO) was used throughout the experiments. Mouse brain and chicken liver tissues were freshly frozen and stored at -80ºC upon use. Garlic and chicken liver tissue samples were purchased from local grocery stores.

Porous Silicon Substrate Preparation Porous silicon substrates were prepared as previously described.[9, 19] Briefly, silicon wafer chips were washed with a 5% HF solution in ethanol for 1 min and then electrochemically etched in a 25% HF/ethanol solution for 1 min at a current density of 5 mA/cm^2. White light from a 50 W tungsten lamp was used to irradiate the silicon surface during etching. The produced porous silicon substrates were then dipped into 15% H_2O_2 for 1 min, followed by a 1-min dip in 5% HF/ethanol solution to refresh the surface prior to analyte deposition.

Synthesis of Ionic Matrix (CHCA/ANI) CHCA/ANI was synthesized by mixing an equal molar CHCA with ANI in methanol as described in the literature.[18] The reaction mixture was stirred for 2 h at room temperature, followed by solvent removal under vacuum. The yellowish product, CHCA/ANI, was stored in a desiccator under vacuum at room temperature prior to use.

Preparation of MS Analyte Two standard solutions of quinidine were prepared for MS evaluation of ionic matrix-based ME-SALDI: (a) 1-μM quinidine in 4.2 mg/mL of CHCA/ANI in acetonitrile/water (1:1, v/v) and (b) 1-μM quinidine in 4.2 mg/mL of CHCA/ANI in acetonitrile/water (1:1, v/v, containing 0.1% TFA). For MALDI-MS analysis, 1 μL of the standard solution (a) or (b) was drop-loaded on a stainless steel MALDI plate. For ME-SALDI analysis, 1 μL of standard solution (a) was drop-loaded on a porous silicon substrate.

To study the impact of acidic additives on vacuum stability, two 10 mg/mL CHCA/ANI solutions were prepared in acetone:ethanol=2:1 with or without 0.1% TFA. The solutions were spin-coated separately onto individual glass slides with a Laurell WS-

400E-6NPP-LITE spin coater (North Wales, PA). UV absorbance of the ionic matrix-coated glass slides was then measured using an 8453 Hewlett Packard spectrometer (Agilent, Palo Alto, CA) before and after being stored in the sample chamber of the mass spectrometer (10^{-7} Torr) for 40 h.

Tissue samples from garlic or chicken liver were first mounted on a metal support with an optical cutting temperature (OCT) compound. The mounted species were then sliced into 10-μm thick sections with a Cryo-cut microtome (American Optical Corp., Buffalo, NY, USA) at -20 °C. The sliced sections were carefully transferred onto a porous silicon substrate for ME-SALDI IMS. Meanwhile, a tissue section microtomed at the adjacent location was placed on a glass slide, stained with methylene blue, and imaged with a Leica DMRX light microscope. In some cases, limited by the view of microscope, the optical images of stained sections were mosaics of several individual images.

The same garlic cloves were also using in homogenized profiling by grinding the cloves and extracting the metabolites in methanol under stirring for 2 d. CHCA/ANI (4.2 mg/mL) was then added to the filtered garlic extracts prior to drop-deposited on a substrate for ME-SALDI and MALDI measurements.

Matrix Deposition through Sublimation. 0.3 g of CHCA/ANI or DHB was added into a sublimation chamber set up in house. A tissue-coated porous silicon substrate was mounted to the flat bottom of the condenser, facing downwards to the matrix. An oil bath was pre-heated to 170 ºC to sublimate CHCA/ANI or to 110ºC to sublimate DHB. In some cases, the temperature of the oil bath was varied from 80 ºC to 120 ºC to deposit

DHB onto chicken liver sections to produce matrix films of different thicknesses. The condenser and the surface temperature of the substrate attached to the condenser were cooled down with running water for vapor condensation. The pressure of the sublimation chamber was maintained at ~50 torr for 2 min before immersing the apparatus into the oil bath. After 5-min immersion, the sublimation setup was removed and the vacuum was released. The substrate was carefully removed and affixed to a MS plate to be loaded into the MS sample chamber.

A transparent glass slide without mounted tissue was coated in the same fashion and the absorbance at 337 nm was used to semi-quantitatively monitor the amount of DHB deposited. Deposition uniformity was evaluated by calculating intra-substrate relative standard deviations of the measured UV absorbance of each coated slide at five different locations. Deposition reproducibility was evaluated by inter-substrate relative standard deviations, which were calculated from UV absorbance of five matrix-coated glass sides prepared under the same conditions. Matrix stability was evaluated by comparing UV absorbance of matrices before and after storage in the sample chamber of the mass spectrometer (10^{-7} Torr) for 40 h. Optical microscopic images were also taken to visually examine the quality of matrix deposition using a Leica DMRX light microscope equipped with a Donpisha XC-003P CCD camera.

MS Instrument Parameters and Data Analysis. An Applied Biosystems Voyager DE-STR MALDI-TOF mass spectrometer (Framingham, MA) was operated at an accelerating voltage of 20 kV, equipped with a 20-Hz N_2 laser. All experiments were operated in a reflector mode. The laser intensity and delay time were varied to achieve

optimal performance. An adjustable pinhole was placed close to the laser entrance window to adjust the diameter of the laser beam and final beam size was determined by the largest measurable laser burn-mark left on a substrate under the highest laser fluence provided by the instrument. A 35-µm laser beam was used in most experiments except for DHB-coated garlic section and CHCA-coated mouse brain section, which were imaged under a 90-µm laser beam at 100-µm stepwise. CHCA/ANI-coated garlic section was imaged at 50-µm stepwise.

Mass spectra were extracted using in-house developed software and plotted using Origin 6.0 (Microcal Software, Inc.). Matrix suppression effect scores (MSE) were calculated using $MSE = \frac{\sum I_{[\text{Analyte Ions}]}}{\sum I_{[\text{Analyte Ions}]} + \sum I_{[\text{Matrix Ions}]}}$ to quantify the impact of matrix interference. During MS imaging, the instrument was controlled by MMSIT MALDI Imaging Tool software V2.2.0. The final ion maps, as well as the Y-axis and X-axis profiles, were reconstructed using BioMap 3.7.5.4. Both programs were provided by Markus Stoeckli, Novartis Institutes for BioMedical Research, Basel, Switzerland.

5.3 Result and Discussion

The gradual loss of matrix molecules in MS imaging was clear in Figures 5.1A and 5.1B where conventional matrix DHB was sublimated atop a piece of garlic section. Panel 5.1A shows the clearly reduced ion intensity of DHB (m/z= 155.0) over ~15 h scanning, following the direction of laser rastering from left to right. A distorted distribution of analyte interested is also observed. As shown in Figure 5.1B, a much

higher ion intensity for ions at m/z=104.1 (likely from γ-aminobutyric acid, one of the major amino compounds produced during germination and early seedling growth) is observed not only in cotyledon portion of garlic but also in the left portion of the tissue where the area was analyzed in the beginning of IMS experiment.[20, 21]

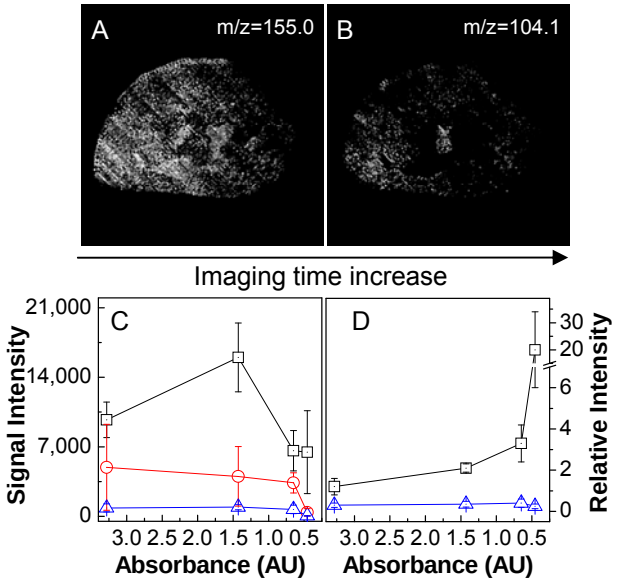

Figure 5.1. Reconstructed 2-D images for ions at (A) m/z=155.0 and (B) m/z=104.1 for a DHB-coated garlic tissue. DHB was sublimated onto chicken liver sections with varied thickness. (C) Signal intensities of an analyte at m/z=103.9 (□), the matrix ion at m/z=155.0 (○) and cholesterol at m/z=369.4 (Δ) from DHB-coated chicken liver sections were plotted against the absorbance of DHB at 337 nm. (D) Normalized signal intensities of ions at m/z=103.9 (□) and m/z=369.4 (Δ) against DHB ions were plotted against the absorbance of DHB at 337 nm.

To better quantitate the effect of matrix loss on MS imaging, MS spectra were collected from several adjacent chicken liver tissue sections coated with different amounts of DHB by controlling the sublimation temperature. The ion intensities of several prominent species were plotted against the absorbance of DHB on the corresponding glass slides (Figure 5.1C). Note that the range of the amounts of DHB examined was designed such that the amount of matrix typically used in MALDI-MS experiments was bracketed. Moreover, within the range studied here, the assumption that

the UV absorbance of DHB semi-quantitatively correlated to the absolute amount of DHB deposited on the surface is valid. Figure 5.1C shows that the MS intensities of analyte ions vary when the amount of DHB changes and the degree of variation differs significantly among the analytes studied. For example, the major ion peaks of DHB ($[M+H]^+$, m/z = 155.0) and cholesterol ($[M+H-H_2O]^+$, m/z = 369.4) remained relative constant initially but decreased sharply when the amount of matrix deposited reached certain thresholds. However, the intensity of ions at m/z = 103.9 increased unexpectedly as the thickness of DHB decreased and decreased faster when the thickness of DHB reduced over certain level. The observation that MS intensities of different analytes vary at different paces when the amount of matrix on the sample surface changes raises concerns that mapping of biological variation of an analyte of interest could be distorted by inconsistent presence of matrix across the surface. Hence the stability of conventional matrix in vacuum during ME-SALDI-IMS could impose a limit to the overall size of the tissue section to be analyzed and the achievable spatial resolution.

It is also worth pointing out that although internal standards have been used to alleviate the arbitrary distortion induced by the loss of matrix over time by normalizing the peak intensities of the analytes against that of the internal standard, the analyte-specific fluctuation to the changes of the amount of matrix makes this approach only partially successful. As shown in Figure 5.1D, after normalization against the molecular ion peak of DHB, the ion intensities of cholesterol was less dependent on the amount of DHB on the substrate where the relative signal variation of cholesterol ions from the samples with different amounts of matrix was reduced from 63% to 20%. However, a

sharp increase in relative intensity was observed for ion at m/z=103.9 after DHB normalization and an increase from 46% to 134% in signal variation from the samples with different amounts of matrix were calculated.

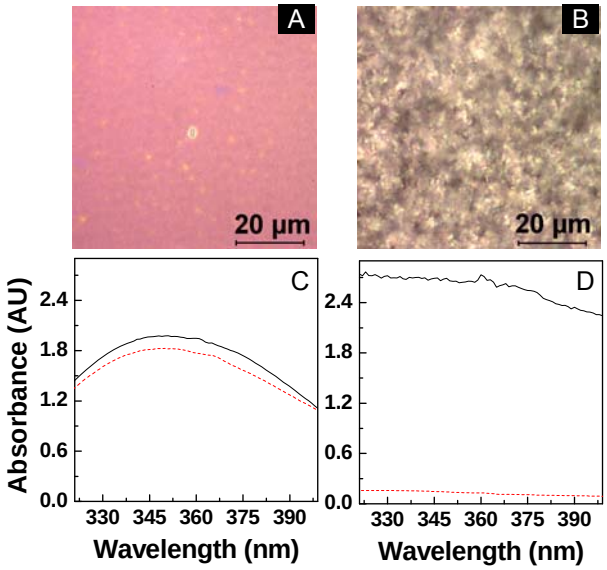

Figure 5.2. Optical images of (A) the solid ionic matrix (CHCA/ANI) layer and (B) conventional matrix (DHB) layer sublimated on glass slides. Representative UV-Vis spectra of (C) the CHCA/ANI layer and (D) the DHB layer collected before (—) and after (---) 40-h vacuum storage.

Advances in matrix optimization suggest that ionic matrix could be the solution to the aforementioned problem. However, before adapting it to ME-SALDI imaging applications, three critical issues need to be addressed first to ensure a homogenous and reproducible matrix coating with minimal analyte delocalization: (1) deposition of ionic matrix can be conducted in a solvent-free format, e.g. through sublimation; (2) matrix stability is indeed improved in the ME-SALDI mode that warrants continuous investigation and optimization; and (3) no compromises on the spectral quality in ME-SALDI when ionic matrix is used. To address these issues, an ionic matrix, CHCA/ANI, was selected as the model molecule to evaluate the performance of ionic matrix in ME-

SALDI for its well-documented MALDI performance. Although in salt forms, many ionic liquid molecules exhibit measurable vapor pressures that allow them to be vaporized at reduced pressure without decomposition.[22] Indeed, CHCA/ANI was found to be vaporizable at an elevated temperature of 170 ºC, noticeably higher than that of CHCA under vacuum (125 ºC) but still manageable with the in-house sublimation apparatus. Dissociation of CHCA/ANI salt was unlikely

Table 5.1. Calculated Relative Standard Deviation (RSD%) of UV Absorbance of Sublimation-coated Matrix Thin Film at 337 nm

	Intra-substrate RSD%						Inter-substrate RSD%
matrix	1#	2#	3#	4#	5#	Average	
CHCA/ANI	0.97	1.97	1.72	2.82	1.97	1.89	4.37
DHB	4.52	1.37	2.95	4.19	1.89	2.98	8.15

during vaporization as drastically different film morphology was observed from the CHCA/ANI-coated slide in comparison to the "puffier" surface coated with DHB (Figure 5.2A-B). Giving that both CHCA/ANI and DHB have strong optical absorption in the UV region, the reproducibility of matrix deposition was quantitatively assessed by comparing the corresponding UV absorbance. The intra-substrate RSD% of five measurements within the same substrate was less than 2% and the inter-substrate RSD% from five CHCA/ANI-coated substrates prepared independently was less than 4.4%. On the other hand, for DHB-coated substrates RSD% of 3% and 8.2% were calculated respectively, suggesting a comparable, if not better, deposition uniformity and reproducibility when ionic matrix was deposited by sublimation (Table 5.1). The vacuum stability of different matrix layers was examined by comparing the change in their UV absorbance before and after 40-h vacuum storage at 10^{-7} Torr. As shown in Figure 5.2C,

the UV absorbance of the CHCA/ANI layer changed less than 4% (from 1.81±0.05 to 1.75±0.03). In contrast, the UV absorbance of the substrate coated with DHB was significantly reduced from 2.68±0.05 to 0.15±0.02, equivalent to more than 94% loss of original materials (Figure 5.2D).

Significant reduction of the matrix interference is another attractive characteristic of using CHCA/ANI as the matrix, yet it was often accompanied by reduction of analyte signals. As shown in Figure 5.3A, a clean but fairly weak analyte signal was observed when CHCA/ANI was used as the MALDI matrix in detection of 1 pmol quinidine (m/z=325.2), an anti-arrhythmic pharmaceutical compound. The Matrix Suppression

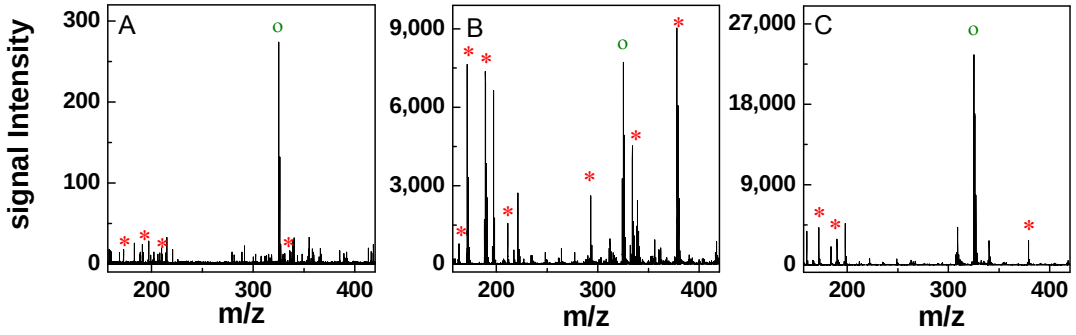

Figure 5.3. Representative spectra of 1 pmol quinidine collected with (A) CHCA/ANI using MALDI, (B) CHCA/ANI contained 0.1% TFA using MALDI and (C) CHCA/ANI using ME-SALDI. The matrix and analyte peaks were labeled with asterisks and circles, respectively.

Effect score ($MSE = \frac{\sum I_{[\text{Analyte Ions}]}}{\sum I_{[\text{Analyte Ions}]} + \sum I_{[\text{Matrix Ions}]}}$) was quantitatively calculated as 72±7%. Proton transfer between matrix ions and analyte molecules in desorbed plume has been reported as the major ionization pathway for analyte ionization in MALDI. Decrease of the plume density was suspected for ionic matrix, which likely led to the observed reduction of both analyte and matrix signal. Acidic additives, such as

Scheme 5.1. Competitive reaction of TFA with solid ionic matrix CHCA/ANI.

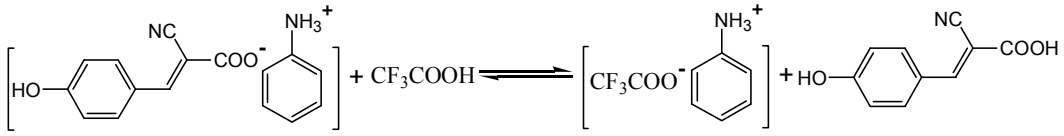

trifluoroacetic acid (TFA) or phosphoric acid, have been frequently used with ionic matrices to overcome this limitation and enhance analyte ionization efficiency (Figure 5.3B). However, they are not suitable for MS Imaging because TFA can not be co-vaporized with CHCA/ANI due to their drastically different vapor pressures; therefore solution-based matrix deposition has to be employed, which raises the risks of redistribution of analytes. More importantly, although these acidic additives facilitate analyte ionization by providing extra protons to the system, they compete with CHCA in complexation with aniline, resulting in release of conventional MALDI matrix from the corresponding solid ionic matrix (Scheme 5.1). Recurrence of matrix signal after addition of TFA is the first sign of dissociation of CHCA/ANI complexes where MSE decreased to 21±5%. The suspected dissociation was further confirmed by the lessened vacuum stability where the UV absorbance of CHCA/ANI co-deposited with TFA decreased from 0.73±0.16 to 0.50±0.11 after 40-h storage, a 32% reduction.

Using porous surfaces to assist efficient ionization of analytes, ME-SALDI provides an alternative solution to improve analyte signals without applying any additives. Figure 5.3C shows that the ion intensity of quinidine was enhanced near 2 orders of magnitude in ME-SALDI in comparison to using CHCA/ANI in the MALDI mode without TFA and more than 3 folds to using CHCA/ANI in the MALDI mode with TFA additive. Moreover, the ability of ionic matrix to reduce matrix interference

(MSE=69±5%) and improve vacuum stability (less than 4% loss after 40-h vacuum storage) was preserved in ME-SALDI. The usage of ionic matrix in complex biological sample was also examined through the detection of garlic extracts (Figure 5.4). The intensity of ion at m/z=104.1 was ~7 folds stronger in ME-SALDI than in MALDI (without acidic additives) and the matrix background signal was negligible. Furthermore, the molecular ions of fructooligosaccharides with the degree of polymerization (DP) from 5 to 12 were only detectable in ME-SALDI with an acceptable signal-to-noise ratio and resolution (Table 5.2). Further examination of MS spectra confirmed that the use of ionic matrix in the ME-SALDI mode did not compromise other important MS characteristics, such as ion intensity, signal-to-noise ratio, mass range and spectral resolution of analytes.

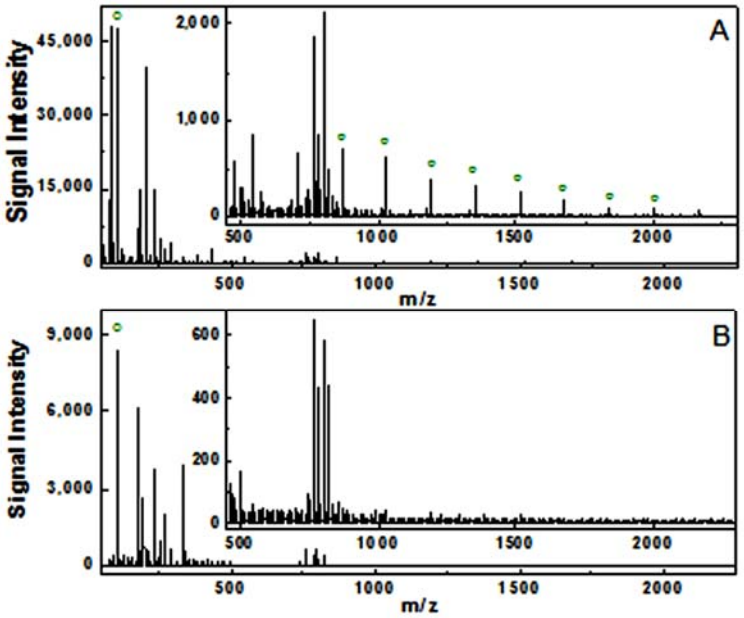

Figure 5.4. The usage of solid ionic matrix without acidic additive in complex biological sample was also examined through the detection of garlic extracts using (A) ME-SALDI and (B) MALDI. The analyte peaks were label with circle.

The usage of ionic matrix as ME-SALDI matrix in revealing the spatial distribution of natural biomolecules was demonstrated through the analysis of garlic

Table 5.2 Detection of Fructooligosaccharides in Garlic Extract with CHCA/ANI using ME-SALDI MS

	DP5 m/z=867.2	DP6 m/z=1029.3	DP7 m/z=1191.3	DP8 m/z=1353.4	DP9 m/z=1515.4	DP10 m/z=1677.5	DP11 m/z=1839.5	DP12 m/z=2001.6
Signal Intensity	611±126	490±111	363±36	295±52	209±30	146±21	93±9	75±15
S/N	31	113±27	85±9	72±12	51±9	38±7	26±4	19±4
Resolution	5598±710	7439±985	6288±674	7120±878	7299±1021	9305±1212	8240±2129	8132±1941

tissue samples. Figure 5.5A displays an optical image of a 10-µm thick garlic tissue section, where the storage leaf (i.e. endosperm) was clearly distinguishable from the cotyledon in the center. A piece of garlic section at the adjacent position was placed on a porous silicon substrate and coated with a thin layer of CHCA/ANI through sublimation, followed by scanning with a 35-µm laser beam at 50-µm step wise. A major matrix ion (*m/z* = 190.1) was uniformly observed across the whole scanning area, which confirmed homogenous matrix deposition on the tissue and negligible matrix loss over ~46 h scanning (Figure 5.5B). In comparison to the distorted distribution in DHB-coated garlic section (Figure 5.1B), signal for ions at m/z=104.1 was found highly expressed in the cotyledon portion with a weak but uniform background across the tissue, as expected (Figure 5.5C). On the other hand, the potassium adducts of fructooligosaccharide DP5 (m/z=867.2), one of the primary carbohydrate storage materials in garlic, was spatially distributed mainly in the endosperm portion (Figure 5.5D).

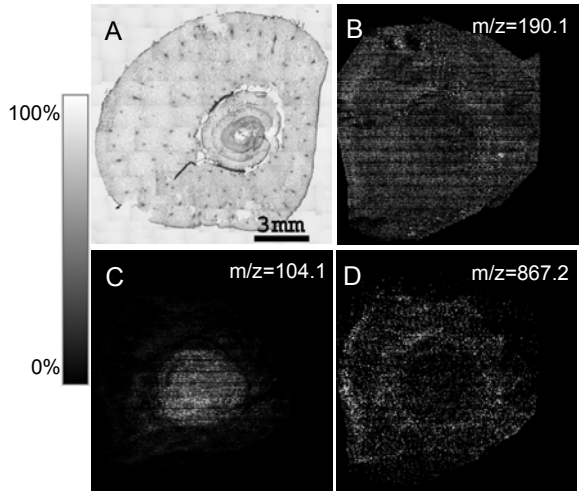

Figure 5.5. (A) An optical image of 10-μm thick garlic section. (B) Reconstructed 2-D images for ions at (B) m/z=190.1, (C) m/z=104.1 and (D) m/z=867.2 for a CHCA/ANI coated garlic section in ME-SALDI IMS.

5.4 Conclusions

In summary, we have demonstrated that the usage of ionic matrix in ME-SALDI provides an attractive approach to the analysis of small molecules, especially in the imaging application. The demonstrated benefits include extended imaging duration under vacuum, enhanced analyte ionization, lower background noise, and solvent-free deposition capability. The potential of quantitative analysis using ionic matrix in ME-SALDI was demonstrated but quantitative comparison with other imaging methods needs to be further evaluated.

5.5 References.

(1) Alimpiev, S.; Grechnikov, A.; Sunner, J.; Borodkov, A.; Karavanskii, V.; Simanovsky, Y.; Nikiforov, S. Anal. Chem. 2009, 81, 1255-1261.

(2) Dattelbaum, A. M.; Iyer, S. Expert Rev. Proteomics 2006, 3, 153-161.

(3) Kailasa, S. K.; Kiran, K.; Wu, H.-F. Anal. Chem. 2008, 80, 9681-9688.

(4) Kawasaki, H.; Sugitani, T.; Watanabe, T.; Yonezawa, T.; Moriwaki, H.; Arakawa, R. Anal. Chem. 2008, 80, 7524-7533.

(5) Lo, C.-Y.; Lin, J.-Y.; Chen, W.-Y.; Chen, C.-T.; Chen, Y.-C. J. Am. Soc. Mass Spectrom. 2008, 19, 1014-1020.

(6) Northen, T. R.; Lee, J.-C.; Hoang, L.; Raymond, J.; Hwang, D.-R.; Yannone, S. M.; Wong, C.-H.; Siuzdak, G. Proc. Natl. Acad. Sci. 2008, 105, 3678-3683.

(7) Zhang, H.; Cha, S.; Yeung, E. S. Anal. Chem. 2007, 79, 6575-6584.

(8) Taira, S.; Sugiura, Y.; Moritake, S.; Shimma, S.; Ichiyanagi, Y.; Setou, M. Anal. Chem. 2008, 80, 4761-4766.

(9) Liu, Q.; Guo, Z.; He, L. Anal. Chem. 2007, 79, 3535-3541.

(10) Liu, Q.; Xiao, Y.; Pagan-Miranda, C.; Chiu, Y. M.; He, L. J. Am. Soc. Mass Spectrom. 2009, 20, 80-88.

(11) Samuel Carda-Broch, A. B. D. W. A. Rapid Commun. Mass Spectrom. 2003, 17, 553-560.

(12) Hankin, J. A.; Barkley, R. M.; Murphy, R. C. J. Am. Soc. Mass Spectrom. 2007, 18, 1646-1652.

(13) Tholey, A.; Heinzle, E. Anal. Bioanal. Chem. 2006, 386, 24-37.

(14) Fukuyama, Y.; Nakaya, S.; Yamazaki, Y.; Tanaka, K. Anal. Chem. 2008, 80, 2171-2179.

(15) Laremore, T. N.; Zhang, F.; Linhardt, R. J. Anal. Chem. 2007, 79, 1604-1610.

(16) Zabet-Moghaddam, M.; Heinzle, E.; Lasaosa, M.; Tholey, A. Anal. Bioanal. Chem. 2006, 384, 215-224.

(17) Mank, M.; Stahl, B.; Boehm, G. Anal. Chem. 2004, 76, 2938-2950.

(18) Lemaire, R.; Tabet, J. C.; Ducoroy, P.; Hendra, J. B.; Salzet, M.; Fournier, I. Anal. Chem. 2006, 78, 809-819.

(19) Finkel, N. H.; Prevo, B. G.; Velev, O. D.; He, L. Anal. Chem. 2005, 77, 1088-1095.

(20) Bai, Q.; Fan, G.; Gu, Z.; Cao, X.; Gu, F. Eur. Food Res. Technol. 2008, 228, 169-175.

(21) Popov, V. N.; Eprintsev, A. T.; Fedorin, D. N.; Fomenko, O. Y.; Igamberdiev, A. U. Appl. Biochem. Microbiol. 2007, 43, 341-346.

(22) Earle, M. J.; Esperanca, J. M. S. S.; Gilea, M. A.; Canongia Lopes, J. N.; Rebelo, L. P. N.; Magee, J. W.; Seddon, K. R.; Widegren, J. A. Nature 2006, 439, 831-834.

Chapter 6 Ordered Mesoporous Titania Film in Matrix-Enhanced Surface-Assisted Laser Desorption Ionization Imaging Mass Spectrometry (ME-SALDI-MS)

6.1 Introduction

Revived in recent years, surface-assisted laser desorption ionization (SALDI) IMS has demonstrated as a complementary approach to illustrating spatial distribution of low-mass species of biological importance for various applications. Efforts have been made to improve its imaging performance, including fundamental understanding on the desorption/ionization mechanism, exploratory usage of different nanoparticles in SALDI IMS, and optimization of sample preparation.[1-7] In particular, a hybrid ionization approach - matrix-enhanced surface-assisted laser desorption ionization (ME-SALDI), has been demonstrated to minimize matrix background and improve sensitivity for small molecules imaging.[8] Porous silicon (pSi), which was developed by Siuzdak *et al.* in late 90s and is recognized as one of the most successful SALDI substrates, was used in ME-SALDI in the previous report.[9] However, preserving the performance of freshly prepared pSi and extending its shelf-life have been a daunting task, due to fast surface oxidation. The few measures with certain degree of success to extend substrate lifetime, such as by storing substrates in ethanol or under vacuum, were ineffective in practice of imaging mass spectrometry due to dissolution/redistribution of small molecules on tissue. A substrate with better in-air stability is highly desirable for ME-SALDI IMS to ensure reproducible chemical imaging of analytes of interest. In addition, the ability of imaging surface features in sub-micrometer spatial resolution is crucial to understand the spatial

activity of bio-molecules, such as phospholipids, RNA, and pharmaceutical compounds in the sub-cellular level.[10-15] ME-SALDI IMS is shown to afford sufficient detection sensitivity under reduced laser beams and could provide a complementary imaging tool to secondary ion mass spectrometry (SIMS) to reveal molecular distribution at the cellular level. However, at such high imaging resolution, the porous structures used in energy mediating process need to be small and uniform where variation of signal intensities across the surface and consequently inaccurate report of analyte spatial distribution can be prevented.

Substrate stability refers to chemical inertness towards its storage environment over time and substrate uniformity refers to consistent surface features at the nanometer scale. In addition, an ideal ME-SALDI IMS substrate should possess following characteristics: a strong photon absorption band at 337-nm to allow effective energy absorption; high surface area (i.e. high porosity) and deep pore channels to improve analyte desorption and ionization efficiency[16]; and regular and controllable surface morphology to allow comparable MS performance between substrates. In addition to pSi, a broad range of stable inorganic materials has been examined for SALDI-MS, such as carbon nanotubes, gold nanoparticles, and titania nanoparticles, etc, but few display all characteristic features entailed.[17-19] Among the few successful materials is porous titania film, prepared by a sol-gel method using polyethylene glycol as a porogen.[20] The titania-sol-gel film was then converted to crystalline titania through calcination at 500 ºC, while polyethylene glycol was burned out. It showed promises but the resulting porosity of this film, originated from interparticle voids, was low and the pores were randomly shaped.

Here, we describe the use of an improved sol-gel synthetic method that yields a highly ordered, highly porous titania film for ME-SALDI IMS. The fabrication protocol is simpler and more robust, and the substrate stability is extended from hours to months. Its superior MS performance over porous Si substrates in MS imaging is demonstrated by imaging distribution of cholesterol and phospholipids in mouse brain.

6.2. Experimental Section

Materials. N-type Sb-doped (100) single-crystalline silicon wafers at 0.005-0.02 Ω/cm from Silicon Sense, Inc. (Nashua, NH) were used to prepare pSi substrates. 1,2-Dimyristoyl-*sn*-glycero-3-phosphocholine (DMPC) from Avanti Polar Lipids, Inc. (Alabaster, AL), citric acid diammonium salt and titanium isopropoxide from Alfa Aesar (Ward Hill, MA), citric acid and 2,5-dihydroxybenzoic acid (DHB) from Sigma Aldrich (St. Louis, MO), methylene blue zinc chloride double salt from MP Biomedicals (Solon, OH) were used as received. Commercial triblock copolymer surfactant, Pluronic F127 (polyethylene oxide –b- polypropylene oxide -b- polyethylene oxide, BASF), was used as a template in sol-gel synthesis. Bradykinin was purchased from Fisher Scientific (Pittsburgh, PA). Angiotensin I, ACTH clips (1-17, 18-39 and 7-38), insulin (bovine), thioredoxin (E. coli) and apomyoglobin (horse) were supplied from Applied Biosystems (Framingham, MA).

Preparation of Ordered Mesoporous Titania Films Preparation conditions of ordered mesoporous titania films were optimized based on a published protocol.[21] First, 0.72 g of concentrated HCl was mixed with 1.05 g titanium isopropoxide, and the mixture solution

was stirred for 15 min. To this solution, the alcoholic solution of the surfactant, prepared by dissolving 0.2 g of pluronic F127 in 2.8 g ethanol, was added under stirring. The reactant solution thus prepared was then filtered through a 0.45 μm filter. A pre-cleaned silicon substrate was coated with this reactant solution by spin coating at 4,000 rpm for 1 min. The Si substrate after coating was kept under the atmosphere at RT-95 % relative humidity (RH) for 20 min, followed by overnight aging at -20 ^{o}C. The substrates after aging were then calcinated under atmosphere from RT to 400 ^{o}C at a ramping rate of 1 ^{o}C/min and remained at 400 ^{o}C for 4 h to remove the surfactant. The mesoporous titania films thus prepared were stored in desiccator prior to analyte deposition. Additional preparation conditions were evaluated and details were described in the text.

Preparation of Porous Si (pSi) Substrates pSi was prepared as previously described[5]. A 1-cm^2 of square-shaped Si wafer was dipped in a 5% HF solution in ethanol for 1 min to remove the oxidized layer, followed by electrochemical etching in a 25% HF/ethanol solution for 1 min at a current density of 5 mA/cm^2 under the white light irradiation using a 50 W tungsten lamp. The porous Si thus prepared was refreshed by sequential dipping in 15% H_2O_2 and 5% HF/ethanol solution prior to analyte deposition.

Sample Preparation for MS Measurements A citrate buffer solution was prepared by mixing the aqueous solution of diammonium citrate (50 mM) with citric acid (100 mM) in 3:1 volume ratio. Standard solutions of atenolol (1, 5, 10, 50 and 100 μM) were prepared using the citrate buffer. Three peptide solutions were prepared: peptide mixture 1 included 2 μM angiotensin I, 2 μM ACTH (1-17 clip), 1.5 μM ACTH (18-39 clip), 3 μM ACTH (7-38 clip) and 3.5 μM insulin; and peptide mixture 2 included 0.5 μM

insulin, 2.75 μM thioredoxin, and 4 μM apomyoglobin (horse**);** and peptide solution 3 was bradykinin (5 μM). **.** All solutions were prepared in the citrate buffer solution.

MS Measurements. An Applied Biosystems Voyager DE-STR MALDI-TOF mass spectrometer (Framingham, MA) was operated at an accelerating voltage of 20 kV. All standard analytes were detected in a linear mode, and the reflector mode was used in all MS imaging experiments. The laser intensity and delay time was varied to achieve optimal performance. A variable pinhole was placed close to the laser entrance window to adjust the diameter of the laser beam. Each MS spectrum was recorded with twenty laser shots, and ten spectra were averaged to obtain one accumulated MS spectrum before further data analysis. At any given size of the laser beam, five MS replicates were collected at each laser irradiation energy level.

The mouse heart and brain tissue samples were mounted on a metal support with optical cutting temperature (OCT) compound and was sliced to 10-μm thick sections with a Cryo-cut microtome (American Optical Corp., Buffalo, NY) at -20 °C. The tissue sections were then transferred onto an ordered mesoporous titania film. In mouse brain imaging experiment, matrix DHB was sublimated onto the tissue section at 110 °C under vacuum for MS imaging. Meanwhile, a similar section microtomed at the adjacent location was placed on a glass slide and stained with methylene blue for optical visualization. Optical micrographs were taken with a Leica DMRX light microscope equipped with a Donpisha XC-003P CCD camera. All tissue sections were MS-imaged under a 35-μm laser beam at 50-μm stepwise. The MS instrument was controlled by MMSIT MALDI Imaging Tool software V2.2.0. Fifty shots were averaged to yield one

accumulated spectrum at each imaging pixel. The final ion maps, as well as the Y-axis profiles, were reconstructed using BioMap 3.7.5.4. Both software were provided by Markus Stoeckli, Novartis Institutes for BioMedical Research, Basel, Switzerland.

6.3 Result and Discussion

Scheme 6.1. The fabrication procedure in preparing porous titania substrate

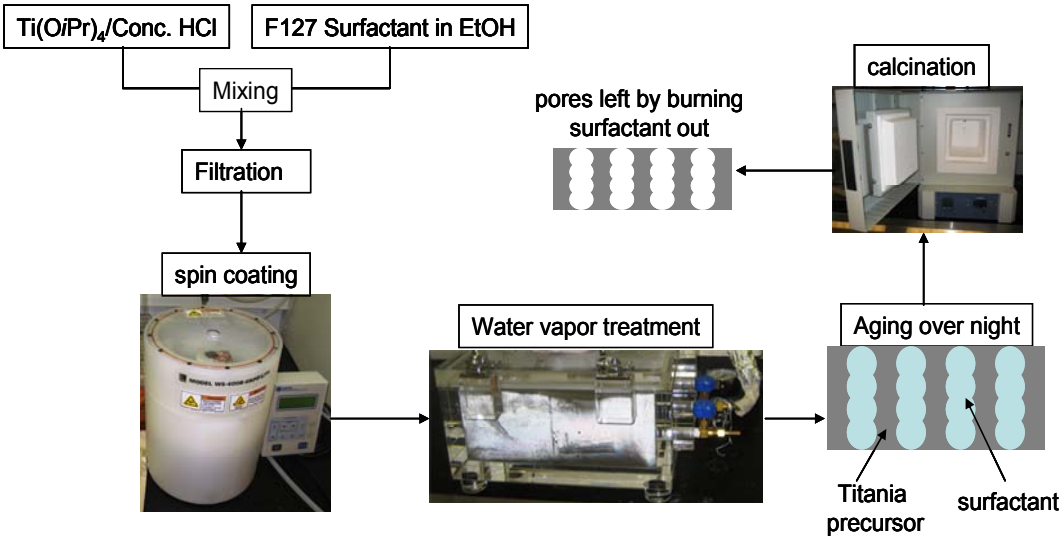

Scheme 6.1 shows the fabrication procedure in preparing porous titania substrates. Figure 6.1A displays the SEM image of the top view of a mesoporous titania film with pores of an average of 10 nm in diameter. The 3-D structure of the film was further revealed by the cross section image, in which open channels of high aspect ratios were formed perpendicular to the substrate where well-aligned pores were connected from calcination (Figure 6.1B), as described in the previous report.[21] In comparison to porous silicon, a much more uniform and ordered porous surface was observed from the titania substrate (Figures 6.1C and 6.1D). The small and identical features minimize the

potential signal variation across the surface, which can be especially important in direct quantification of analytes in the absence of internal standards during high resolution MS imaging of animal tissues.

Preparation of mesoporous titania film was straightforward and robust. Moderate variation in the fabrication parameters did not cause significant changes in its subsequent MS performance. For instance, the aging temperature was varied from -20ºC to 4ºC and

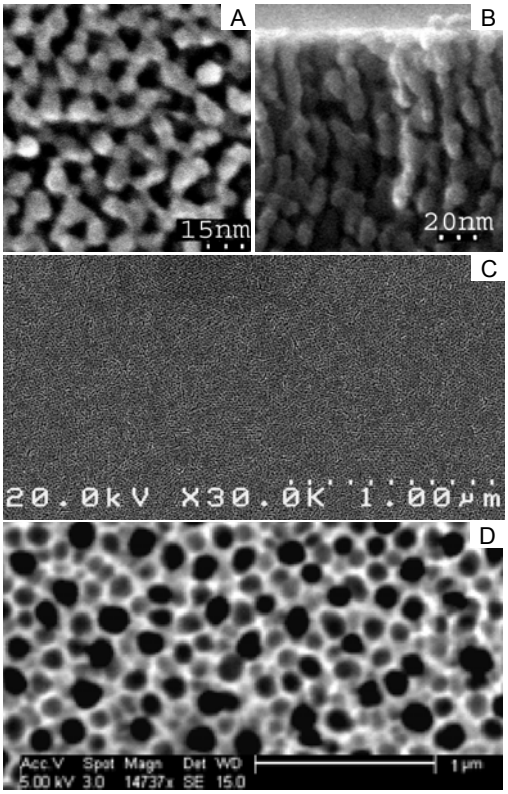

Figure 6.1. SEM images of titania film with (A) top view and (B) cross section. Zoom out SEM images of (C) titania film and (D) porous silicon with top view.

the aging time was varied from overnight to 5 h during the preparation; yet comparable analyte signal was observed regardless which of the mesoporous titania film was used (Figure 6.2A to 6.2D). The change of solvent from ethanol to pentanol made little

difference, (Figure 6.2E to 6.2F) nor did the change of the template surfactant from F127 to P123 or F108, which have different segment length of polyethylene oxide and polypropylene oxide (Figure 6.3). In contrast, the porous structure of porous silicon is known to be very sensitive to the preparation conditions where slight change in anodic current or etching time would adversely affect subsequent MS performances (data not shown).[22]

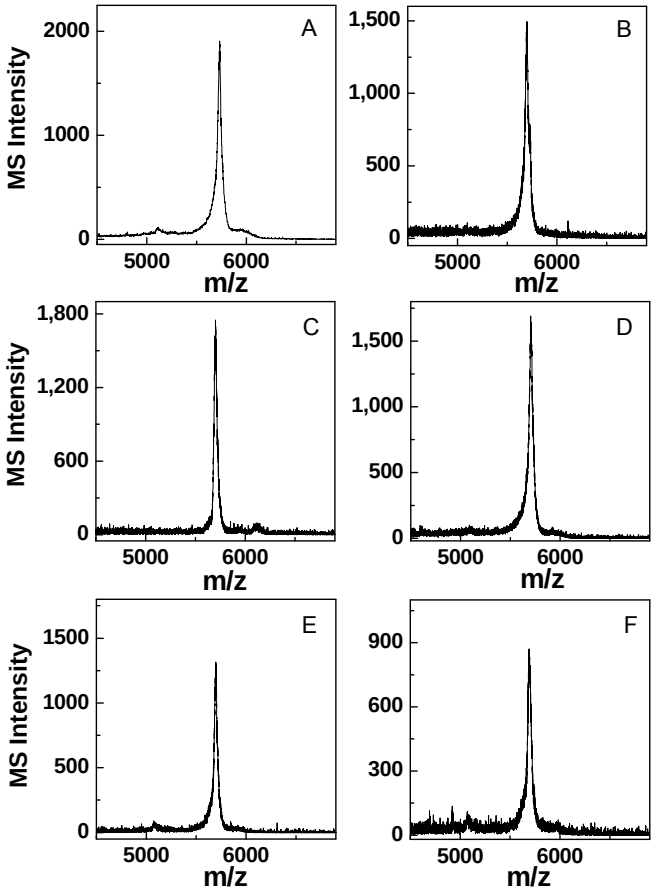

Figure 6.2. 10 μM of insulin solution was used as standard to compare the MS performance of titania films prepared under different conditions. Representative spectrum were collected from the titania film (A) aged at -20ºC overnight, (B) aged at -20ºC for 5 hours, (C) aged at 4ºC overnight and (D) aged at 4ºC for 5 hours where ethanol was used as solvent during fabrication. Representative spectrum were collected from the titania film aged at -20ºC overnight where (E) butanol and (F) pentanol was used as solvent during fabrication.

The use of ordered mesoporous titania film as a ME-SALDI substrate is demonstrated in Figure 6.4. Atenolol, a drug commonly used for cardiovascular diseases treatment, was used as the model molecule to establish the quantitative capability of porous TiO2 substrates. Its protonated molecular ion is clearly observed at m/z = 267.3 with S/N=117±44 in the detection of 1 pmol materials (Figure 6.4A), which is comparable to that from freshly prepared pSi. Direct quantitative analysis of atenolol without internal standard was carried out, where the calibration curve was plotted as the S/N of the molecular ion against the atenolol concentration from 1μM to 100 μM (Figure 6.4B). The first few data points were fitted with a linear relationship with the correlation

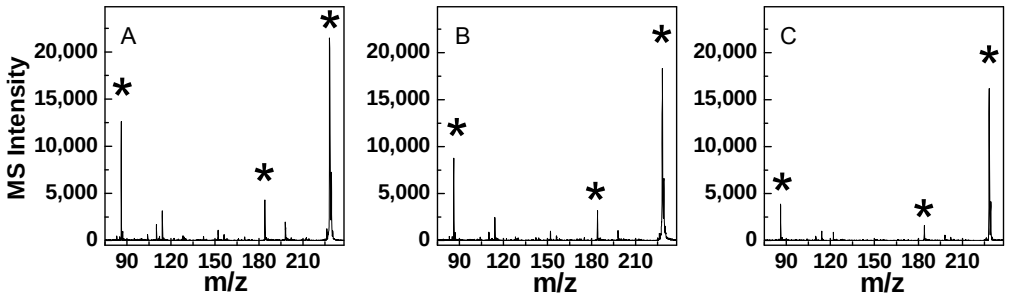

Figure 6.3. The surfactant used for titania film preparation was optimized. The Representative ME-SALDI MS spectrum on titania mesoporous film prepared with surfactant (A) P123, (B) F127 and (C) F108. The head groups of DPPC at m/z=86, m/z=184 and the molecular ion of DTMA at m/z=228 were labeled with asterisks.

coefficient of 0.94. With the increasing concentration to 100 uM, the signal-to-noise ratio decreases mainly due to increased background signals. Figure 6.4C and 6.4D display the analysis of two peptide/proteins mixtures on a titania film. Positive detection for all peptides from 1,000 Da to near 20,000 Da was clearly observed.

The stability of the mesoporous titania film in air was investigated and compared with that of porous silicon using 1 μl of 5 μM bradykinin solution as a analyte. Figure 6.5A and 6.5B are the spectra recorded using the mesoporous titania film soon after the

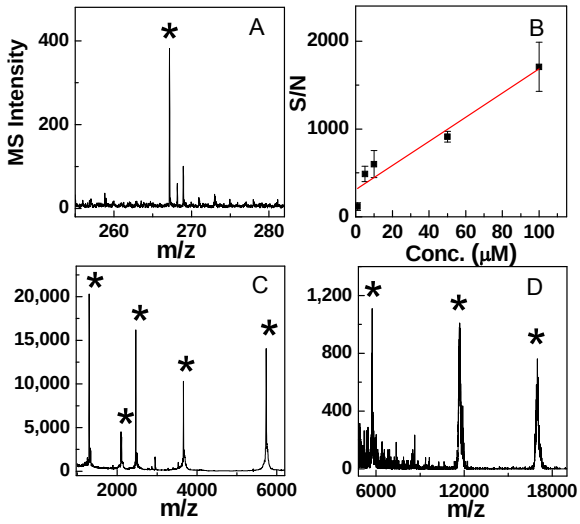

Figure 6.4. Representative spectrum of (A) 1 μM Atenolol and (B) the calibration curve for Atenolol. Representative spectrum of (C) peptides mixture 1 and (D) peptides mixture 2. All analyte solution prepared with citric acid/diammonium citrate buffer. The peptides mixture 1 includes angiotensin I, ACTH clips (1-17, 18-39 and 7-38 clip) and insulin. The peptides mixture 2 includes insulin, thioredoxin and apomyoglobin. All analytes were labeled with asterisks.

preparation and that stored in desiccator for 10 months, respectively. The S/N of bradykinin molecular ion was estimated to be 390±181 and 336±119 for fresh and aged titania film, respectively. No significant changes are observed between these two spectra, showing that exposure to air did not adversely alter the MS performance of the substrate in bradkinin detection. On the other hand, the stability of porous silicon in air is much poorer. Although comparable detection was achieved using a fresh porous silicon (Figure 6.5C, S/N= 342±185) for the same bradykinin solution, the MS capability of porous silicon was almost completely lost (~95% loss) after only one day storage in desiccator (Figure 6.5D, S/N=18±10). The remarkable difference in the stability between these two substrates in air is attributed to their resistance to oxidation. Porous silicon is easily oxidized under an oxygen-rich atmosphere to form insulating silicon dioxide, which is much less SALDI-active. On the other hand, titania is in its highest oxidation

state that can not be further oxidized. Its physical and chemical properties are therefore preserved and the corresponding MS performance unchanged. It is also interesting to note that the photocatalytic behavior of titania may also contribute to the consistent MS performance by preventing unnecessary adsorption of contaminants and reducing background noises overtime.[23]

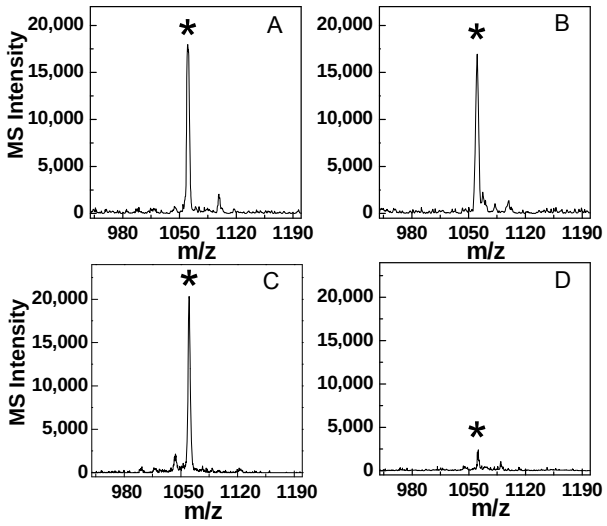

Figure 6.5. Representative spectrum of bradykinin using (A) freshly prepared titania film, (B) titania film after 10-months storage, (C) fresh prepared porous Si and (D) porous Si after one-day exposure in air. Analyte peak was labeled with asterisk.

Inert to its chemical environment, good sensitivity, and large mass window made the ordered mesoporous titania film an ideal substrate for MS imaging in the ME-SALDI mode. Figure 6.6 shows MS images of a piece of horizontally dissected mouse brain placed on a titania substrate and coated with a thin layer of DHB by sublimation. The sublimation conditions were systematically optimized to yield a thin and homogeneous thin matrix film. During the ME-SALDI-IMS experiment, the laser energy was efficiently absorbed by the titania film while DHB acted as the major proton source to

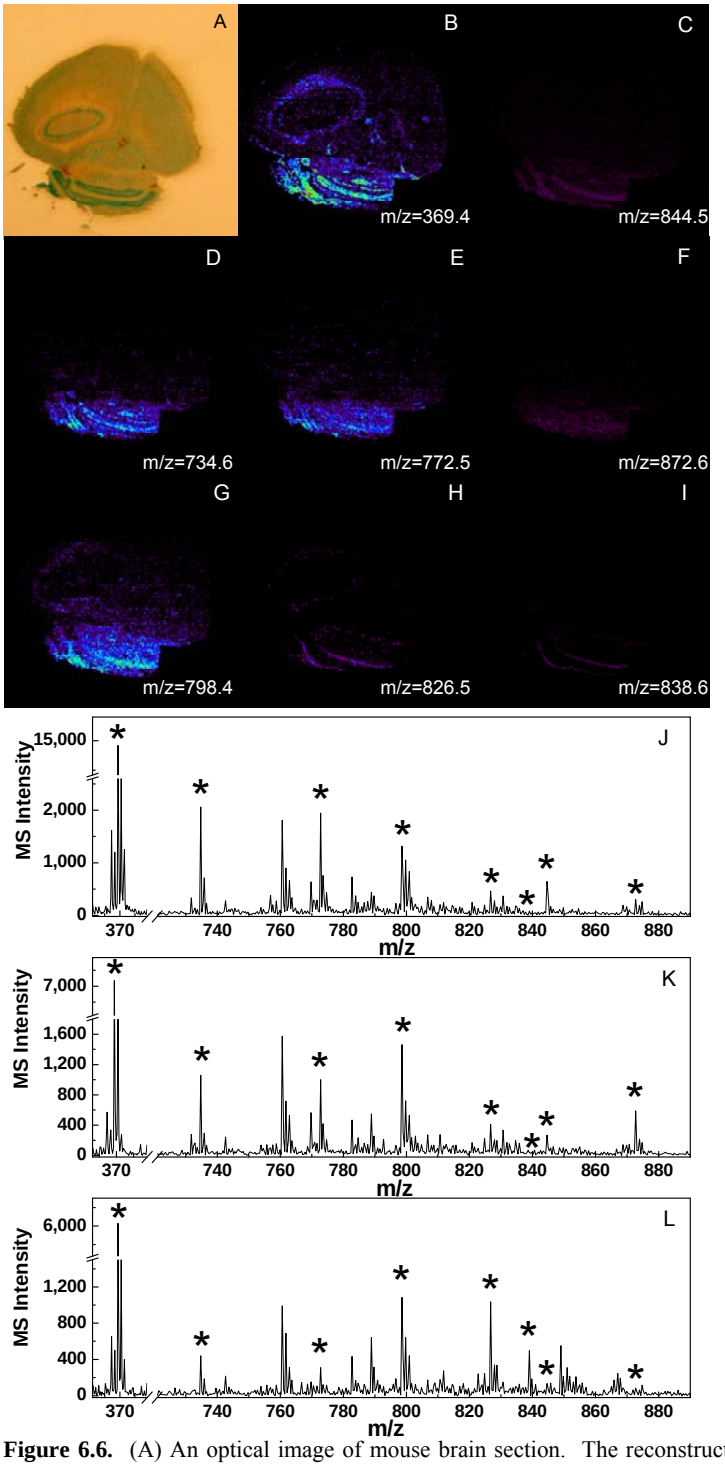

Figure 6.6. (A) An optical image of mouse brain section. The reconstructed ion maps at (B) m/z=369.4, (C) m/z=844.5, (D) m/z=734.6, (E) m/z=772.5, (F) m/z=872.6, (G) m/z=798.4, (H) m/z=826.5, (I) m/z=838.6. Representative spectrum collected from (J) the granular layer, (K) the molecular layer and (L) the white matter of mouse brain cerebellum during the IMS process. Analyte peaks were labeled with asterisks (∗).

facilitate the ionization of analyte. Cerebral cortex, cerebellum (molecular layer, granular layer and white matter), and the left side of corpus callosum of mouse brain can be clearly visualized under an optical microscope after methylene blue staining. Figure 6.6B displays reconstructed ion image of cholesterol concentrated in granular layer at corpus callosum and cerebellum. As expected, full MS spectra from pixels within ,granular layer, molecular layer, and white matter of mouse brain cerebellum showed more than 2-fold less cholesterol in the latter matter (Figure 6.6J to 6.6L). PC 38:6 is also found dominantly expressed in the granular layer in the reconstructed ion image as well as in the representative MS spectra where its potassium adduct peak is ~3 times stronger than in other area of cerebellum (Figure 6.6C). PC 32:0 is more concentrated (3~5 folds) in both the granular layer and the molecular layer (Figure 6.6D, 6.6E). The signal of PC 40:6 is stronger (~2 folds) in molecular layer than that in granular layer, while that in white matter is negligible (Figure 6.6F). PC 34:1 is highly expressed in cerebellum and the concentration seems to be higher in granular layer and white matter (Figure 6.6G). In contrast, PC 36:1 and PC 40:4 were almost exclusively expressed in white matter (Figure 6.6H, 6.6I).

6.4 Conclusion

A mesoporous titania film, prepared through self-assembly of surfactant, has been developed as a novel ME-SALDI substrate. The superior stability of the mesoporouas titania film as well as high performance in detecting both metabolites and small proteins (<10,000 Da) have been demonstrated. Spectral variations across the tissue sample and

between different imaging experiments have been minimized due to the nanometer-sized, homogenously distributed mesoporous features and the robust fabrication procedure. The spatial distribution of hormone and phosphor lipids in mouse brain has been spatially profiled to prove the usefulness of the mesoporous titania film in ME-SALDI-IMS imaging.

6.5 References.

(1) Zhang, H.; Cha, S.; Yeung, E. S. Anal. Chem. 2007, 79, 6575-6584.

(2) Taira, S.; Sugiura, Y.; Moritake, S.; Shimma, S.; Ichiyanagi, Y.; Setou, M. Anal. Chem. 2008, 80, 4761-4766.

(3) Chen, Y.; Chen, H.; Aleksandrov, A.; Orlando, T. M. J. Phys. Chem. C 2008, 112, 6953-6960.

(4) Alimpiev, S.; Nikiforov, S.; Karavanskii, V.; Minton, T.; Sunner, J. J. Chem. Phys. 2001, 115, 1891-1901.

(5) Liu, Q.; Guo, Z.; He, L. Anal. Chem. 2007, 79, 3535-3541.

(6) Liu, Q.; He, L. J. Am. Soc. Mass Spectrom. 2008, 19, 8-13.

(7) Northen, T. R.; Yanes, O.; Northen, M. T.; Marrinucci, D.; Uritboonthai, W.; Apon, J.; Golledge, S. L.; Nordstroem, A.; Siuzdak, G. Nature 2007, 449, 1033-1036.

(8) Liu, Q.; Xiao, Y.; Pagan-Miranda, C.; Chiu, Y. M.; He, L. J. Am. Soc. Mass Spectrom. 2009, 20, 80-88.

(9) Wei, J.; Buriak, J. M.; Siuzdak, G. Nature 1999, 399, 243-246.

(10) Piehowski, P. D.; Carado, A. J.; Kurczy, M. E.; Ostrowski, S. G.; Heien, M. L.; Winograd, N.; Ewing, A. G. Anal. Chem. 2008, 80, 8662-8667.

(11) Subhash, C. J. Microsc. 2008, 232, 27-35.

(12) Wittig, A.; Arlinghaus, H. F.; Kriegeskotte, C.; Moss, R. L.; Appelman, K.; Schmid, K. W.; Sauerwein, W. A. G. Mol. Cancer Ther. 2008, 7, 1763-1771.

(13) Chandra, S.; Tjarks, W.; Lorey, D. R., II; Barth, R. F. J. Microsc. 2007, 229, 92-103.

(14) Altelaar, A. F. M.; Van Minnen, J.; Jimenez, C. R.; Heeren, R. M. A.; Piersma, S. R. Anal. Chem. 2005, 77, 735-741.

(15) McDonnell, L. A.; Piersma, S. R.; Altelaar, A. F. M.; Mize, T. H.; Luxembourg, S. L.; Verhaert, P. D. E. M.; Van Minnen, J.; Heeren, R. M. A. J. Mass Spectrom. 2005, 40, 160-168.

(16) Xiao, Y.; Retterer, S. T.; Thomas, D. K.; Tao, J.-Y.; He, L. J. Phys. Chem. ASAP.

(17) Su, C.-L.; Tseng, W.-L. Anal. Chem. 2007, 79, 1626-1633.

(18) Najam-ul-Haq, M.; Rainer, M.; Szabó, Z.; Vallant, R.; Huck, C. W.; Bonn, G. K. J. Biochem. Biophys. Methods 2007, 70, 319-328.

(19) Chen, C.-T.; Chen, Y.-C. Anal. Chem. 2005, 77, 5912-5919.

(20) Chen, C.-T.; Chen, Y.-C. Rapid Commun. Mass Spectrmo. 2004, 18, 1956-1964.

(21) Wu, C.-W.; Ohsuna, T.; Kuwabara, M.; Kuroda, K. J. Am. Chem. Soc. 2006, 128, 4544-4545.

(22) Lewis, W. G.; Shen, Z.; Finn, M. G.; Siuzdak, G. Inter. J. Mass Spectrom. 2003, 226, 107-116.

(23) Andrew, M.; Stephanie, H.; Soo Keun, L. Research Chem. Intermediates 2005, 31, 295-308.